TECHNISCHE UNIVERSITÄT WIEN
Vienna | Austria

DIPLOMARBEIT

Approaches and advancements towards NCN and SCS pincer complexes with first row transition metals

ausgeführt zum Zwecke der Erlangung des akademischen Grades eines

Diplom-Ingenieurs

unter der Leitung von

Univ.Prof. Dipl.-Ing. Dr. techn. Karl Kirchner

Univ. Ass. Dipl.-Ing. Wolfgang Eder
Univ. Ass. Dipl.-Ing. Jan Pecak

Institut für Angewandte Synthesechemie E163
Getreidemarkt 9/163, A-1060 Wien

eingereicht an der Technischen Universität Wien
Fakultät für Technische Chemie

von

Matthias Georg Käfer, BSc

Matr.Nr. 01526123

[redacted]

March 30, 2022

Matthias G.Käfer

Declaration

Ich habe zur Kenntnis genommen, dass ich durch Drucklegung meiner Arbeit unter der Bezeichnung

Diplomarbeit

nur mit Bewilligung der Prüfungskomission berechtigt bin.

Ich erkläre weiteres Eides statt, dass ich meine Diplomarbeit nach den anerkannten Grundsätzen für wissenschaftliche Abhandlungen selbstständig ausgeführt habe und alle verwendeten Hilfsmittel, insbesondere die zugrunde gelegte Literatur, genannt habe.

Weiters erkläre ich, das ich dieses Diplomarbeitsthema bisher weder im In- noch Ausland (einer Beurteilerin/einem Beurteiler zur Begutachung) in irgendeiner Form als Prüfungsarbeit vorgelegt habe und dass diese Arbeit mit der vom Begutachter beurteilten Arbeit übereinstimmt.

Danksagung

Zu aller Anfang möchte ich Prof. **Karl Kirchner** meinen Dank ausprechen. Zum einen für das spannenede und fordernde Forschungsthema und die Möglichkeit daran in seiner Forschungsgruppe zu arbeiten, zum anderen für die prosperiernde Arbeitsatmosphäre die in der Arbeitsgruppe implementiert wurde.

Ebenso möchte ich meinen beiden Co-Betreuern **Wolfgang Eder** und **Jan Pecak** danken. Dir Wolfgang, für all die unterhaltsamen und lehrreichen Gespräche über alle möglichen Dinge. Weiters noch dafür, dass du mir und allen anderen Mitgliedern der Gruppe immer wieder vor Augen führst, wie viel Spielraum die österreichische Interpretation der deutschen Sprache zulässt. Ebenso beachtlich ist dein Engagement mit dem du deinen Bildungsauftrag als einziger Lungauer der Arbeitsgruppe wahrnimmst, regionale Bräuche nicht in Vergessenheit geraten zu lassen. Dir Jan möchte ich explizit dafür danken, dass du mir die Grundzüge der DFT Rechnung im Kontext dieser Arbeit beigebracht hast. Die vielen unterhaltsamen Gespräche werden mir noch lange in Erinnerung bleiben.

Weiterer Dank gilt **Bertold Stöger**, der sich immer wieder die Zeit genommen hat die Kristallstrukturen dieser Arbeit aufzulösen und diese eloquent zu beschreiben.

Folgende Mitglieder der Arbeitsgruppe dürfen selbstverständlich nicht unerwähnt bleiben: **Gerald Tomsu** möchte ich vorallem dafür danken, mit mir den ein oder andern Feiertag und das ein oder andere Wochendende arbeitend verbracht zu haben. **Stefan Weber** gebührt ob seines hilfsbereiten, genauen Charakters ebenfalls Dank. Du bist ein gutes Beispiel dafür, was mit einer disziplinierten Arbeitsweise alles zu erreichen ist. **Ines Blaha** möchte ich vor Allem für einen neuen Spitznamen, die vielen lustigen Momente im Labor und die Näherbringung einer neuen Farbpalette danken. **Daniel Zobernig** möchte ich dafür danken, immer ein offenes Ohr für allfällige Belange zu haben, und dafür, dass du dein fundiertes Fachwissen über kulinarische Belange so bereitwillig teilst. **Heiko Schratzberger** möchte ich für seinen erheblichen Beitrag in der wissenschaftlichen Klassifikation von, unter anderen paramagnetischen Reaktionsprodukten danken. Ich finde es alarmierend, wie wenig ich doch über die Vielfältigkeit mancher Getränke gewusst habe. **Sarah Fleissner** möchte ich dafür danken, dass du dir die Zeit genommen hast, zu versuchen die Substanzen dieser Arbeit via HRMS zu charakterisieren.
Meinen beiden Diplomarbeitskolleginnen **Claudia Rabijasz** und **Dina Iebed** möchte ich für die gegenseitige Unterstützung während des(der) vergangenenen Jahre(s) danken.

Ebenso zu erwähnen sind **Ludwig Enzlberger** und **Katharina Obleser**, durch die das Absolvieren unzähliger Prüfungen und Präsentationen zu einem Hochgenuss wurde. Weiterer Dank gilt **Felix Seitz** für die jahrelange Freundschaft. Durch euch Drei wurden die vergangenen Jahre zu dem was sie sind, gefüllt mit Erinnerungen und Geschichten, an die ich mich sehr gerne erinnere und die ich sehr gerne erzähle.

Ebenso möchte ich **Peter Weinberger** und den Mitgliedern seiner Arbeitsgruppe, **Martin Huber, Willi Zeni, Matthias Schöbinger, Frieda Kapsamer** für die gute Zusammenarbeit im Stockwerk danken. Ebenfalls erwähnen möchte ich an dieser Stelle die Personen, die mich während meiner Studienjahre an der TU Wien mehr oder weniger begleitet haben: **Flora Jessl, Tina Gurmann, Florian Mayer, Moritz Mitterhofer, Anna-Maria Fuchsberger**.

An dieser Stelle möchte ich allen Kollegen, die mich bei der Firma MSD Intervet über die letzten Jahre begleitet haben, für die lehrreiche Zeit und die vielen geknüpften Kontakte danken.

Großer Dank gilt hier auch meiner besseren Hälfte- ohne ihre emotionale Unterstützung wären die letzten Wochen und Monate bestimmt anders verlaufen. Abschließend möchte ich meiner Familie, meinen Eltern und meiner Schwester für die überschwängliche Unterstützung in jeder Lebenslage und ihre Liebe danken.

Abstract

The investigation of pincer ligands and their transition metal complexes has received significant attention in the last years. Due to easily achievable modifications in their molecular scaffold, they provide for a huge variability and a rich chemistry. Although there are numerous works dealing with the preparation of pincer complexes bearing ligands which utilise phosphorus atoms as their main donating groups, there are significantly less reports in conjunction with the utilisation of nitrogen and sulfur. Most of them report back to the works of van Koten in the 1980s and 1990s, although a slight increase in reported works in the last few year has to be noted. Both elements exhibit very different donating properties and in doing so they enable a wide variety of binding modes to a metal atom. This allows for a variety of new coordination geometries and therefore the possibility to stabilise metal centres in more unusual oxidation states.

In the course of this thesis new pathways to prepare base metal (i.e. Ti, Cr, Fe, Co) NCN pincer complexes and further base metal (i.e. Co, Ni) SCS pincer complexes were investigated. Further their reactivity towards gaseous ligands (CO, NO) was exploited.

The isolated compounds were characterized by the means of single crystal X-ray diffraction, EPR-, IR-, NMR- spectroscopy (for paramagnetic compounds via the utilisation of the Evans method) and studied computationally by the means of DFT.

Kurzfassung

Der Untersuchung von Pincerliganden und ihren Übergangsmetallkomplexen wurde in den letzten Jahren große Aufmerksamkeit geschenkt. Da sich ihr molekulares Gerüst leicht verändern lässt, bieten sie eine große Variabilität und eine reichhaltige Chemie. Obwohl es zahlreiche Arbeiten gibt, die sich mit der Herstellung von Pincerkomplexen mit Liganden befassen, die Phosphoratome als Hauptdonorgruppen verwenden, gibt es deutlich weniger Berichte in Verbindung mit der Verwendung von Stickstoff und Schwefel. Die meisten von ihnen gehen auf die Arbeiten von van Koten in den 1980er und 1990er Jahren zurück, wenngleich in den letzten Jahren ein leichter Anstieg der gemeldeten Arbeiten festzustellen ist. Beide Elemente weisen sehr unterschiedliche Donoreigenschaften auf und ermöglichen dadurch eine Vielzahl von Bindungsmodi an ein Metallatom. Dies ermöglicht eine Vielzahl neuer Koordinationsgeometrien und damit die Möglichkeit, Metallzentren in ungewöhnlicheren Oxidationszuständen zu stabilisieren.

Im Rahmen dieser Arbeit wurden neue Wege zur Herstellung von NCN-Pincerkomplexen für unedle Metalle (z. B. Ti, Cr, Fe, Co) und weiteren SCS-Pincerkomplexen für unedle Metalle (z. B. Co, Ni) untersucht. Außerdem wurde ihre Reaktivität gegenüber gasförmigen Liganden (CO, NO) untersucht.

Die isolierten Verbindungen wurden mittels Einkristall-Röntgenbeugung, EPR-, IR- und NMR-Spektroskopie (bei paramagnetischen Verbindungen unter Verwendung der Evans-Methode) charakterisiert und mit Hilfe von Computerbasierten Methoden wie DFT rechnerisch untersucht.

List of Abbreviations

NBS N-bromosuccinimide

AIBN 2,2-Azobis(2-methylpropionitrile)

MeOH methanol

NaOH sodium hydroxide

Na_2SO_4 sodium sulfate

EtOH ethanol

NMR nuclear magnetic resonance

TEA triethylamine

HBr hydrobromic acid

IR infra red

Mes 1,3,5 trimethylbenzene

DFT density functional theory

CO carbon monoxide

***n*-BuLi** *n*-butyllithium

THF tetrahydrofuran

Å angstrom

PTFE polytetrafluoroethylene

HR-MS high resolution mass spectrometry

HOMO highest occupied molecular orbital

LUMO lowest unoccupied molecular orbital

SOMO single occupied molecular orbital

EPR electron paramagnetic resonance

NaBAr$_4^F$ sodium tetrakis (3,5-(bis(trifluoromethyl)phenyl)borate

PPh$_3$ triphenyl phosphine

py pyridine

Contents

1 Introduction

At a time when society and the environment, indeed the entire ecosystem of the earth, are undergoing tremendous change, every human being has a part to play in preserving this unique jewel to the best of our knowledge and belief. And in such a way that it can also be a home for many future generations. The ways of modern science to achieve such enormous goals are more advanced than ever before in the history of mankind, but there is still a lot to learn on the way to fulfilling this goal. However, we cannot hope that one specific group of scientist will be able to solve the problem alone. Everyone must and can make a small, significant contribution.
The involvement of organometallic chemists in this process, for example, is to develop new catalysts in order to make energy-consuming reactions more economical. One of the prime targets here is the development of a new system for producing ammonia from the elements. Nevertheless, there is still an almost innumerable amount of reactions that can still be improved today. Another aspect is the attempt to replace already established systems based on precious metals, which are time and energy consuming to produce, with metals that are much more abundant in the earth's crust and thus make production easier.

The process of catalysis is best described as the acceleration of a chemical reaction with the help of an additional substance, the so called catalyst. The catalyst is a substance or material, which increases the rate of reaction, by lowering the activation energy of a reaction. The process of catalysis does not change the overall thermodynamics of a given reaction. Therefore, the catalyst achieves its function by providing alternative reaction pathways during the reaction.[1,2]

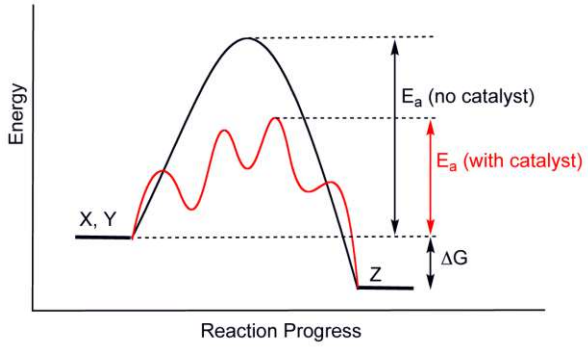

Figure 1.1: Visual depiction of Energy vs. reaction progress[1,2]

The field of catalysis is subdivided in two main categories: homogeneous and heterogeneous catalysis. The main difference between the two is the way in which the reaction is carried out. Whereas in homogeneous catalysis the catalyst and substrate are present in the same phase, for example both in liquid phase, dissolved in a solvent, in heterogeneous catalysis the substrate and catalyst are in different phases.
The main distinctions in property can be made in the fields of activity, selectivity, turnover, and required reaction conditions. Homogeneous catalysts normally work at much lower temperatures, often close to ambient conditions, and achieve high selectivities. Despite those advantages, one main problem in this field is catalyst recycling, separation and purification of possible reaction products. In this sense, heterogeneous catalysis has a major advantage, as here catalyst separation is not necessary.[3–5]

If one takes a look at the field of catalysis from an economic point of view, it is a field in which billions of dollars are turned over each year. Chemical industry relies heavily on the use of a catalyst to provide economically lucrative processes. Prominent representatives of homogeneous catalysis are the process of hydroformylation and the production of acetic acid, with the utilization of molecular rhodium catalysts. To name prominent heterogeneous counterparts, the Haber-Bosch- process and the production of nitric-acid, which operate via iron and platinum catalysts, respectively, must be listed here.[3–5]
Due to the wide applicability of precious metals such as platinum group elements, rhodium ruthenium and others in a variety of industrial processes, and the simultaneous low availability of these elements in the earth's crust, the application of these elements can lead to a risk of supply. (*cf.* Figure 1.2, red box[6])
The rise in global population and increasing technological development are accelerating this trend.[7,8] Therefore it is of increasing interest, to find alternatives which do not pose such risks of shortages in the next decades. Such alternatives, include, for example, to substitute the noble-metal catalysts, with catalytic systems which utilize elements that are more abundant in the earth's crust.

Figure 1.2: Elements of high economic importance and high supply risk (red bracket) as declared by the European commission[6]

1.1 Pincer chemisty

Since the first synthesis of a PCP pincer complex by *Shaw*[9] in the 1970s and the subsequent definition by *van Koten*[10] in the 1980s, pincer complexes have been a well-established class of compounds in homogeneous catalysis and coordination chemistry. Although the underlying intention of these first syntheses was not to achieve high catalytic activities, metal-catalysed C-H activation is now one of the broadest areas of research in organometallic synthetic chemistry today. A generalized depiction of what to expect from a pincer complex is demonstrated in figure 1.3.

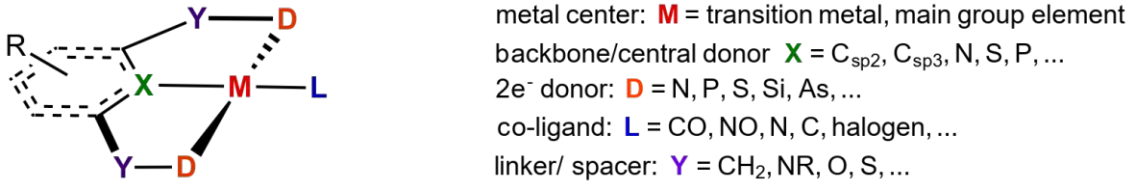

Figure 1.3: generalized schematic framework of a pincer complex

Pincer complexes are a class of compounds, which most commonly contain a transition metal (M) as central atom, ligated by chelating, tridendate ligand frameworks. In recent years there have also been reports, where main group elements have been utilized as central atoms. These ligand frameworks are roughly subdivided into the coordination atom groups depicted as (X) for the central donor, and the two 2-electron donor groups (D). This subdivision is mainly responsible for the naming of the ligand types and is done according to the DXD pattern. Therefore, the thematic focus of this work will be on

complexes with ligand types that have nitrogen and sulphur as their 2-electron donors and carbon as their central donor.

Those 2-electron donors are connected to the ligand backbone via linking groups (Y). This central donor forms a σ-bond towards the metal center. Due to properties of common linking groups, such as CH_2, various amines or oxygen, the resulting ligands are rigid to the extent, that a meridional coordination mode is favoured. Ligands which allow for a facial coordination, are excluded from the definition as pincer.

The great versatility of this generalized framework allows for a wide variety of modifications to fine tune the electronic and steric properties towards the demands, without changing the mode of coordination. Thus, pincer ligands offer to be a mighty instrument in coordination chemistry.

1.2 General considerations on modifiability

When one dissects the individual contributions of the involved groups in the ligand framework, it is clear that the central donor has the main task of forming a stable σ-bond towards the metal center. Here, although other elements have been reported as suitable candidates, nitrogen and carbon are widely utilized.[11–17] This donor influences the complex's properties of exertion of a trans-influence, thus possibly destabilizing co-ligands in *trans*-position to the central donor. The destabilisation can lead to an increase of reactivity of the complex in catalytic transformations.[18,19] Further worth mentioning is the fact that, when X consists of a sp^3 carbon, a shift from meridional coordination to a facial one is possible.[18,20]

Moreover, the choice of the 2-electron donating groups (D) is of great importance for the observed properties of the resulting complex. Over the last few years, phosphorus has proven to be one of the most versatile donors, as its steric and electronic properties can be modified separately from each other. *Tolman* and coworkers have done considerable preliminary work in this area, so that the σ-donor and possible back-donation properties of phosphine-donors are now widely known. The fact that phosphorous has a monoisotopic nucleus (i.e. ^{31}P) with spin 1/2 makes routine analysis via phosphorus ^{31}P-NMR much more convenient.[18,21,22]

When considering nitrogen as a donating group, distinctions in the resulting properties in comparison to those of phosphorus have been made. Nitrogen is classified as a hard Lewis base capable of lone pair donation to form coordinative bonds to a central atom. Moreover, the lack of ability to accept back donation, reduces the suitability as a donor candidate for low-valent transition-metals. However, caused by this hard σ- donation, it has been reported, that nitrogen bearing ligands can stabilize transition metals in higher formal oxidation states.[10,23]

Another significant discrepancy can be seen in the sterics of the systems obtained. Here the cone angle θ is substantially higher in amine-donor-groups, therefore the steric demand of these groups is drastically increased in comparison to analogous phosphine systems.[18,22,24]

Regarding sulphur, it should be mentioned that it has the most versatile donor/ acceptor properties of all three donor systems mentioned so far. Sulphur can act as weaker σ- donor, as moderate π-acceptor and even π-donor ligand. When compared to phosphorus, where bulky ancillary ligands are required to achieve a certain degree of air-stability, sulphur can accept a multitude of hard and soft ancillary ligands without any considerable changes in its stability. Furthermore, it has been shown that sulphur bearing ligand systems allow for the preparation of a multitude of ionic and neutral compounds, as well as bridged systems.[25–29]

Concluding the main building blocks of a pincer ligand, the linking groups (Y) can also play substantial roles in ligand design. Their main objective is the connection of the donating groups onto the ligand backbone, but can further introduce and regulate the electronic and steric properties of the system. Especially when utilizing phosphine donors, the linking groups can drastically change the ligand's electronic properties, when a CH_2 group gets substituted for an oxygen atom.[30–35] Furthermore, the linking groups are a great way to introduce chirality into the ligand system, although ancillary ligands on the donating moieties are also suitable locations for such a transformation.[36–39]

1.2.1 Complex Formation

Despite the favourable properties of a carbon-atom as a central donor, the formation of stable σ carbon-metal bonds is one major obstacle to overcome en route to the synthesis of stable pincer complexes. This can be mainly attributed to the high stability of the C-H bond of the carbon atom on the *ipso*-position. Three methods have become established for successfully accomplishing this task.

Direct C-H Activation

Noble metals have been reported to directly activate the C-H bond and establish stable σ-bonds to the *ipso*-carbon. Although nickel is reportedly the only metal from the first row of transition metals capable of undergoing direct C-H activation pathways,[40] the outcome is also dependent on the utilized ligand framework, as reports with palladium show. When comparing the results of *Venanzi*[41] to those of *van Koten*,[42] the PCP ligand is capable of forming the desired PCP complex, whereas the NCN ligands used by *van Koten* formed bimetallic bidendate complex, making it clear that the type of ligand takes great influence in the products obtained.

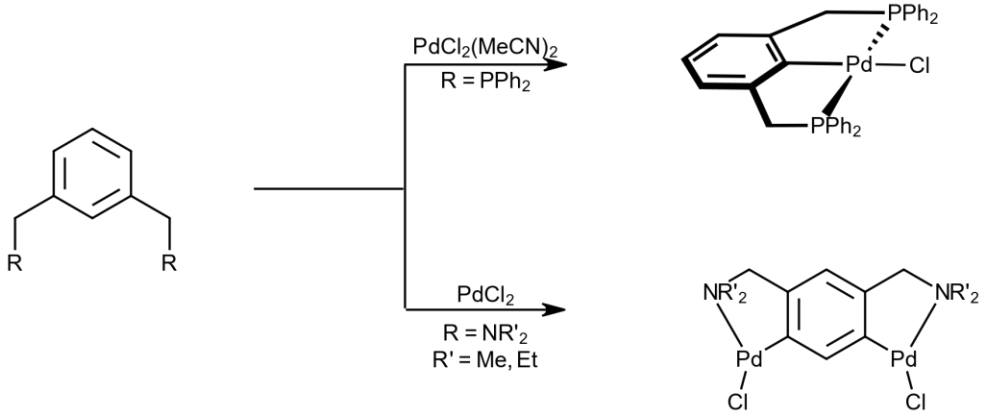

Figure 1.4: Product variety in direct C-H activation

However, the obstacle of product selectivity can be circumvented by the introduction of directing groups. Therefore, a substitution on the *ipso*-position with halogen, silyl or stannyl moieties have proved to be successful routes towards pincer-like coordination patterns. In the case of such a substitution, the term direct C-H activation is no longer applicable.

Oxidative Addition

Another method of σ-bond formation is the so called oxidative addition. Mechanistically, it follows a σ donation of the C-H bond towards a vacant metal orbital, creating a agostic-bond. This agostic bond formation is then followed by backdonation of a populated metal orbital towards an anti-bonding σ^* orbital of the partaking C-H bond. The result of this method is largely determined by the amount of electron density returned, so that if it is not sufficient, the reaction does not proceed beyond this agostic state In this case, the complex featuring a two-electron three-center bond, is thermodynamically favored and is therefore isolatable. In the case of sufficient backdonation, the bond is cleaved and the metal undergoes a formal oxidation. However, this mechanism is not exclusively limited to C-H bonds. Substituted bonds can also form reactions in compliance with this mechanism.

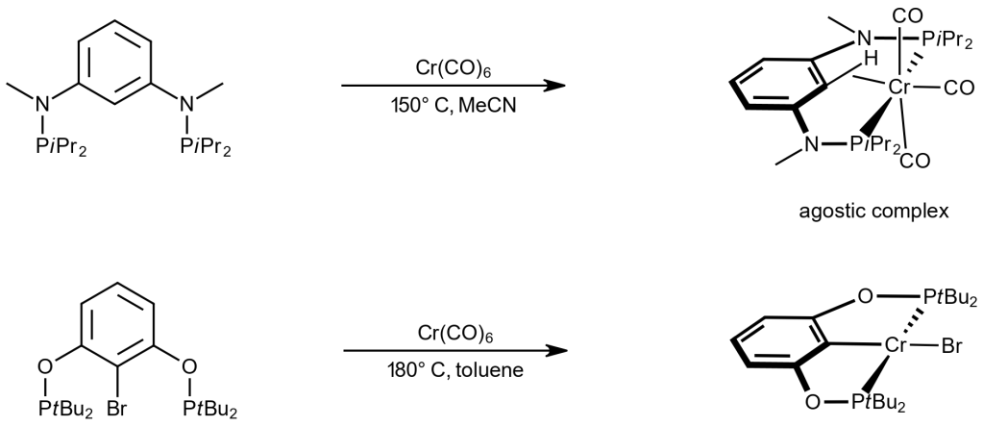

Figure 1.5: Various reaction products of the oxidative addition approach[34,43]

As it was demonstrated numerous times by the *Kirchner* group and others,[44] a substitution of the *ipso*-C-H bond with halogen atoms, as well as higher reaction temperatures increase the probability of success of this method.[30–35,43] Furthermore, this method is preferably successful with low-valent transition metals, which are capable of a change in formal oxidation state by +2. Therefore, the likelihood of a successful oxidative addition increases from chromium towards nickel. (*cf* Figure 1.6)

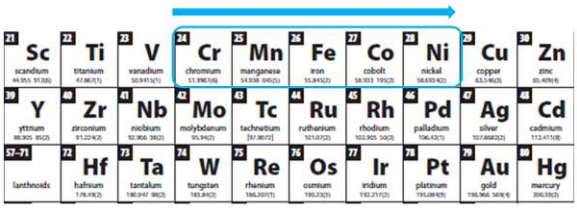

Figure 1.6: Selected part of the periodic table, with the trend of readiness to undergo an oxidative addition highlighted

Transmetallation

This method relies, in principle, on the capabilities of strong bases to deprotonate the *ipso*-position on the ligand. In most cases, *n*-BuLi is used to serve this purpose, creating a lithium-ligand salt in the process. When a metal salt is now reacted with the lithium species, a lithium salt is eliminated, and a metal-ligand σ-bond is formed.

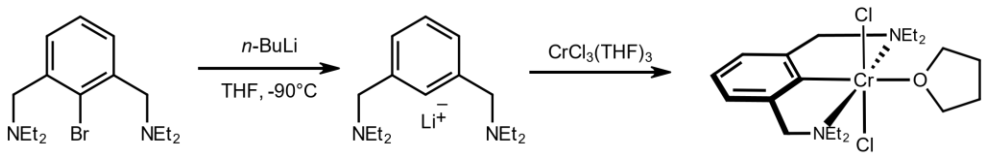

Figure 1.7: exemplary transmetallation protocol, subject to this thesis

Unfortunately, due to the low acidity of aromatic C-H bonds, this position has to be substituted, eg. with bromine, in most cases. The formed lithium salts can then be separated from the desired product. Due to the reactivity of the lithium reagents used, these types of reactions are usually carried out under low temperatures. Normally, an atmosphere of protective gases, like argon, is used.

1.3 Aim of this thesis

The *Kirchner*-group has been successful in the past years with the introduction of new, and quite efficient catalyst systems for homogeneously catalysed reactions. These earlier works featured neutral ligand systems, mainly utilizing a PNP ligand system. Two noteable examples are iron PNP hydrides (*cf.* Figure 1.8), which showed remarkable activities and selectivities in hydrogenation reactions.[45,46] Further works include monoanionic PCP systems, which could be successfully implemented in catalytic hydrosilylation and hydroboration reactions.[34,47]

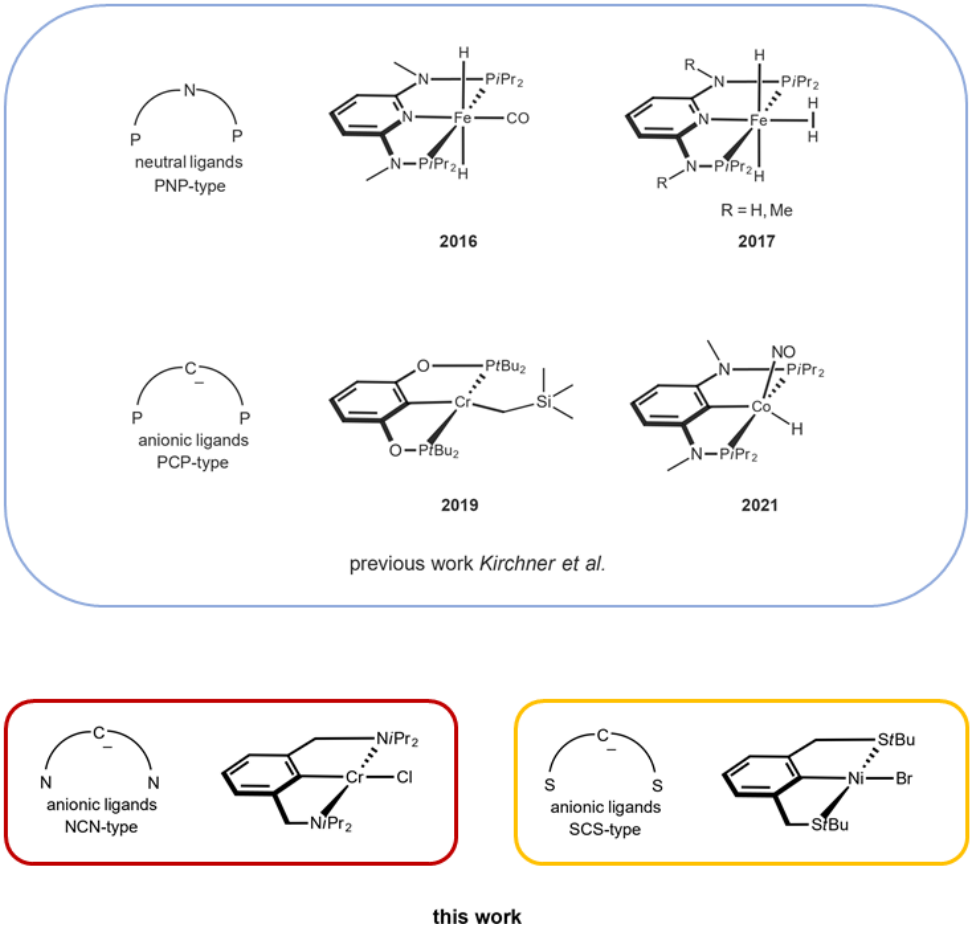

Figure 1.8: Aim of this work.

The goal of this work was to expand the group's capabilities towards ligand systems featuring drastically altered donor groups such as NCN and SCS pincer ligands. The resulting variation in electronic and steric properties should lead the way towards new complexes in possibly unprecedented oxidation states. The development of synthetic strategies towards those complexes, modifications and the evaluation of possible catalytic potentials complete the aim of this work.

1.4 Spectroscopic Methods

A ubiquitous problem behind the analysis of a variety of transition metal complexes is the fact that many of these compounds have unpaired electrons. These unpaired electrons result in these complexes being paramagnetic, and are therefore open shell systems. If one tries to use NMR spectroscopy, which is widely established in organic and organometallic chemistry, with these systems, this leads to spectra that are not trivial to analyse and to broad and poorly resolved spectra. For this reason, two further possibilities are presented here to analyse these compounds promptly.

1.4.1 Evans Method

The method first published by *Evans* in 1959,[48] turns out to be a very simple way of obtaining the magnetic susceptibility using commercially available NMR spectrometers. The chemical shift of a reference material, is compared with the chemical shift of this reference material in which a paramagnetic substance is dissolved. Practically, this can be achieved via a co-axial setup, with a capillary inside an outer Evans-tube.

$$\chi_g = \frac{3\Delta f}{2\pi f m} + \chi_0 + \frac{\chi_0(d_0 - d_s)}{m} \tag{1.1}$$

where:

χ_g = mass susceptibility of the solute (cm^3/g)
Δf = observed frequency shift of reference resonance (Hz)
f = spectrometer frequency (Hz)
χ_0 = mass susceptibility of the solvent (cm^3/g)
m = concentration of the sample (g/cm^3)
d_0 = density of solvent (g/cm^3)
d_s = density of the solution (g/cm^3)

When now applying equation 1.1 , one can directly calculate the susceptibility of the sample, from which conclusions can be drawn about the number of unpaired electrons in a system. Here, the mass susceptibility has to be converted into the molar susceptibility, which has to be further corrected by the contribution of the diamagnetic moment. With this effective magnetic moment, the amount of unpaired electrons can be calculated.

$$\mu_{eff} = 2.8\sqrt{\chi_g T} \tag{1.2}$$

where:

μ_{eff} = effective magnetic moment (μ_B)
μ_B = Bohr's magneton

Important to note is, that by increasing the spectrometer frequency and/or increasing the concentration of the sample, the recorded chemical shift difference will also increase. This allows for accurate estimates, even with low sample loadings. Furthermore, it must be

noted, that the measurement is temperature-dependent to a certain degree. With some solutions, this can lead to significant volumetric changes, which then leads to inaccuracies for obvious reasons.[48–50]

1.4.2 EPR-Spectroscopy

Electron paramagnetic resonance (EPR) spectroscopy is a powerful analytical tool which has a wide range of possible applications. These range from obvious use in solid state physics, detection of electrons in organometallic chemistry,[51] towards spin-trapping experiments in biology,[52,53] possible dosimetry experiments in teeth[53] and in cardiology and biological systems.
The method offers numerous possibilities and the individual mechanisms and observed phenomena are correspondingly extensive. Therefore, only the absolute minimum of information for understanding the physical principle is given here. For further information refer to the relevant literature.

In short, molecules featuring one unpaired electron in the SOMO, are prone to EPR analysis. This one unpaired electron with its spin of 1/2 features a magnetic moment, which will align itself, when exposed to an external magnetic field. Due to the Zeeman effect, each alignment has a specific energy whose splitting is directly proportional to the strength of the applied magnetic field. An excited electron can now change its spin by absorbing or emitting a photon, provided the resonance condition is met. This allows to calculate the proportionality factor for a given sample, which can also be cautiously referred to as the fingerprint for paramagnetic-substances.[54]

In the case of EPR spectroscopy, other influences on the g-value are also included, such as the interaction of the unpaired electron under consideration with magnetic nuclei in the vicinity, e.g. nucleus-electron hyperfine couplings (e.g. isotropic fermi contact interaction and anisotropic electron-nucleus dipole interaction) . To conclude this brief insight, it should be mentioned that these interactions are dependent on the orientation of the molecule in the applied magnetic field.[55–57]

1.5 NCN Pincer Complexes in Literature

Some of the first pincer complexes featuring a NCN-type scaffold were published by *van Koten* in the 1980s.[10,58,59] In this early study he reported the geometry of various pincer complexes with platinum, iridium and nickel and further concluded, that a change of the neutral donation moiety leads to a higher electron-density on the metal center and thus increasing its nucleophility. These early compounds where synthesized by the reaction of the lithium derivative of a CH_2-linked NCN ligand with common palladium and platinum precursors.

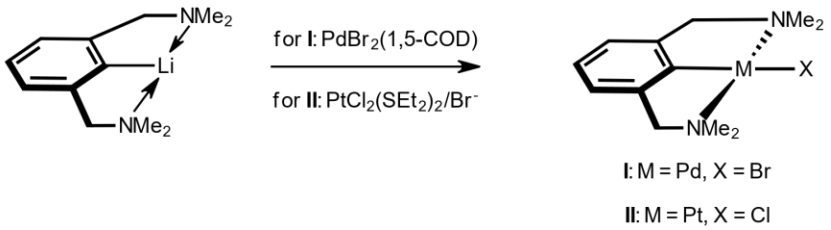

Figure 1.9: First examples of *van Koten's* NCN complexes.[58]

Furthermore, *van Koten* and coworkers described the first NCN complexes featuring cobalt as the central atom. Due to the fact, that it was not possible to crystallize these compounds at the time, they conducted EPR measurements to find further evidence for their proposed structure. They reported patterns in proximity to isoelectronic nickel(III) complexes, which were subject to their earlier studies. Furthermore, they were able to report hyperfine couplings to the ^{59}Co nucleus ($I = 7/2$) and superhyperfine couplings to the ^{14}N nuclei ($I = 1$) of the donating groups.[60]

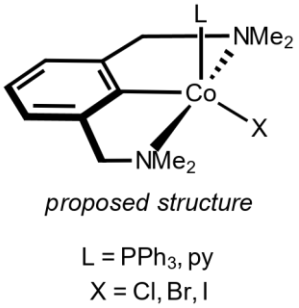

Figure 1.10: Proposed structure of the first NCN cobalt pincer complexes by *van Koten*.[60]

Building on these results, research of the reactivity of these first compounds led to the discovery of, for example, platinum(IV) compounds via oxidative addition reactions. In the following years, the possibility of enabling solid-phase fixation via ligand modifications was also explored.[10,61]

It was further found that the reaction towards **III** also works with Cl_2. Furthermore, the analogon featuring bromine as a halogen co-ligand can also be obtained by the reaction of the bromine-analogue of **II**. Treatement of **II** with the halogen scavenger $AgBF_4$ resulted in the formation of the cationic species **IV**, featuring a water molecule as a neutral co-ligand.[10]

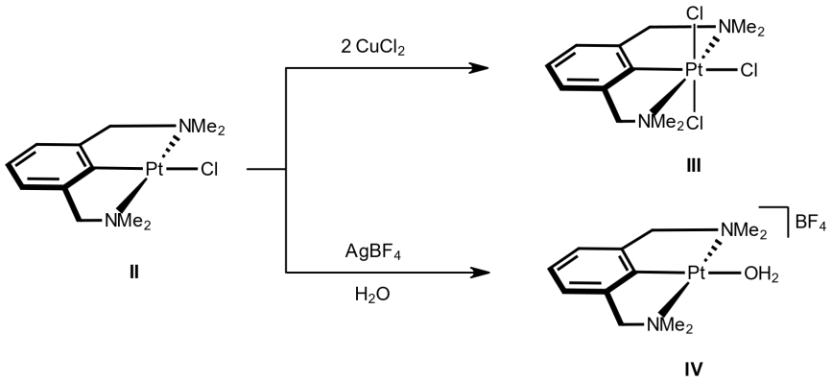

Figure 1.11: Reactivity of NCN platinum complexes

In order to obtain suitable anchor groups on the ligand framework, a number of possibilities were explored. It was found, that due to the remarkable stability of the synthesised palladium and platinum complexes, the functionalisation could also be carried out by strong acids on the final complex, although in moderate yields.[62] Another possibility to introduce functionalisation was the complexation of a ligand, which already featured functional groups on its framework. As a result, it was found that these complexes can be used as catalysts in C-C coupling reactions, as bio-markers and also as selective gas detectors (e.g. for SO_2).[61,62] As research on the topic continued to evolve, implementations of analogues of **I** in catalytic reactions were reported.

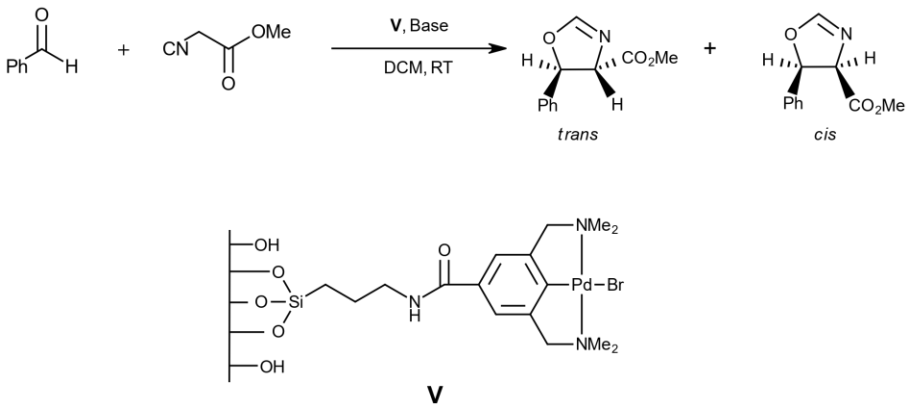

Figure 1.12: Aldol-reaction catalyzed by a silica supported NCN-palladium complex

In 2006 *van Koten* and coworkers reported the catalytic activity of a silica supported NCN

palladium complex towards aldol reactions. After successful optimization, it was possible to isolate the *trans* product in a 50 % selectivity after a reaction time of 3 hours at the given reaction conditions. A increase in catalyst loading from 1 mol% to 2.5 mol% led to a significant increase in overall conversion to 84 %. Throughout all reported experiments, $(i\mathrm{Pr})_2\mathrm{EtN}$ was used as base.[63] Some interesting results have also been published in this field, such as rigid nanosized cartwheel structures of those pincer complexes and their activity as lewis-acid catalysts.[64] Structurally related complexes are also active for Miyaura-Michael reactions and complexes, which are active as catalysts in Friedel-Craft alkylation reactions, have also been discovered.[65,66]

In analogy to the reported palladium and platinum complexes, most reported NCN complexes with nickel can be obtained via similar routes as described for the analogous platinum and palladium counter-parts.[67–70] When it comes to the choice of precursor materials, $\mathrm{Ni(COD)_2}$[67] on the one hand and $\mathrm{NiBr_2(NC\text{-}}i\mathrm{Pr})_n$[69,70]on the other hand have already been published.

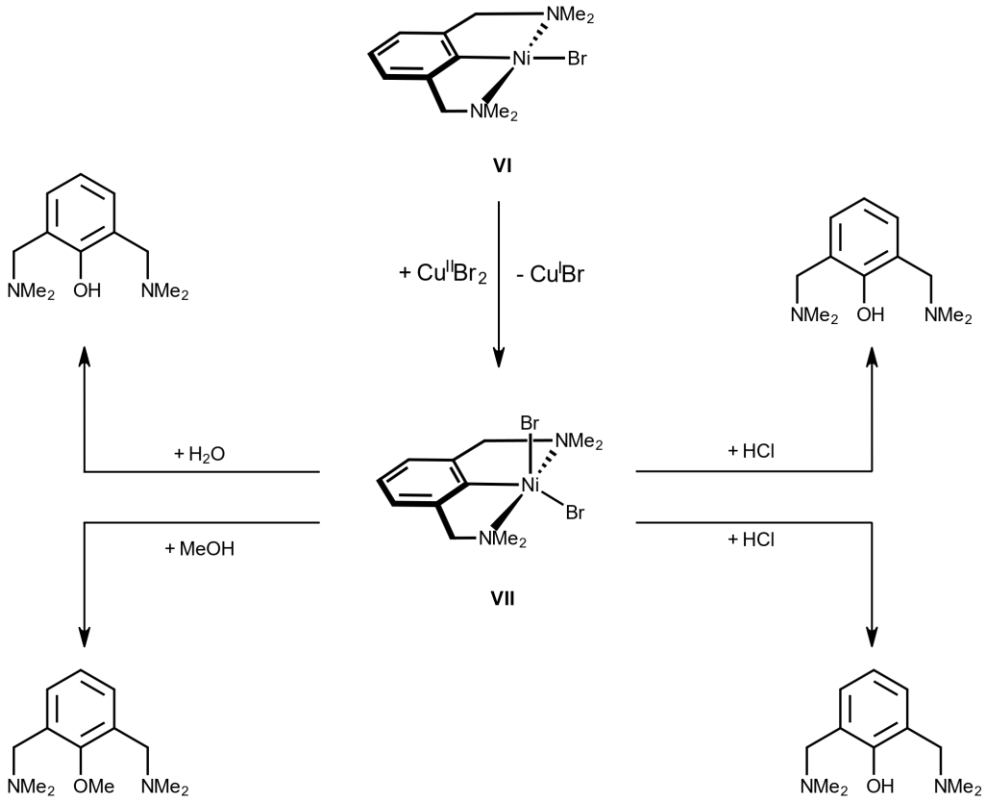

Figure 1.13: Reactivity of reported NCN-Nickel pincer complexes.[69]

In 2018 *Zagarian* and coworkers reported that, one can achieve a direct heterofunctionalization via nickel(III) complexes like **VII**.[69] **VI** is accessible via several routes known from literature.

The oxidation to the nickel(III) species **VII** was achieved via the reaction of **VI** with $CuBr_2$. It has to be mentioned here, that **VII** is also accessible through the reaction with elemental bromine (Br_2). The reaction with the chlorine or iodine analogues of **VI** to the corresponding analogues of **VII**, can also be achieved with $CuCl_2$ and CuI_2 or with the elemental halogens (Cl_2, I_2).[68]

It was found, that if **VII** is treated with Brönsted acids like HCl, a halofunctionalization of the ligand takes place. This heterofunctionalization also takes place if **VII** is reacted with aliphatic alcohols, water or ammonia, resulting in the formation of the functionalized ligand framework. The results of this publication are in good agreement with results previously observed in research on the reactivity of structurally related NCN nickel complexes. The difference between the complexes used is that here tertiary-amine functionalities were used, whereas pyrazole-based functionalities were used as nitrogen donors in earlier reports.[71]
In summary, a large number of these reports have agreed that, although unexpected reactivities have been observed, these nickel(III) compounds have shown remarkable stability.

In 2011 *van Koten* and coworkers reported on the synthesis of pincer coomplexes, featuring early transition metals like titanium, vanadium an niobium. They utilized a different approach towards the complexation of these compounds: using a bimetallic orano-gold(I) compound led the way towards the synthesis of those complexes at room temperature.[37]

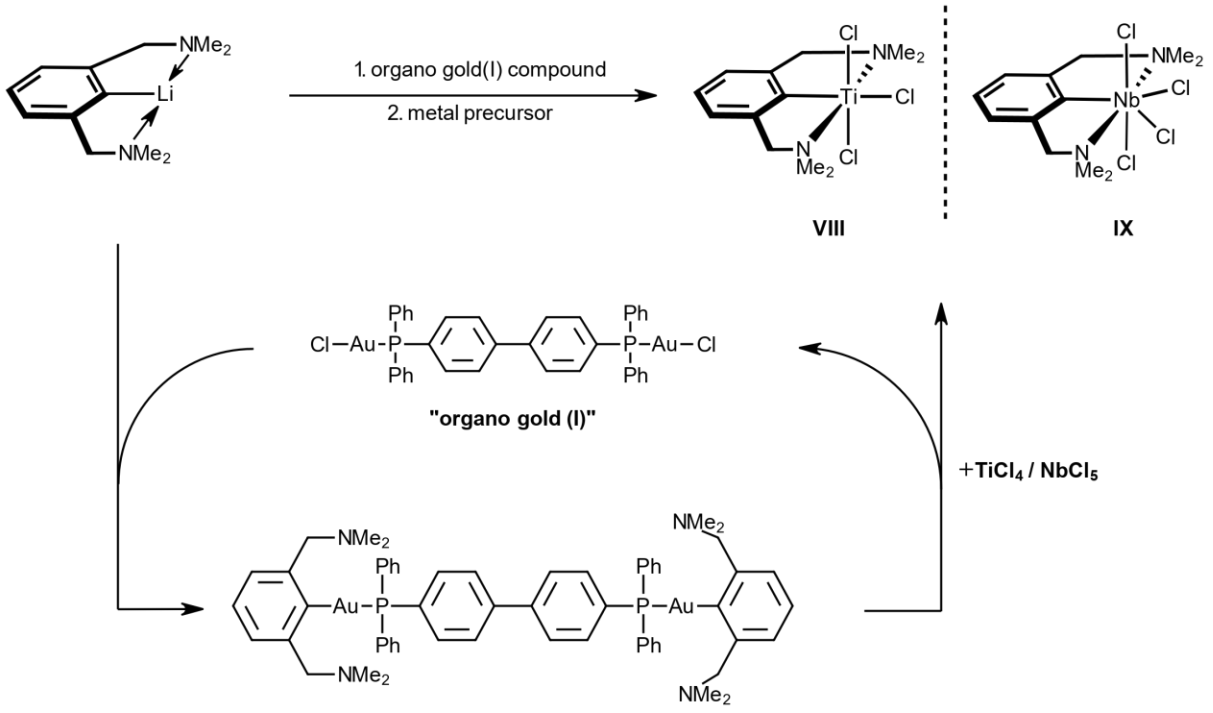

Figure 1.14: Organo-gold(I) transmetalation route.[37]

The insoluble 4,4'-bis[*p*-(chloro gold(I))diphenylphosphino]biphenyl (**organo gold(I)**) can be recovered quantitatively and recycled after the reaction. Interestingly, this method does not work, when using a titanium(III) precursor like $TiCl_3$. Therefore, attempts have been made to obtain the corresponding pincer complex by reacting the lithium species of the NCN ligand directly with $TiCl_3$ in benzene. Unexpectedly, this reaction did not result in the formation of any soluble titanium(III) complex in a desired pincer coordination geometry. Only a rearranged titanium(IV) compound **X**, featuring two ligand moieties bound to the titanium atom could be isolated in 16 % yield.

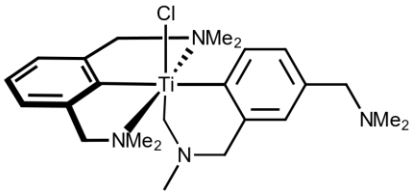

X

Figure 1.15: Titanium(IV) rearrangement-product.[37]

This result is best described by the formation of numerous titanium(II) and titanium(IV) byproducts, which are insoluble in organic solvents, which has been observed before upon reaction with organolithium reagents.[72] To shed light onto the question why this rearrangements takes place, a number of reports have been published in literature. Since this is not a phenomenon specific to titanium, structures involving metals like tantalum, ruthenium and iridium have been published, just to mention a few of them.(*cf.* Figure 1.15)[23,73,74] It was found that, in these compounds, the rearrangement is mostly kinetically driven and therefore irreversibly towards the rearranged product.

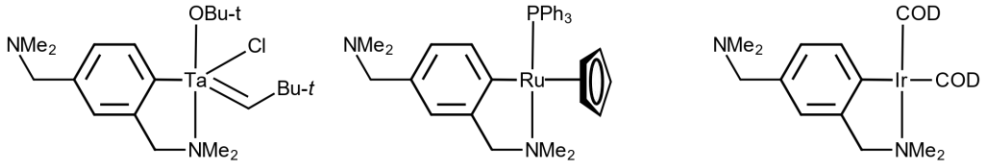

XI **XII** **XIII**

Figure 1.16: Literature known rearrangement-products[23,73,74]

It was found, that when the methodology which was developed for the synthesis of **VIII** and **IX** gets applied to vanadium with the commercially available VCl_4, the disproportionation product **XV** can be isolated. The formation of this vanadium(III) complex has been explained by the simultaneous formation of a vanadium(V) species, which then

decomposes to the halogenated ligand and VCl_3.[37]

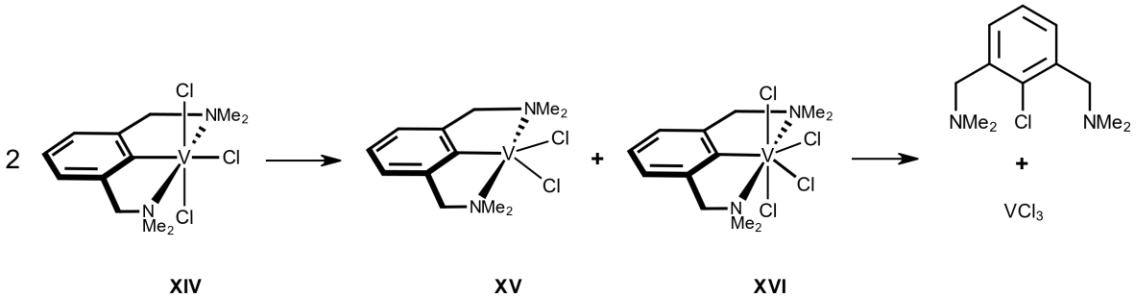

XIV XV XVI

Figure 1.17: Disproportionation of vanadium NCN-pincer complexes[37]

Moreover, complexes **VIII** and **XV** were investigated for their catalytic activity in polymerisation reactions of ethylene. In homogeneous conditions with methylaluminoxane as activator, the activity was low. After immobilisation of the compounds on $MgCl_2$, however, both compounds showed high catalytic activity for the reaction. Furthermore, no inactivation occurred for temperatures up to 70° C, whereby the vanadium complex produced polymers with a higher molecular weight.[37]

When the organo-gold(I) method gets applied to different types of NCN ligands, for example a chiral (S,S)-2,6-Bis(4'-isopropyl-2'-oxazolinyl)phenyl ("**phebox-ligand**") moiety, similar results to those with a non-chiral example like 2,6- bis[(dimethylamino) methyl]phenyllithium were observed. Complexes **XVII** - **XIX** can be obtained by a methodology analogous to that used to obtain **VIII** and **IX**, using $TiCl_3(O\textit{i-Pr})$, VCl_4 and $CrCl_3Py$ as precursor materials, in yields of 75%, 82% and 75% respectively.[38]

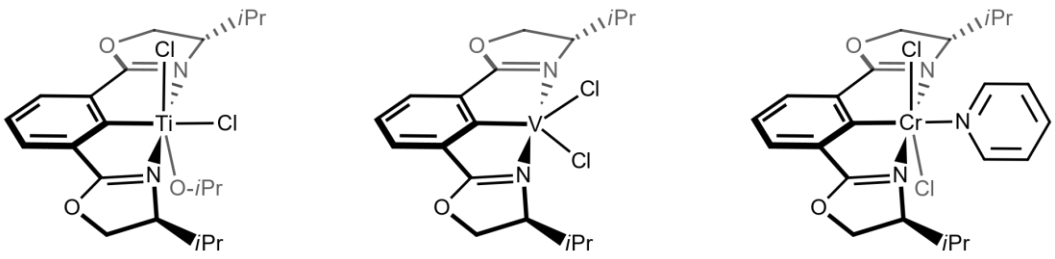

XVII XVIII XIX

Figure 1.18: NCN complexes featuring the "phebox"-ligand[38]

When the organo-gold(I) method is applied to heavier group 4 elements, such as zirconium and hafnium, or heavier group 5 elements such as niobium, chlorine- and oxygen- bridged di-nuclear complexes are obtained. By the reaction of the "phebox"- ligand with $ZrCl_4$, $HfCl_4$ and $NbCl_3O$, the complexes **XX** - **XXII** can be isolated in a 82%, 83% and 76%

yield respectively.

When the compounds **XVII** - **XXII** were tested for their catalytic activity in homogeneous ethylene polymerisation using methylaluminoxane as a co-catalyst, it was found that only **XVIII** showed any noteworthy activity. Due to the low activity and stability of **XVIII** under homogeneous conditions, experiments under heterogeneous conditions were conducted.

Therefore **XVII** and **XVIII** were immobilized on $MgCl_2$. Under these conditions the titanium complex **XVII** showed higher activities than the corresponding vanadium complex **XVIII**. It is worth mentioning, that **XVIII** achieved activities which were about a magnitude higher under heterogeneous conditions, than those achieved under homogeneous conditions.[38]

Throughout their studies, *van Koten* and coworkers revealed, that $MgCl_2$-immobilized vanadium complexes consistently retain a single- center behaviour, which was not the case for the $MgCl_2$-immobilized titanium complexes.

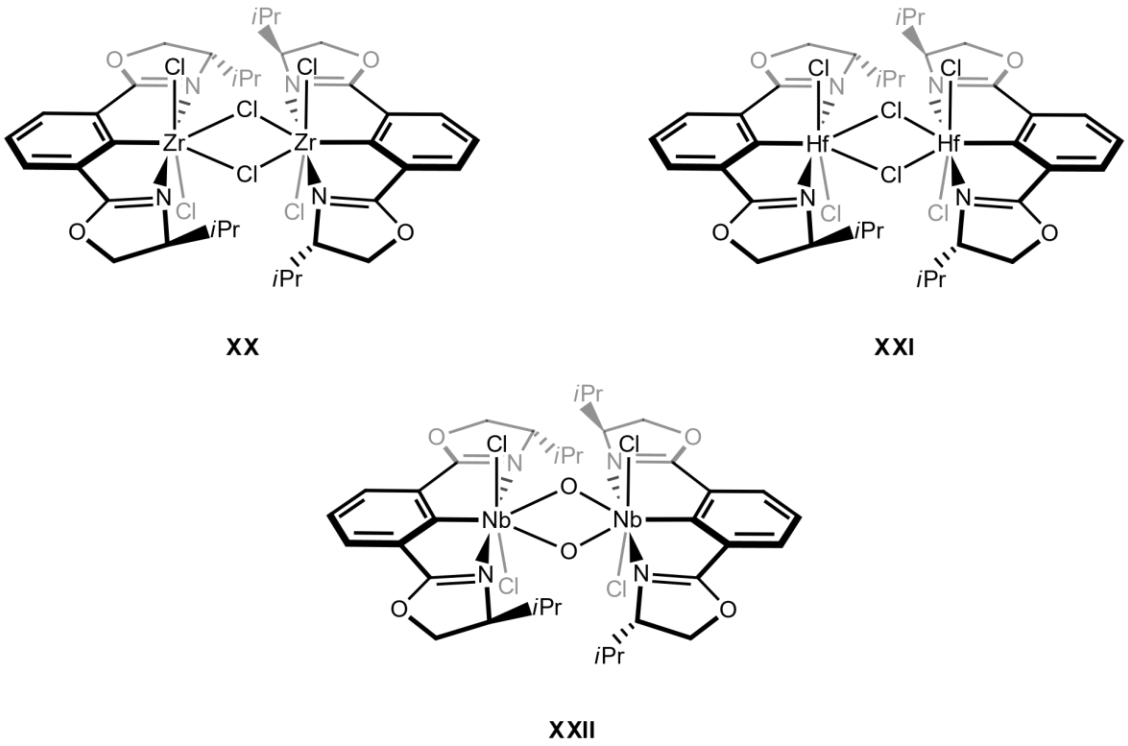

Figure 1.19: Bridged NCN complexes featuring the "phebox"-ligand[38]

In 2010, *Nishiyama* and coworkers investigated the reactivity of phebox-ligands, which were similar to those already described by van Koten, for iron. Therefore, a solution of the corresponding ligands was heated up with $Fe_2(CO)_9$. The resulting complexes showed a remarkable level of stability, so that they even allowed for a purification via silica-gel chromatography.[39]

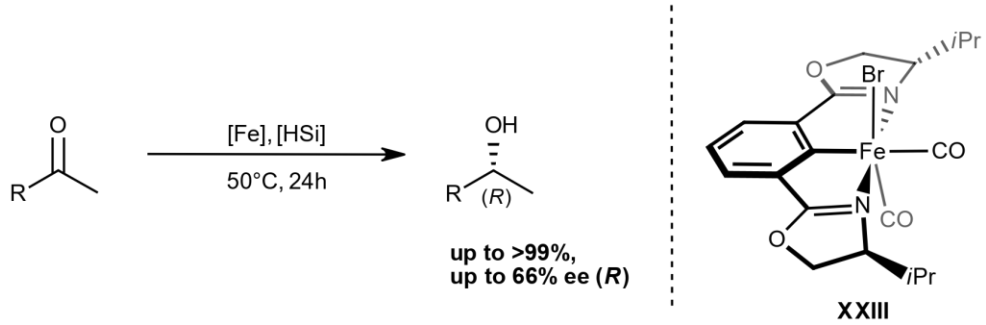

Figure 1.20: Assymetric hydrosilylation of carbonyl-compounds, catalysed by a NCN iron complex[39]

It is therefore worth noting that this iron complex, despite its stability, shows catalytic activity in the chiral hydrosilylation of carbonyl compounds. When **XXIII** is used as a catalyst , with potassium-acetylacetonate as additive and 1.5 equiv. of $HSi(OEt)_2Me$ as hydrogen source, yields up to 99% were achieved with a ee of 66 % towards the (R)-isomer of the corresponding alcohol.

Attempts have been made to foster the catalytic activity in this reaction by the introduction of silyl/stannyl moieties. This was achieved by the complexation of a modified ligand, with $Fe(CO)_5$ as precursor material under UV irradiation. Although it was possible to isolate and characterize the modified complexes, subsequent investigation of the reactivity of **XXIV** towards the asymmetric hydrosilylation of ketones did not lead to the anticipated increase in reactivity and selectivity.

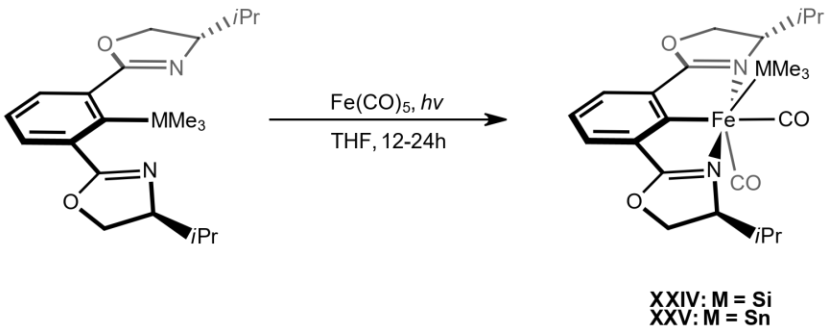

Figure 1.21: Modified iron phebox-NCN complexes[75]

The investigations of *Nishiyama et al.* also included different ligands, where, for most cases, the organic substituents on the positions of the isopropyl moieties (*cf.* Figure 1.21, XXIV) have been varied. The selection of substituents also included benzyl, phenyl and methyl groups, in various combinations. Within these variations, only small margins in obtained yields could be observed. Furthermore, it has been shown, that **XXIII** is prone to ligand substitution reactions. Hence it was possible to illustrate, that the reaction with PMe_2Ph leads to the formation of a cationic complex, which utilizes a bromine atom as counter ion. A cationic complex was also obtained by the reaction of **XXIII** with a tenfold excess of CN*t*-Bu under heating to 50° C.[39,76]

Another interesting result was published in 2013 by *Nishiyama* and coworkers, where they applied the same methodology which was successful for iron towards the complexation of various phebox-type ligands with cobalt. Here it was observed that, under similar conditions, the oxidative addition of cobalt onto the ligand framework remains incomplete, at a cobalt(I) species. The ligands in that case coordinate to the metal center in a κ^2 fashion, with three additional carbonmonoxide co ligands remaining bound to the metal center.[77]

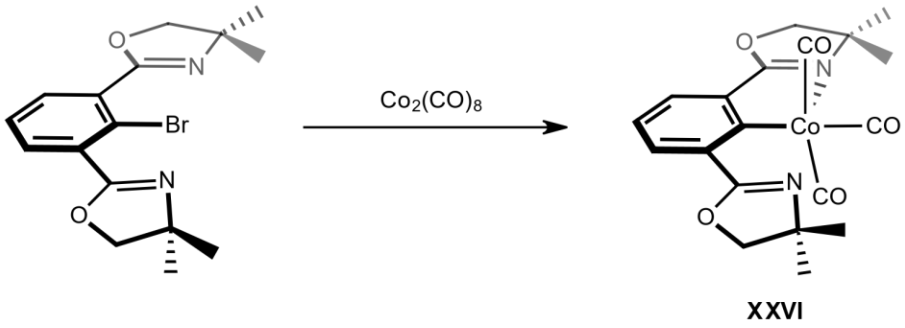

Figure 1.22: Reactivity of selected phebox-type ligand with cobalt[77]

It was only achieved with the subsequent reaction of **XXVI** with iodine, followed by the addition of water, to obtain a complex in a meridional coordination geometry, undergoing a oxidation reaction from cobalt(I) to cobalt (III). Further it was possible to modify complex **XXVII** with CN*t*-Bu to obtain complex **XXVIII**, which does not utilize water as a co-ligand. Moreover, it was possible to obtain a acetate complex by subsequently reacting **XXVII** with 4 equiv. of AgOAc.[77]

Is was also possible to comprehensively study the molecular structure of the complexes **XXVI** to **XXIX**, because crystals of sufficient quality for single-crystal XRD measurements could be obtained for all substances listed above.

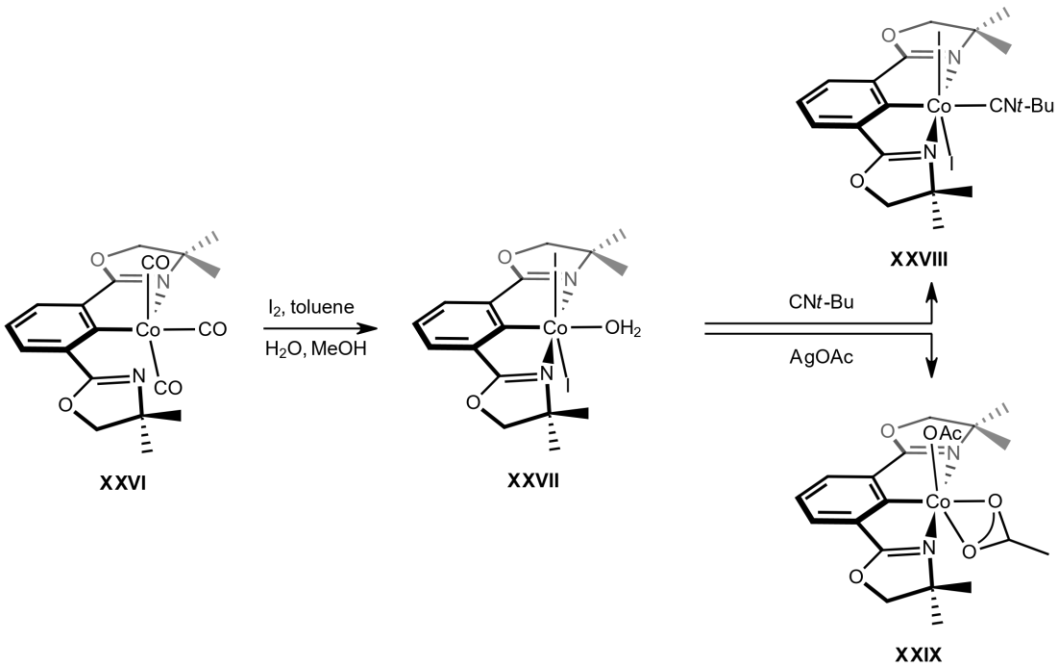

Figure 1.23: Reactions towards modified cobalt phebox-type-NCN complexes[77]

In 2011, *Liu* and coworkers reported the successful synthesis of some of the first known chromium NCN pincer complexes. They used a different set of ligands, featuring imine donating moieties, which differ in the steric demand of the alkyl groups bound to the donating nitrogen. As a result, they reported selectivity controlled by the sterics of the ligands to various reaction products.[78]

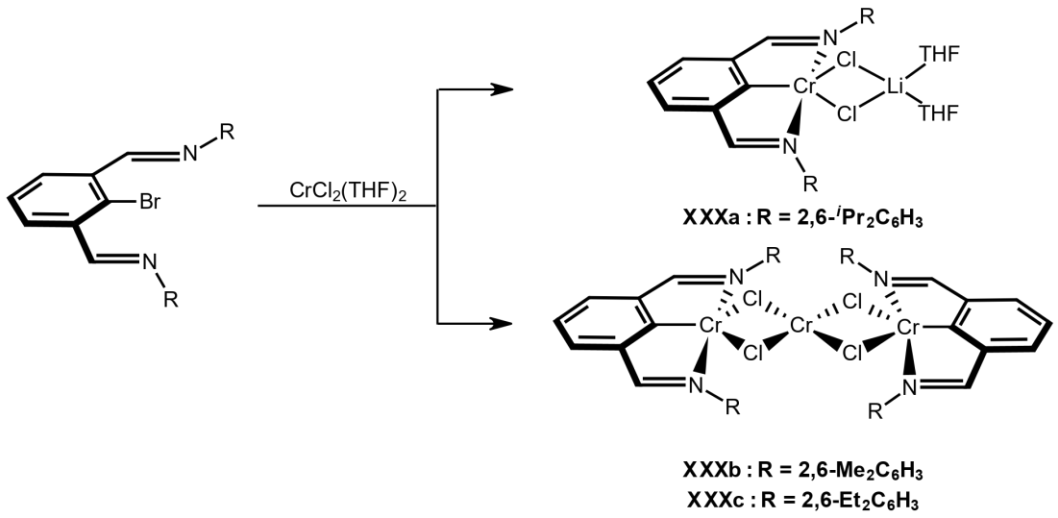

Figure 1.24: Reactions towards NCN chromium(II) complexes[78]

When the ligand with the highest steric demand gets reacted with a chromium(II) precursor, **XXXa** is obtained, where a lithium cation gets stabilized between the chlorine co-ligands and THF solvent molecules. If this reaction is conducted with similar ligands with less sterically demanding substituents, complexes like **XXXb** and **XXXc** can be isolated, where two pincer units are connected via a additional chromium center and bridging chlorine coligands. All complexes reported have shown distorted trigonal pyramidal geometries around their ligand bound chromium central atoms.[78]

When the same set of reactions gets carried out with chromium(III) precursors, no variation in coordination occurs. Complexes **XXXa-c** reportedly all feature the same distorted octahedral coordination geometry to the chromium central atoms.

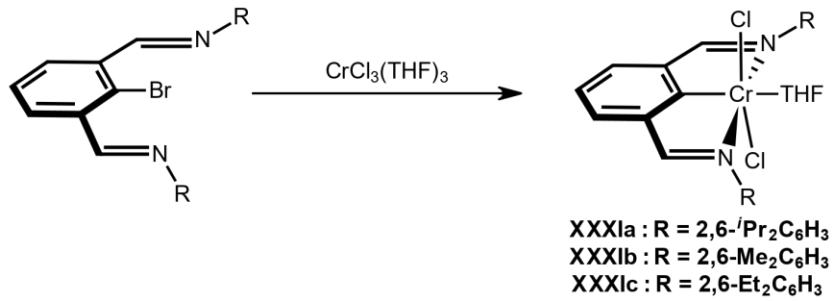

Figure 1.25: Reactions towards NCN chromium(III) complexes[78]

Liu and coworkers then subsequently endeavoured to implement the Cr(II)-complexes **XXXa** to **XXXIc** as catalysts in isoprene polymerisation reactions. They found out, that complexes **XXXa-c** showed no catalytic activity under activation with various trialkylaluminium reagents, various borates or methlyalumnoxane. They explained this result by the fact, that the cation resulting from the activation does not carry an alkyl group and thus cannot continue the polymerisation, although isoprene can coordinate to the metal centre.

The chromium(III) complexes showed the opposite result, with moderate to high activity. Here, the aluminium alkyls used had a significant influence, so that the alkyls with the most sterically demanding properties achieved the highest activities. Furthermore, **XXXIb** showed the highest activity. This was attributed to the fact, that the steric demand of the ligand forms a good average in the shielding of the resulting cation after activation.
Interestingly, when methylaluminoxane gets used as a co-catalyst, the activity of **XXXIb** is decreased drastically. Nevertheless, the selectivity towards the *trans*-1,4- product gets increased substantially, yielding over 90% selectivity towards the *trans* product.[78]

Most recently, in the beginning of 2022, *Aldridge* and coworkers reported the reversible CO_2 uptake into tin-tin and germanium-germanium bonds, which were supported by NCN-typer pincer ligands.[79] It was further found, that the mode of CO_2 insertion is dependent

on the type of the utilized group 14 element.
Their study showed, that dimetallynes like **XXXIIa-b** are able to insert CO_2 fragments, even at low temperatures of -30° C. The mode of insertion however depends, mostly on the size of utilized group 14 element. Furthermore it is possible to isolate the carbonate compounds, when compounds like **XXXIIIa-b** are exposed to harsher conditions under a constant CO_2 atmosphere.

Although, it must be mentioned that the compound featuring germanium (**XXXIIIa**) required substantially higher temperatures to undergo the conversion towards the carbonate species **XXXIVa**.

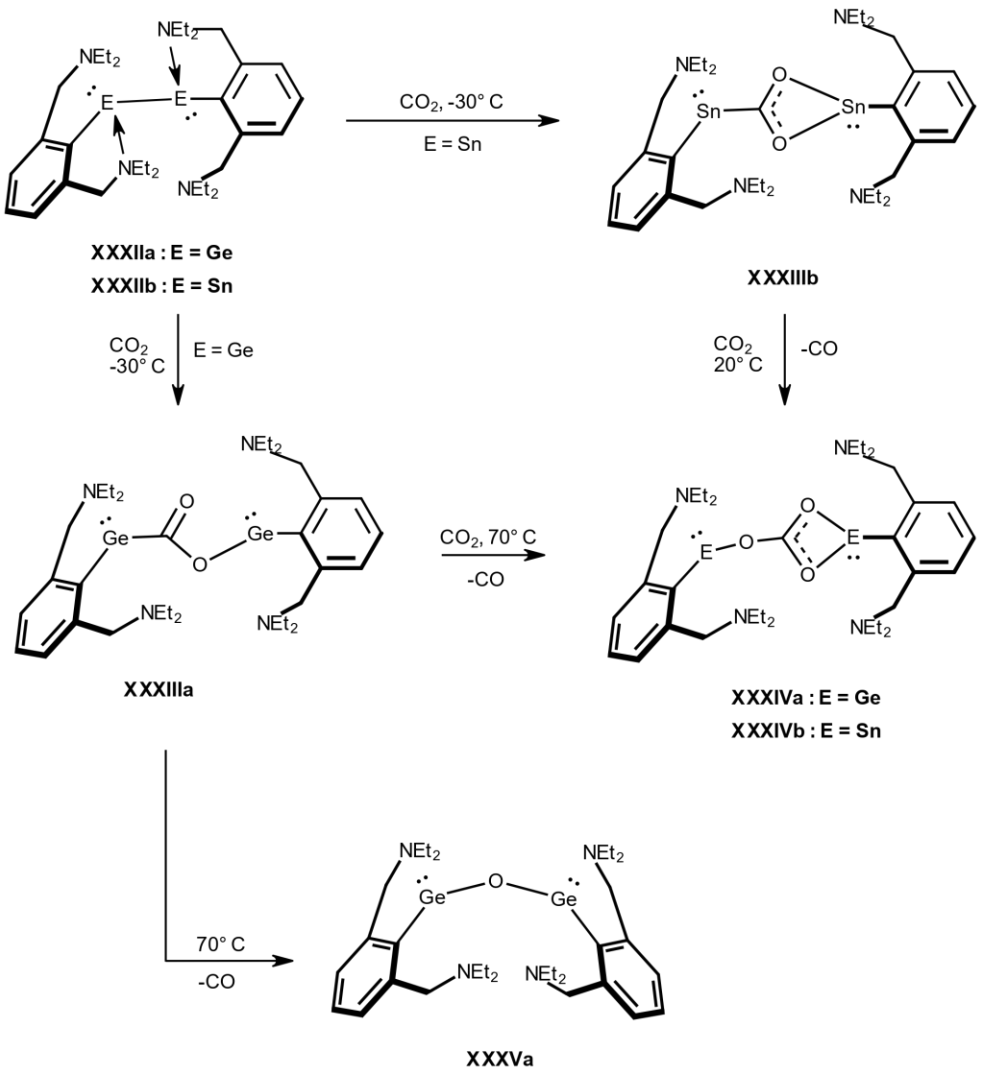

Figure 1.26: Reversible CO_2 uptake of NCN supported complexes[79]

Investigations on the thermal stability concluded their work, with the result, that the

corresponding germanium compounds turned out to be more thermally stable than the corresponding tin analogous, without the presence of additional CO_2. Interestingly, when **XXXIIIa** gets heated up without additional CO_2 being present, the bridged species **XXXVa** gets formed selectively.

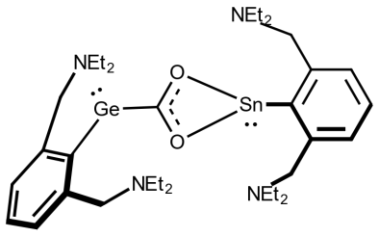

XXXVI

Figure 1.27: NCN complex featuring mixed group 14 elements[79]

In contrast to that, when **XXXIIIb** gets stored without a CO_2 atmosphere, it disintegrates to a 1:1 mixture of **XXXIVb** and **XXXIIb** over the time of several days. This reaction is proposed to feature an intermediate in analogy to **XXXVa**, which then disproportionates to the before described reaction products. Interestingly, when **XXXIIIa** and **XXXIIIb** get combined in a 1:1 mixture, a mixed group 14 NCN complex is formed selectively.

1.6 SCS Pincer Complexes in Literature

The field of SCS pincer systems known from the literature is significantly smaller compared to the amount of NCN systems known from the literature. Here, the published complexes are almost exclusively limited to the representatives of group 10, which have precious metal character, such as palladium and platinum.

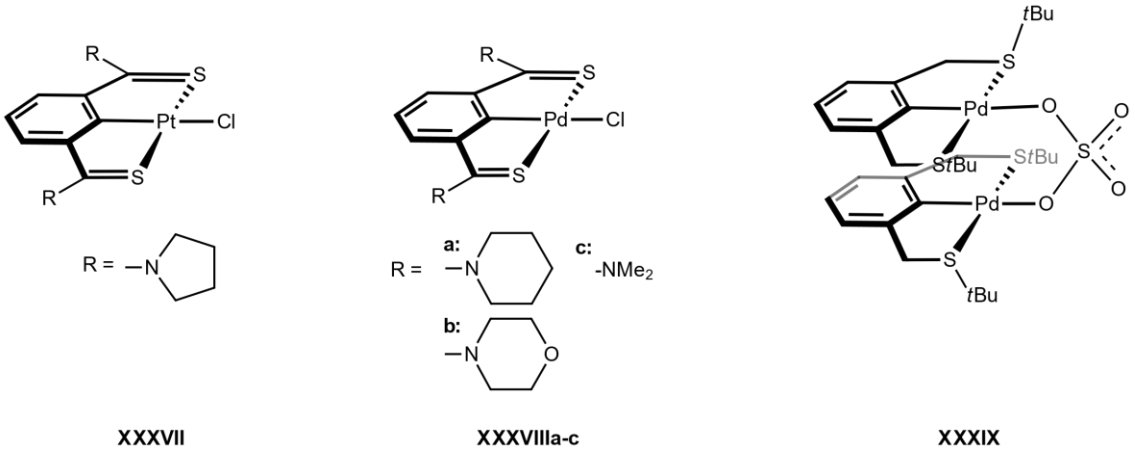

XXXVII **XXXVIIIa-c** **XXXIX**

Figure 1.28: Overview of literature known SCS complexes[80–82]

Whereas compounds like **XXXVII** and **XXXVIIIa-c** (published by *Inoue et al.*[80] and *Yamamoto et al.*[81] respectively) exhibited distinct luminescent behaviour, **XXXIX** was thought to be implemented as a catalyst in Suzuki-Miyaura C-C cross-coupling reactions.[82] The field of luminescent pincer complexes features broad applications, eg. LEDs.[83,84] To this effect, **XXXVII** displays red electroluminesence, and strong emissions in a frozen, glass like state of matter.[80] Furthermore it was reported that **XXXVIIIa-c** also exhibits strong emissions, both in the solid state and in the frozen state. Here, the decay time of the emission allows a classification as phosphorescence.[81]

In regard to the investigation of the catalytic activity of **XXXIX**, it can be concluded, that it performs worse than analogous NCN or PCP complexes, in the investigated cross coupling reactions. One property that can be attributed to most reported SCS platinum and palladium complexes is their remarkable stability to water. In order to increase the solubility of these complexes in water and possibly increase their activity in catalytic reactions, some attempts have been made to modify these complexes in this way. These attempts ranged from embedding these systems in supramolecular assemblies,[85] fixating these complexes on different sugar substrates[86] and embedding them in ambiphilic polymer chains,[87] just to mention a few. Some of the methods chosen achieved their goal and for example, catalyst loadings could be significantly reduced.[87]

In 2008, *van Koten* and coworkers examined the structural properties of SCS based pincer complexes with group 10 metals in more detail. Here the molecular structure of sulfur donating moieties allows for the existence of different orientations of the sulphur bearing alkyl substituents in relation to each other.

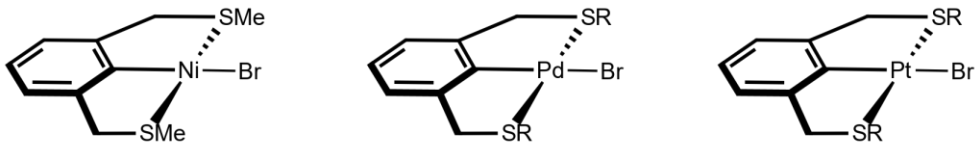

XL **XLIa: R = Me** **XLIb: R = Ph** **XLIIa: R = Me** **XLIIb: R = Ph**

Figure 1.29: Triad of SCS pincer complexes investigated by *van Koten*[88]

They discovered that the palladium complexes, due to the triple-coordinating sulphur, can occur in three different conformers, which also crystallise in solid phase in a single unit cell. These *rac*, *meso* and *assymmetric* conformers of **XLIa** and **XLIb** could be distinguished from each other via ^{1}H-NMR measurements at low temperatures. Furthermore, by utilizing ^{195}Pt-NMR measurements on **XLIIa** and **XLIIb** the ratio of *rac* : *meso* could be directly inferred. Interestingly, **XL** was only found to exist in the *rac*-conformer.[88]

Since it is literature known,[88,89] that further substituents on the ligand framework, can take significant influence on the electronic properties of pincer complexes, *van Koten* and coworkers investigated the effects of different substituents on SCS palladium pincer complexes. In this endeavour, they connected four pincer complex units to a porphyrin cage, and investigated the effects, possible substitutions of co-ligands inside the porphyrin cage might have on the catalytic activity of the SCS palladium complex.(*cf.* Figure 1.29)

They chose the Heck reaction between iodobenzene and styrene as a model reaction. Here it became apparent, that the metalloporphyrin-hybrid, featuring a manganese(III) (*cf.* **XLIII**, Figure 1.22) center exhibited the lowest catalytic activity, whereas the magnesium(II)-porphyrin-pincer-hybrid showed the highest observed activity in this study. They attributed these results to the electron donating properties of the porphyrin moieties. The authors concluded, that the chemical nature of the porphyrin exerts immediate influence on the peripheral palladium pincer complexes.[89]

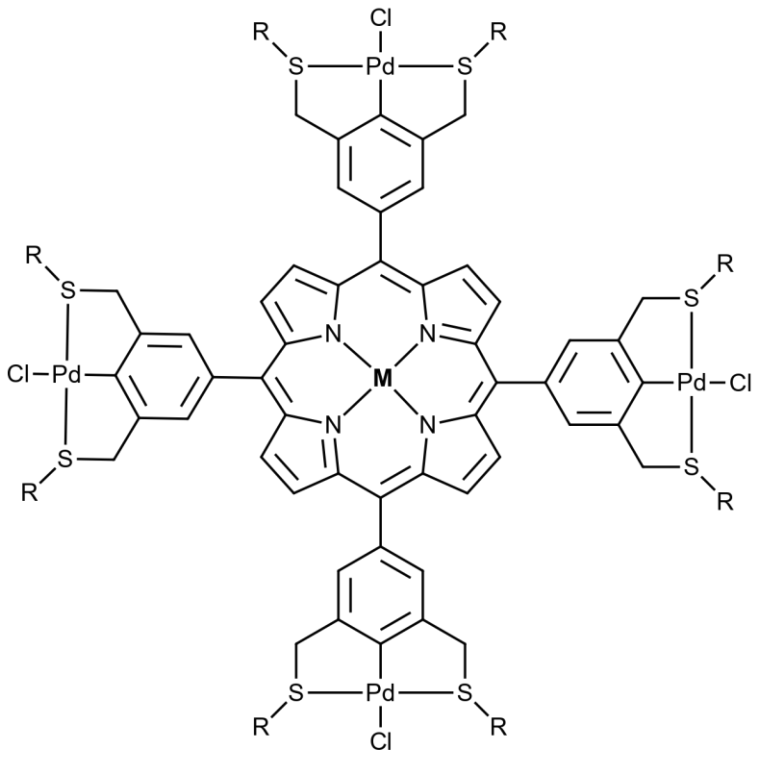

Figure 1.30: Multimetallic SCS-pincer-(metallo)porphyrin hybrid[89]

Unfortunately the observed activities of these hybrid-complexes, did not exceed those of the unsubstituted palladium complexes, like **XLIb**, which disproves the usefulness of such a modification.[89]

In 2010, *Klein Gebbink* and coworkers also published bimetallic SCS palladium complexes. They modified the Pincer complex by η_6 coordination of $Ru(C_5R_5)$ cations (R = H, Me) towards the aromatic framework of the pincer complex. Furthermore, the effect of the modificaiton was tested on the catalytic properties of **XLIVa-b** towards the cross coupling reaction between *trans*-phenylvinylboronic acid and vinylperoxide.

It was found, that the sterically more demanding rest on the cyclopentadiene unit of **XLIVb** slows down the inversion of the isopropyl moieties on the sulfur donors. Furthermore it was found that, both cationic complexes exhibit modest catalytic activity towards the investigated reaction. Additionally, it has to be mentioned, that if the sulphur donors get exchanged for phosphine moieties, no significant catalytic activity can be observed anymore. The authors mostly contributed this phenomenon to the increased steric shielding of the palladium center.[90]

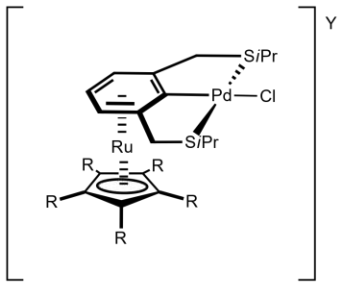

XLIV a : R = H, Y = PF_6
XLIV b : R = Me, Y = BF_4

Figure 1.31: SCS palladium - ruthenium complexes[90]

In 2018, a triad of nickel SCS complexes, coordinated via thioamide groups, was investigated towards their activity against estrogen-responsive human breast cancer cells. To do so, bovine serum albumin as model protein was chosen, due to its proximity to human serum albumin.
Furthermore it exhibits unusual coordination properties. As a result, it was demonstrated that **XLVc** exhibits the strongest coordination towards the bovine serum albumin, mostly attributed to the hydrogen bonding interactions with the hydrogen atoms bound to the amine substituents.[91]

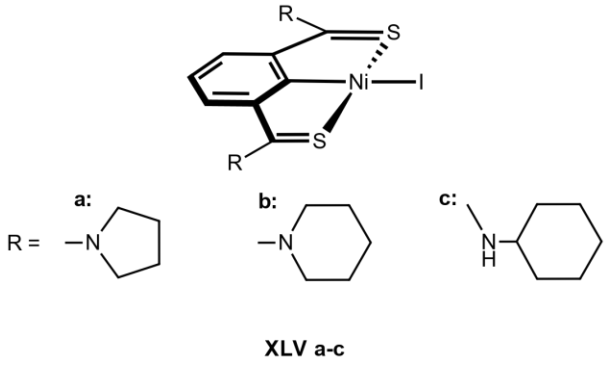

XLV a-c

Figure 1.32: SCS nickel complexes subject to anti cancer studies[91]

The experiments on the anti-cancer activity of the complexes against estrogen-responsive human breast cancer cells showed *in vitro* that, **XLVa** has a higher cytotoxicity and selectivity towards the cancer cells of interest. Therefore **XLVa** was chosen for *in vivo* experiments in female mice with mammary cancer. The group of mice treated with with **XVLa** exhibited augmented greater tumor regression, when compared to the animals of the control group.[91]

In much of society, research means to investigate something you do not know or understand.

Neil Armstrong

2 Results and Discussion

As previously demonstrated by the Kirchner group, halogen bearing xylene derivatives can serve as suitable building blocks for a multitude of different, monoanionic PCP type pincer complexes.[30?] Therefore, this work focuses on the synthesis of NCN type ligands with special attention being paid to their abilities to from stable complexes with early transition metals. Because it was known in advance that base metals, except for nickel, are not able to activate C-H bonds, ligands featuring an *ipso*-halogen were chosen to facilitate cyclometalation. Consequently, 2-bromoxylene was selected as the starting material to obtain the various ligands. Only one example of a ligand without a halogen atom at the *ipso*-carbon was synthesized. This is because it was already shown that tungsten is indeed, despite the general trend, able to activate the C-H bond of the *ipso*-carbon under solvothermal conditions, therefore directly creating a tungsten-hydride species.[92]

2.1 Synthesis of the Ligands

In Figure 2.1 a brief overview of the ligands subject of this thesis is given. These compounds are mostly literature known.[82,93–95] Compound **13** is not literature known to our knowledge.

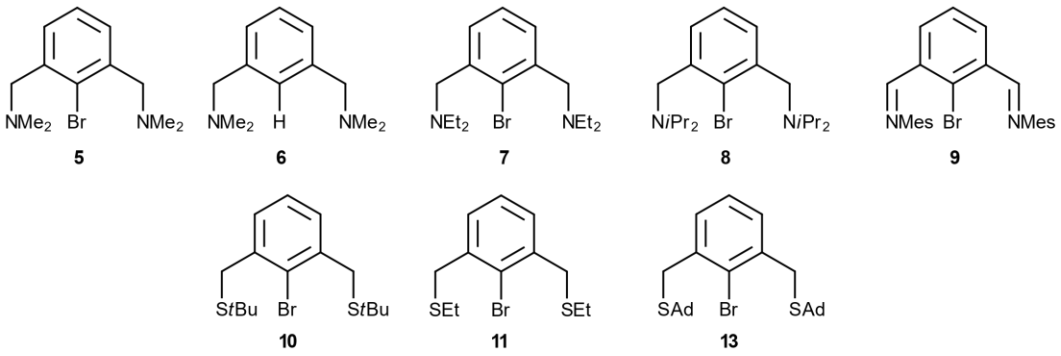

Figure 2.1: Overview of the pincer ligands subject to this thesis.

In order to create the universal building block, from which both, NCN and SCS type ligands could easily be synthesized, 2-bromoxylene was reacted with NBS in presence of AIBN as a radical starter in CCl_4 as solvent. Further it was found that subsequent addition of more radical starter increases the yield substantially. The choice of solvent, despite the environmental concerns, provides an advantage in reaction-workup because of its semi-heterogeneous character. This is due to the fact, that the resulting succinimide is insoluble in this solvent and therefore can be separated easily via filtration. In this case, filtration over a short plug of silica was found to be the best choice. Due to the need for starting materials of formidable purity, and because unreacted 2-bromo-xylene is still soluble in CCl_4, the crude product was recrystallized carefully from *n*-hexanes affording the analytically pure 2-bromo-bis(bromomethyl)xylene **1** as colourless needles. In order to obtain the building block for the NCN ligand **6** featuring an *ipso* C-H bond, this procedure was carried out in analogy, using *m*-xylene as a starting material.

To afford the desired NCN pincer ligands, **1** was reacted with the corresponding amines to undergo a nucleophilic substitution reaction with the benzylic bromides. For the ligands featuring bulkier substituents on the nitrogen donor site i.e. N-ethyl and N-isopropyl, the corresponding amine could be used as internal base, by simply doubling the amount of amine added to the reaction. $HNMe_2$ being a gas, which would impose a multitude of difficulties in reaction handling, the corresponding hydrochloride salt was used. In order to liberate the amine in situ, TEA was added as base. Using the salt as source of the nucleophile also had an impact on the choice of solvent used in this reaction: whereas with the ethyl and isopropyl amines toluene could be used as solvent, chloroform had to be used in order to get hydrochloride salt into solution. After reacting all amines with the building block at room temperature overnight, the crude products underwent standard procedures before the solvents got evaporated in *vacuo*. Purification of the crude products of (2-bromo-

1,3-phenylene)-bis-(N,N-dimethylamine) **5**, 1,1' (1,3-phenylene)-bis-(N,N-dimethylamine) **6** and 1,1' (2-bromo-1,3-phenylene)-bis-(N,N-diethylamine) **7** ligands could be achieved via distillation at reduced pressure, yielding the products as beige to slightly orange-coloured oils. In contrast, the 1,1' (2-bromo-1,3-phenylene)-bis-(N,N-diisopropylamine) ligand (**8**) had to be recrystallized from *n*-hexane, to afford the purified product as slightly orange solid. It was observed, that the discoloration of the ligands could be reduced by carrying out the reactions under an argon atmosphere, although the coloration had no noticeable impact on the recorded ^{1}H-NMR spectra of the products.

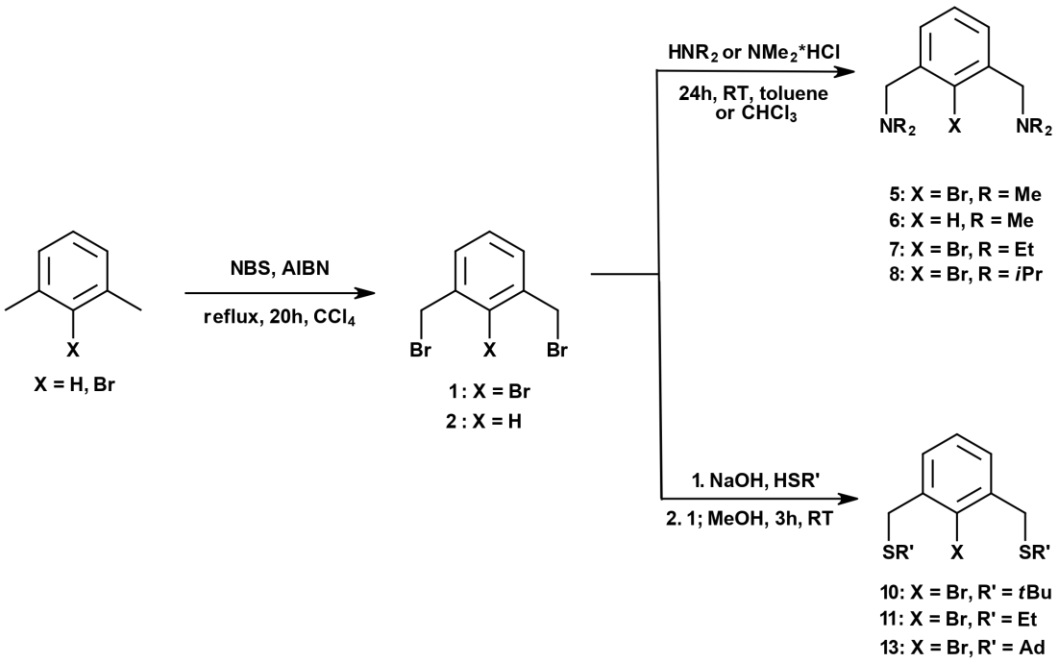

Figure 2.2: Synthesis of NCN and SCS pincer ligands

To obtain the SCS type ligands, first a MeOH solution of NaOH was produced, to which the corresponding thiole was added. During the deprotonation reaction, slight change of color took place, which was used as an indicator for the subsequent addition of the 2-bromo-1,3-bis(bromomethyl)benzene (**1**) to the mixture. After reaction times of up to 4 hours at room-temperature, water and EtOH were added to the mixture, and the crude products extracted into the organic phase. After washing with NaOH, drying over Na_2SO_4 and evaporation of the solvents, the ligands **10**, **11** and **13** could be obtained in sufficient purities to be used in further reactions without any further purification steps. In order to synthesize the SCS-type ligand featuring the unusual adamantane subsitutents on the sulfur donors **13**, the 1-adamanthylthiol **12** had to be prepared according to literature procedures, including slight modifications, beforehand.[96]

First, 1-bromoadamantane and thiourea where suspended in glacial acid and 48% HBr before heating up the mixture to reflux for 4h under an argon atmosphere. After cooling, hydrolysis of the formed isothiouronium salt over night resulted in the formation of the desired product. Isolation of the 1-adamantylthiol **12** as a white solid could be achieved by acidifying the mixture prior to extraction with chloroform, followed by a standard work-up routine.

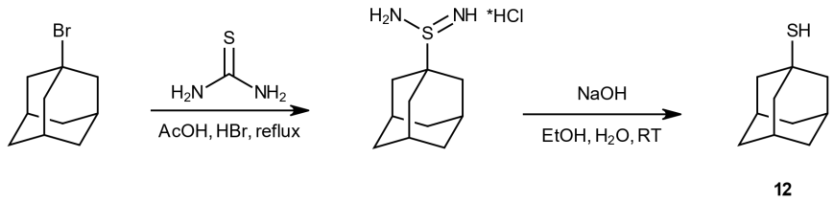

Figure 2.3: Synthesis of 1-adamantanethiol

In order to achieve further flexibility in the donating properties of the nitrogen donor groups, one more ligand was synthesized. Ligand **9** features imine-moieties, which are, in some cases, able to accept back bonding to a certain degree, giving them the ability to stabilize metal-centres in lower oxidation states as well. Furthermore, this donor features non-innocent character.

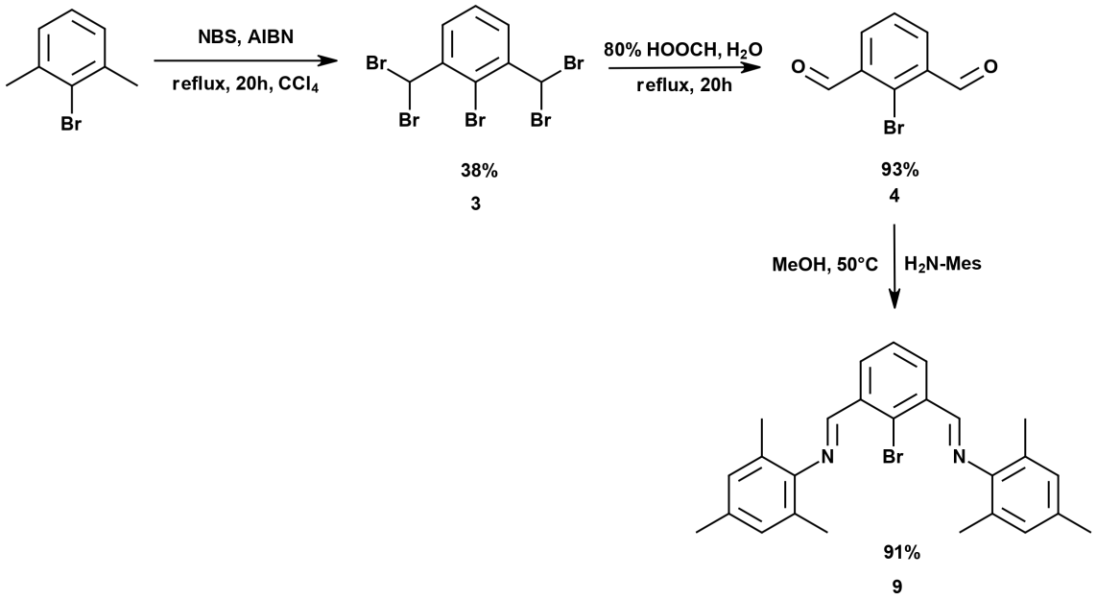

Figure 2.4: Synthesis of the Ligand **9**

Therefore, 1,3-bis(dibromomethyl)benzene **3** was produced in analogy to the previously described 2-bromo-1,3-bis(bromomethyl)benzene **1**, varying the amount of used NBS. After creating the 1,3-bis(dibromomethyl)benzene **3** the crude product was hydrolysed according to literature procedures with slight modifications. A methanolic solution of **4**

was heated up to about 50° C wereafter 2,4,5-trimethylaniline was added slowly. Due to the spontaneous crystallisation of **9**, the product could be easily collected. The product could be obtained as an analytically pure, yellow crystalline powder without any further purification.

2.2 Synthesis of the NCN Pincer Complexes

As demonstrated by *Himmelbauer* and *Eder*,[30–35] reactions of PCP pincer ligands with transition metal carbonyl complexes under solvothermal conditions are a viable option for the formation of the corresponding PCP-Pincer complexes. In some cases, the method was so successful that the complexes could be obtained directly from the reaction solution in qualities suitable for single crystal x-ray diffraction measurements.

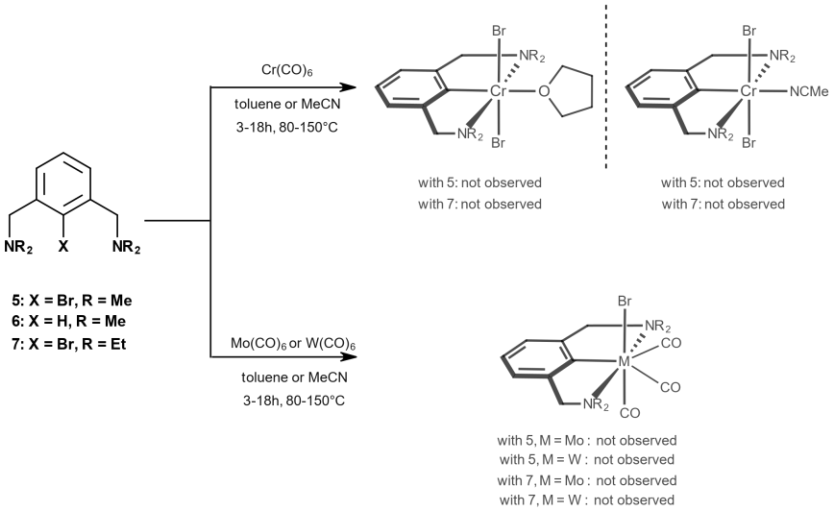

Figure 2.5: Reactions of ligands **5** and **7** with group 6 carbonyl-complexes.

Therefore, first attempts have been made with analogous NCN ligands to investigate, if similar qualities in forming the corresponding complexes could be observed. Various precursor complexes featuring first row transition metals (i.e. $Mn_2(CO)_{10}$, $Fe_2(CO)_9$, $Co_2(CO)_8$, $Cr(CO)_6$, $Mo(CO)_6$, $W(CO)_6$) have been reacted with the synthesized ligands in different solvents, at various reaction temperatures and reaction times. A general overview can be seen in figure 2.5 and 2.6. When reacting the ligands **5** and **7** with group six metal-carbonyl complexes, different results have been obtained when compared to various PCP ligands. In reactions of the NCN ligands with chromium, formation of the direct analogues to the complexes *Himmelbauer*[34] obtained when reacting $Cr(CO)_6$ with his PCP ligands could not be observed.

Due to the fact that the residues obtained were hardly soluble in common solvents, it can be concluded that metallic chromium formed under the conditions. The soluble parts exhibited aromatic frequencies in IR spectroscopy and ^{1}H-NMR analyses confirmed the assumption that unreacted ligand has been recovered. No evidence of the formation of chromium(III) complexes was found. Further, a change in solvent, reaction temperature and prolonging the reaction time had no change in outcome. The same result was obtained when interchanging chromium for molybdenum or tungsten. No evidence of the formation of the seven coordinated species were found in the IR spectrum. Here it was also possible to partially recover the starting materials.

Changing the *ipso* substitution to an hydrogen-atom in ligand **6** no change in reactivity towards molybdenum and tungsten could be observed. Furthermore, no more evidence of the starting materials could be found here during the workup.

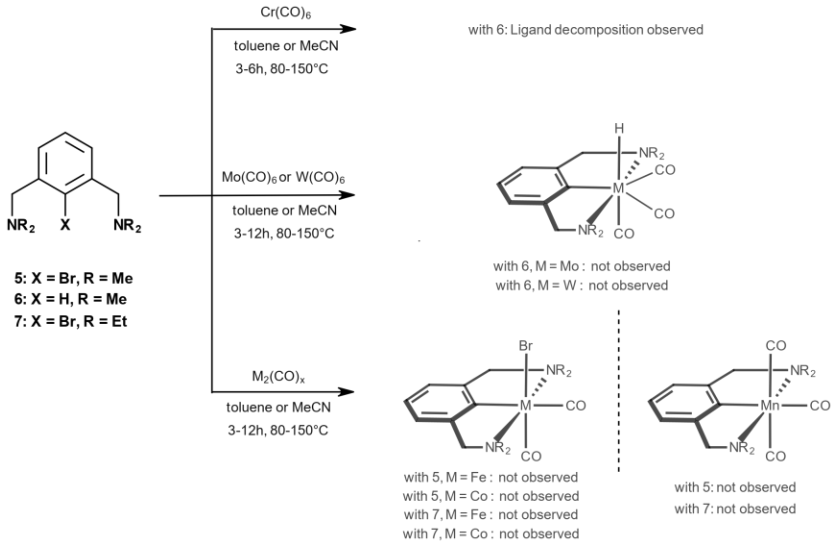

Figure 2.6: Overview of solvothermal reactions with selected NCN pincer ligands.

It can therefore be concluded that ligand **6** is more unstable under these conditions than the analogues **5** and **7** featuring a halogen moiety at the *ipso*-carbon. Attempts to synthesize the desired NCN-analogues of the complexes obtained by *Eder*[30] and *Himmelbauer*[31–33,35] with other first row transition metals were conducted under the similar protocols as before with group 6 metals. Unfortunately, using $Mn_2(CO)_{10}$, $Fe_2(CO)_9$, $Co_2(CO)_8$ did not result in the formation of the desired complexes as shown in Figure 2.6. During the reactions with $Co_2(CO)_8$ formation of a metallic cobalt mirror could be observed on the walls of the reaction vessel. Even slower heating rates resulted in this phenomenon. The reactions with $Fe_2(CO)_9$ led to a change in color of the reaction-mixture towards red. First it was believed, that the reaction vessel had leakage somewhere. But even with repeated implementation, the phenomena persisted. After opening the reaction vessel under argon atmosphere and careful work-up of the residue, no evidence of the formation of the desired species could be found via IR and NMR spectroscopy.

Interestingly, when performing the reactions with $Mn_2(CO)_{10}$, even though no evidence for the complexation with the ligands could be found, all starting materials including the $Mn_2(CO)_{10}$ precursor could be recovered. Unfortunately, no different result was observed when investigating the reactivity of $Fe_2(CO)_9$ and $Mn_2(CO)_{10}$ as precursor material with ligand **9**, and only starting materials could be detected.

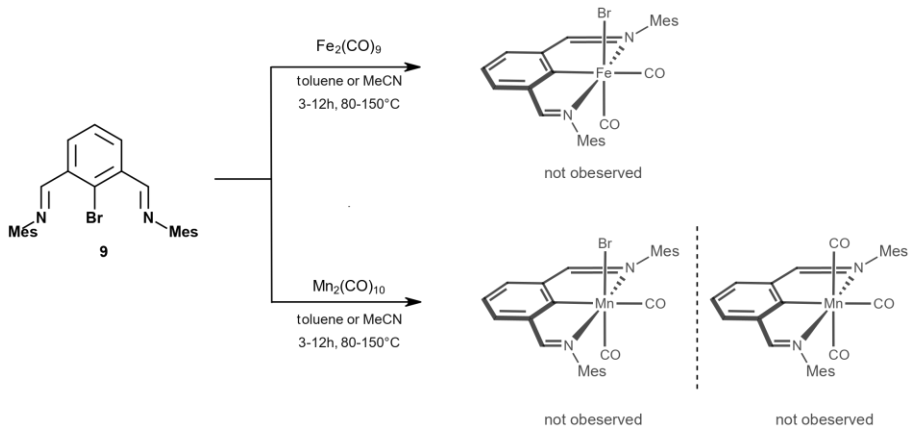

Figure 2.7: Overview of carried out under solvothermal reactions with ligand **9**.

A different result could be obtained when ligand **9** was heated up to 80° C with $Co_2(CO)_8$ for 4 hours. After evaporation of the initial reaction solvent, IR spectroscopy revealed two distinct frequencies at 1835 cm^{-1} and 575 cm^{-1} which did not indicate the pincer species expected at the beginning.[97] Hence there were no signals detectable via NMR spectroscopy, it was assumed that a paramagnetic species must have formed.

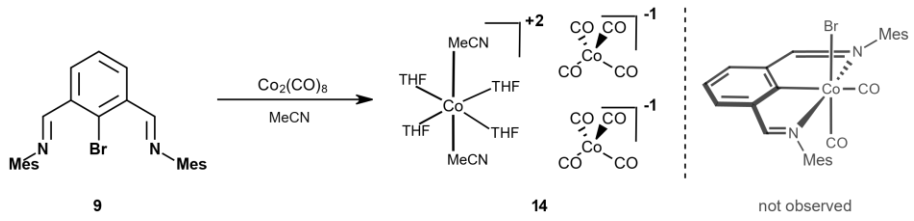

Figure 2.8: Solvothermal reaction of ligand **9** with $Co_2(CO)_8$.

Therefore, attempts have been made to crystallize the compound from diffusion of *n*-pentane into a concentrated THF solution. From this attempt, crystals suitable for x-ray diffraction analysis could be collected. Surprisingly, the diffraction analysis did not confirm the expected pincer coordination geometry.

The product obtained was a species of cobalt(II) and cobalt(-I) in the form of two $Co(CO)_4$ anions and a $Co(II)(MeCN)_2(THF)_4$ cation. The bond lengths of the coordinated THF ligands around the Co1 center range between 2.069 - 2.084 $\AA$, whereas the the bond lengths of the coordinated MeCN ligands range from 2.094 to 2.106 $\AA$. The cobalt(II) species adopts a slightly distorted octahedral geometry, with bonding angles in the THF plane varying between 87.52° and 92.79°. The bonding angles along the axes (O1-Co1-O2,O3-Co1-O4, N1-Co1-N2) are in the range of 176.52°-179.69°. For the cobaltate anions, the bond-lengths for the cobalt-carbon bonds vary from to 1.763 to 1.784 $\AA$. Looking at the

coordination geometry of the cobaltate anions, it is easy to see that they adopt a near perfect tetrahedral geometry around the cobalt atoms. Measurements of the bond angles confirm this assumption, since indeed all angles lie in a range from 106.06° to 110.82° which is very close to the ideal tetrahedral angle.

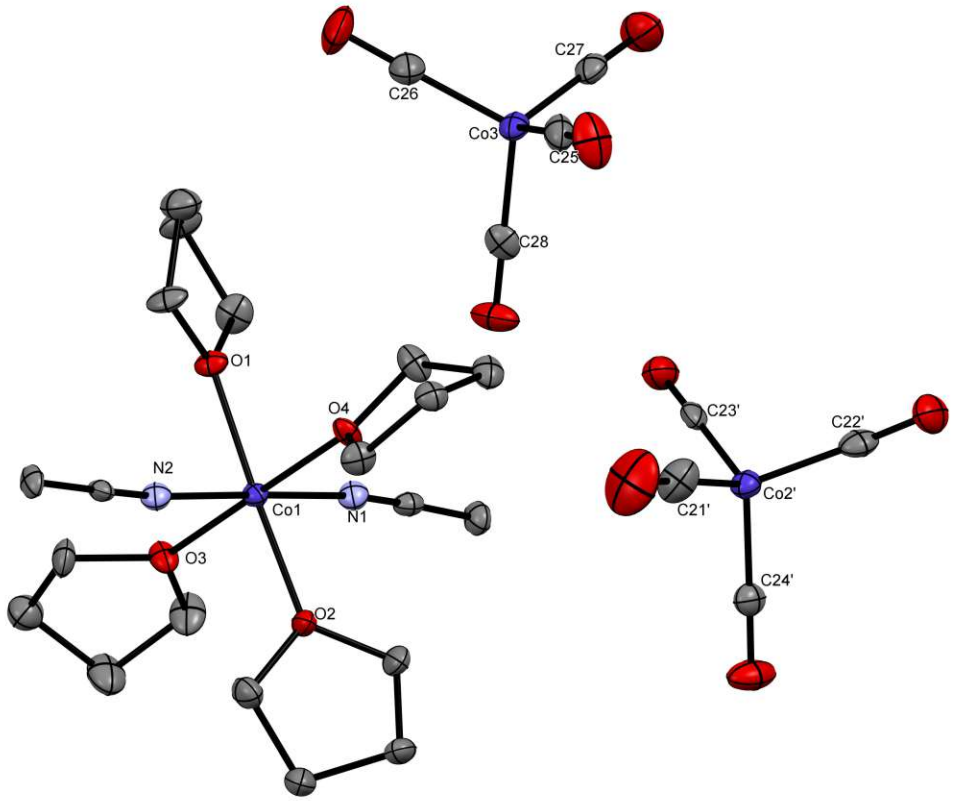

Figure 2.9: Crystal structure of **14** with 50 % thermal ellipsoids. H-Atoms are omitted for clarity. Selected bond lengths (*Å*) and bond angles (°): Co1-N1 2.094, Co1-N2 2.106, Co1-O1 2.084, Co1-O2 2.072, Co1-O3 2.083, Co1-O4 2.069, Co2'-C21' 1.754, Co2'-C22' 1.772, Co2'-C23' 1.784, Co2'-C24' 1.763, Co3-C25 1.774, Co3-C26 1.768, Co3-C27 1.754, Co3-C28 1.775, N1-Co1-N2 178.96, O1-Co1-O2 179.09, O3-Co1-O4 176.52, C22'-Co2'-C24' 108.29, C27-Co3-C28 108.58

After performing DFT calculations, the IR absorption at 575 cm^{-1} could be assigned to the oscillation of the cobaltate anion, which also helped to clarify the reactivity of analogous cobalt PCP pincers with CO, were similar IR frequencies could be observed. In figure 2.10 the d-splitting of the frontier orbitals of **14** is depicted. Orbital-energy values are in hartrees (italics).

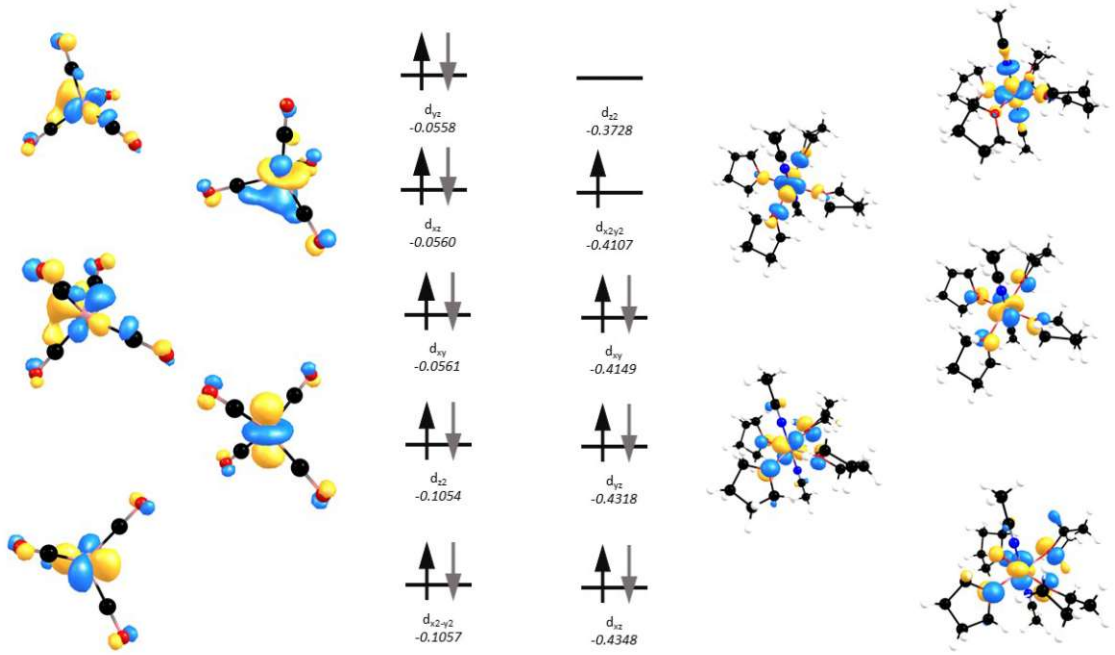

Figure 2.10: B3LYP/def2-TZVP computed frontier Orbitals (d -splitting for **14**. Orbitals computed at an iso-value of 0.05. Left: $[Co(CO)_4]^{1-}$; Right: $[Co(II)(MeCN)_2(THF)4]^{2+}$

Through these experiments it was made clear that solvothermal reaction protocols are not feasible strategies to successfully obtain NCN pincer complexes. Therefore, attempts have been made to obtain NCN pincer complexes via transmetallation methods.

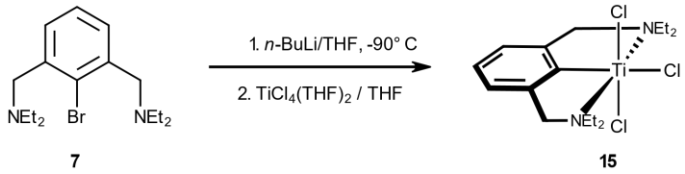

Figure 2.11: Reaction towards **15**

To do so, a solution of ligand **7** was cooled to -90° C and *n*-BuLi was added. The formed solution was then allowed to warm up to 0° C, before it was added to solution of $TiCl_4(THF)_2$, forming a dark red solution almost instantly. The recorded ^{1}H-NMR spectra give rise to a singlet at 3.58 ppm (*cf.* 3.64 ppm for the free ligand **7**), indicating a successful complexation. Unfortunately, **15** proved to be inherently unstable in solution, so that ^{13}C-NMR spectroscopy could not be applied successfully. Moreover, attempts to obtain crystals suitable for XRD measurements have been unsuccessful.

In analogy to the procedure towards **15**, a solution of ligand **7** was cooled to -90° C and *n*-BuLi was added. Then, neat $CrCl_3(THF)_3$ was added after the solution was allowed to warm up to room temperature. Following this procedure, complex **16** could be obtained

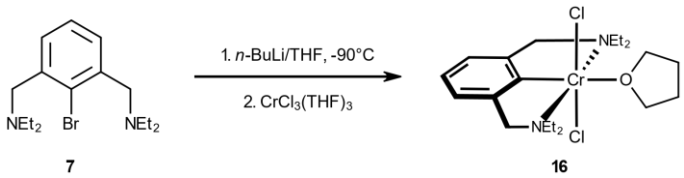

Figure 2.12: Reaction towards **16**

in a 63 % yield. Diffusion of *n*-pentane into a saturated THF solution yielded dark green crystals which were of sufficient quality for single crystal x-ray diffraction analysis. Interestingly, the colour of the compound varies strongly depending on whether it is in solid state (purple) or in solution, where for example in THF, it exhibits an intensive dark green colour. Investigations on the magnetic moment of the formed species are clearly indicating a d^3 high spin system with an effective magnetic moment of μ_{eff} =3.7(2)μ_B. The measurement was conducted in d_8-THF.

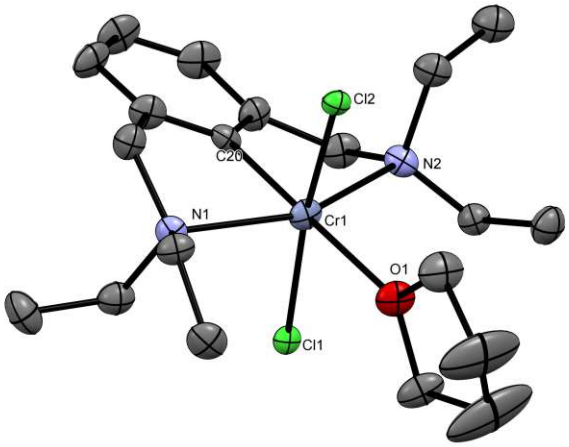

Figure 2.13: Crystal structure of [Cr(NCN^{CH2}-Et)Cl$_2$(THF)] with 50 % thermal ellipsoids. H-Atoms are omitted for clarity. Selected bond lengths ($\AA$) and bond angles(°):Cr1-C20 2.000, Cr1-N1 2.295, Cr1-N2 2.292, Cr1-Cl1 2.294, Cr1-Cl2 2.377, Cr1-O1 2.239, C20-Cr1-O1 179.35, Cl1-Cr1-Cl2 171.59°, N1-Cr1-N2 155.64

The structure is of poor quality due to the fact, that it most likely undergoes a phase transition while cooling down to 100 K during the XRD measurement. Furthermore, it was discovered that complex **16** exhibits significant sensitivity towards air and moisture. These properties lead to a rapid decomposition of **16**, when working with it under these conditions. Furthermore, it was determined, that the chloride atoms are disordered with bromide atoms. A phenomenon, which is well known for transmetalation products, where a chloride-precursor material gets used with a bromide ligand. The LiBr arising during the reaction, reacts with the product in a possbile salt-metathesis reaction to produce disorder-effects in the final product. When comparing the bond-lenghts to corresponding PCP^O-complexes,[34] significant differences can be described. Starting at the *ipso*-carbon-

chromium bond, it can be reported that, the C20-Cr1 distance of 2.000 is noticeably shorter than those of the corresponding PCP^O (*cf* 2.067 (*Å*))[34] and approximately the same length as for Bis(iminoaryl)-NCN complexes (*cf* 1.967 (*Å*)).[78] It is also relevant to mention, that the measured Cr-N distances are significantly shorter than those for Cr-P , with 2.292-2.295*Å* and 2.481 *Å* respectively. Interestingly, Cr-N distances are noticeably longer than those reported in comparable Bis(iminoaryl)-NCN complexes, with 2.163 - 2.186*Å*. One further aspect worth mentioning is, that the measured bond-lengths differ substantially from features observed in chromium NCN-complexes with trianionic ligand frameworks. Veige et al pupblished a chromium(IV) complex, which features a Cr-C bond of 1.953 *Å* and Cr-N bonds which are in the range of 1.887 - 1.905 *Å*.[98]

Another interesting aspect to mention are the torsion angles which are highlighted in figure 2.13. One can easily coonclude from figure 2.13, that the two arms bearing the nitrogen donor groups are strongly bend away from the Cr1-C1-C2 plane. The arm with the **N1** group is bent with a 29.95° angle below the plane, whereas the **N2** bearing arm is bent with an 28.73° angle above the plane. Interestingly, complex **16** features significantly higher torsion angles than those observed in corresponding POCOP-complexes,[34] which is most likely attributed to the higher flexibility of the CH_2-linkers utilized in this work.

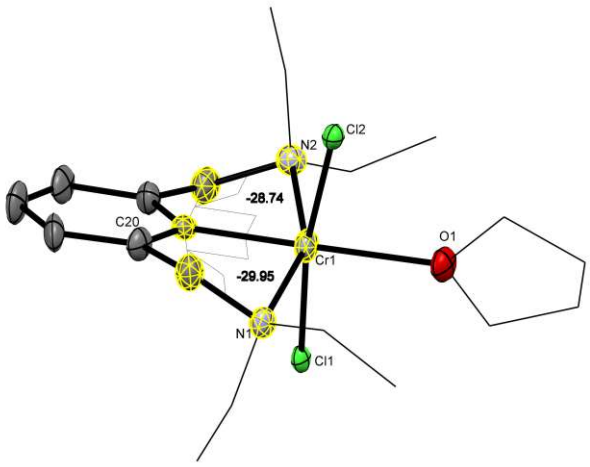

Figure 2.14: Crystal structure of [Cr(NCN^{CH2}-Et)Cl_2(THF)] with 50 % thermal ellipsoids. H-Atoms are omitted for clarity. Ethyl and THF groups are depicted as wireframes for clarity. Torsion angles (°):Cr1-C20-C2-N2: -28.73, Cr1-C20-C6-N1: -29.95

Additionally, it was shown, that when the precursor material gets suspended or dissolved prior to its addition to the lithiated ligand, yields could be improved significantly. When applying the protocol to the ligand **5** and **8** light green (**17**) and dark green (**18**) substances were obtained respectively. Investigations on the magnetic moment of the compounds via the Evans method (d_8-THF) also indicated d^3 high spin systems with a μ_{eff} =3.8(2)μ_B and μ_{eff} =3.8(4) μ_B respectively, indicating three unpaired electrons for both systems. Attempts to crystallize both products from various solvents and solvent combinations has

not been successful yet. Further attempts to characterize complexes **17** and **18** via HR-MS measurements were unsuccessful as well.

It is well known in literature that chromium(II) compounds open up a much broader field of application than the corresponding chromium(III) compounds.[34,78,99,100] Contrary to our expectation, the type of compound obtained and its coordination geometry depend, on the one hand, strongly on the amounts of precursor utilized, whether the precursor is added as a solid or in solution, and, on the other hand, also on the sequence of the addition.
When treating the ligand **7** with *n*-Buli at -90° C and adding neat $CrCl_2$, several products are likely formed. This can most likely be attributed to the poor solubility of anhydrous $CrCl_2$ in common organic solvents. When the $CrCl_2$ gets suspended in small amounts of solvent and gets further dispersed using an ultrasonic bath, it was observed, that the amount of precursor used in the process takes increasing influence on the obtained product.

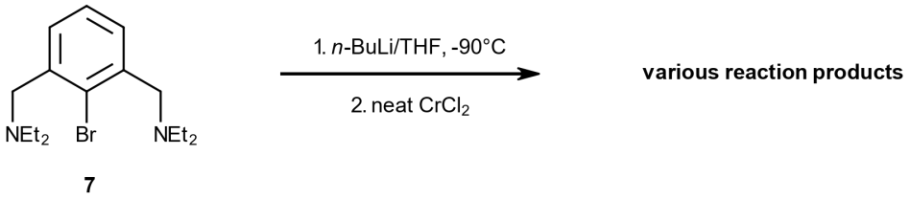

Figure 2.15: Reaction of **7** with neat chromium(II)precursor

Therefore, when using 1.1 equivalents or more, bridged chromium species are formed in the process, which is also known to literature.[78] After several days, these species also start to form clusters, from one of which a crystal suitable for XRD analysis was obtained.

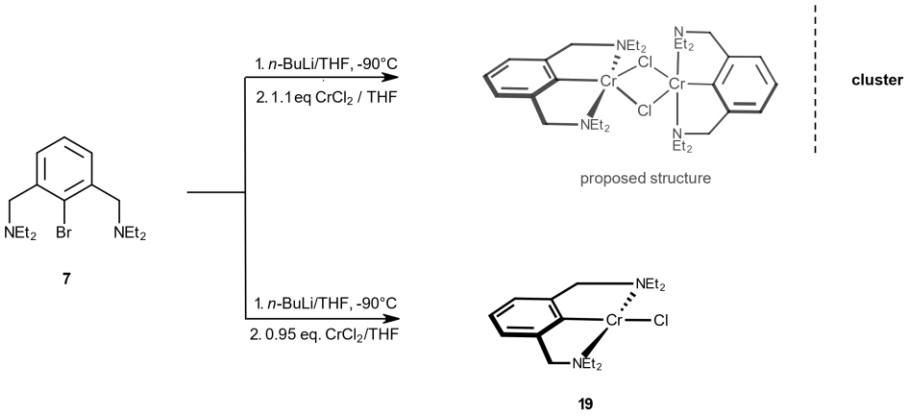

Figure 2.16: Reaction of **7** with $CrCl_2$ at various conditions.

Interestingly, not the proposed bridged structure was obtained, but a cluster where three chromium atoms are linked via bridging chlorine atoms and to our surprise, two oxygen

atoms. These two oxygen atoms are most likely a result of the crystallization process. The crystals as *n*-pentane-solvate were obtained via slow diffusion of *n*-pentane into a saturated THF solution.

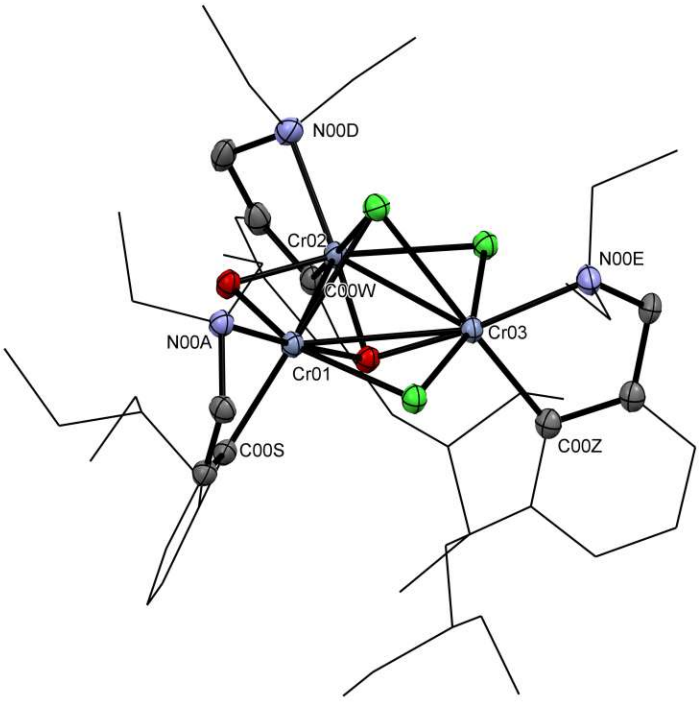

Figure 2.17: Crystal-structure of the chromium(II)cluster with 50% thermal ellipsoids.H-Atoms are omitted, several parts are depicted as wireframe for clarity. selected bond lenghts ($\mathring{A}$) and bond angles(°): C00S-Cr01 2.041, C00W-Cr02 2.043, C00Z-Cr03 2.035, Cr01-N00A 2.205, Cr02-N00D 2.190, Cr03-N00E 2.198,Cr01-Cr02 2.780, Cr02-Cr03 2.955, Cr03-Cr01 2.967, C00S-Cr01-N00A 80.00, C00W-Cr02-NOOD 82.23, C00Z-Cr03-N00E 81.70

The obtained structure features a highly unsymmetrical cluster, consisting of three chromium atoms, with one ligand **7** moiety bond in a κ^2- fashion to the corresponding chromium atoms. Further, the chromium atoms are connected via chlorine and oxygen atoms in a μ_2 and μ_3 fashion. The bond distances of the *ipso*-carbon atoms range from 2.035 to 2.041 $\mathring{A}$. Further the distances of the donating nitrogen groups are in the range of 2.190 $\mathring{A}$ to 2.205 $\mathring{A}$. The distances between the various chromium and chlorine atoms are in the range of 2.398 $\mathring{A}$ to 2.610 $\mathring{A}$. The distances of the oxygen atoms to their bound chromium atoms are in the range of 1.908 $\mathring{A}$ and 1.989$\mathring{A}$. The formal distances between the chromium atoms are in the range of 2.780 $\mathring{A}$ and 2.967 $\mathring{A}$. Due to the fact that this structure represents one of many likely formed products during that uncontrolled reaction described before, it was not further investigated if real chromium - chromium bonds are existent in this structure.

From these results, it was concluded that the pincer species is more accessible when exact equivalents are maintained. When treating ligand **7** with exactly one equivalent of suspended $CrCl_2$, a differently coloured solution formed. The obtained substance could be crystallized from a saturated *n*-pentane solution which was kept at -30°C over night. Unfortunately, most likely to the even higher sensitivity of the compound, the complex disintegrated during the XRD measurements.

From this results the hypothesis arose, that if ligands with steriacally more demanding rests on the donating sites are used, one is capable of sterically shielding the metal center, and therefore able to easier isolate the desired compounds. Henceforth, the same protocol was applied to ligand **8** with its space-demanding isopropyl moieties bond to the nitrogen donor atoms.

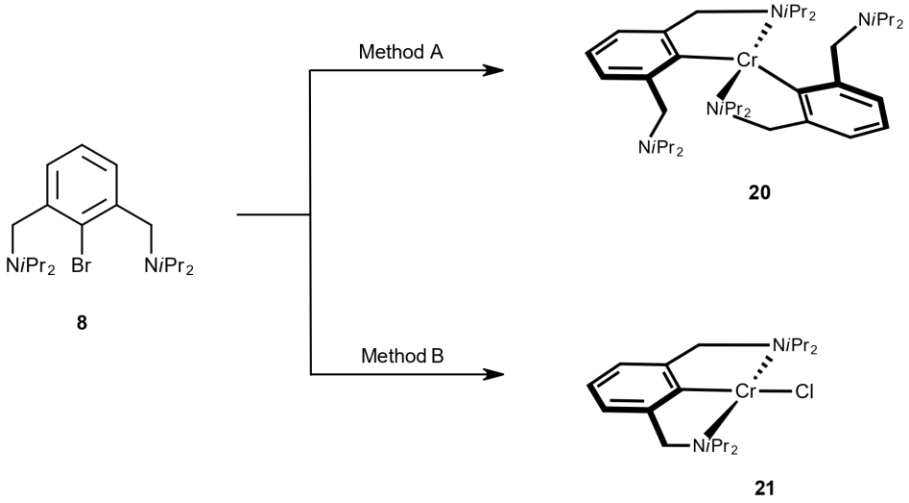

Figure 2.18: Reaction of **8** with towards **20** and **21**

When treating a suspension of $CrCl_2$ in small amounts of THF with the lithiated ligand **8** (**Method A**) a blue suspension formed. After work up, crystals suitable for XRD analysis were obtained via cooling a saturated *n*-pentane solution of **20** down to -30°C over night.

Surprisingly, the obtained structure showed a chromium(II) complex, where the two ligand moieties are bound to the chromium atom in a $\kappa_2\kappa_2$ fashion. Investigations on the magnetic moment via Evans method (d_2 DCM) indicated a d^4 high spin system with a effective magnetic moment of $\mu_{eff} = 4.7(4)\mu_B$.
To get further insights into the coordination geometry of complex **20**, the geometry indices τ_4 and $\tau_4^{'}$ where calculated according to literature.[101–103] Comparison of this two values one can make further assumptions whether a coordination center with four ligands adopts either a square planar, see-saw or a tetrahedral geometry. If those two values equal 0, one has obtained a square planar geometry, if both are equal to 1, a tetrahedral geometry is described. For the also possible seesaw geometry τ_4 equals around 0.43 and $\tau_4^{'}$ equals around 0.24. When calculating the indices for complex **20**, the value 0.50 is obtained

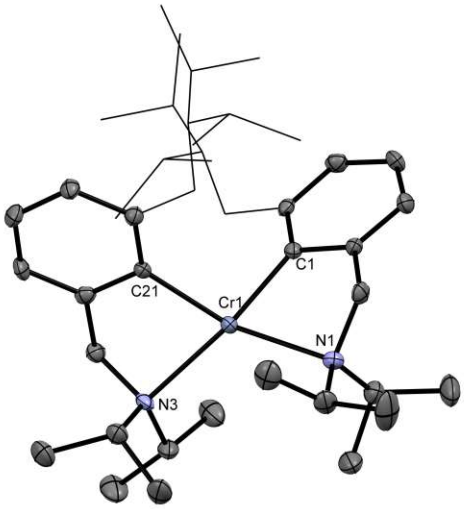

Figure 2.19: Crystal Structure of [Cr-(κ^2-NCN^{CH2}-iPr)$_2$] (**20**) with 50 % thermal ellipsoids. H-atoms omitted for clarity. Selected bond lengths (A) and bond angles (°): Cr1-C1 2.074, Cr-C21 2.090, Cr1-N1 2.381, Cr-N3 2.371, C1-Cr1-N3 144.99, C21-Cr1-N1 143.75

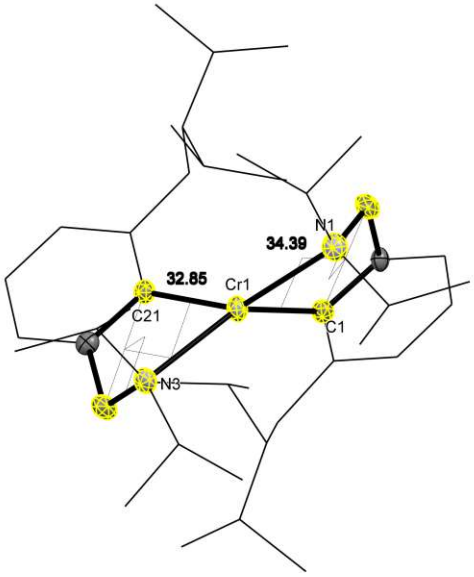

Figure 2.20: Crystal Structure of [Cr-(κ^2-NCN^{CH2}-iPr)$_2$] (**20**) with 50 % thermal ellipsoids. H-atoms omitted, iPr-groups and non coordinating arms are depicted as wireframes for clarity. Torsion-angles between the highlighted atoms (°): N1-C14-C1-Cr1 34.39, N3-C27-C21-Cr1 32.86

for τ_4 and the value 0.50 for $\tau_4^{'}$. This result is not surprising when analysing the crystal structure and leads to the conclusion, that complex **20** adopts a intermediary structure between a square planar geometry and a tetrahedral geometry.
Whereas if the $CrCl_2$ gets completely dissolved in large amounts of THF and exposed to the ultrasonic bath a light-blue solution of the $CrCl_2(THF)_2$ can be obtained. If now the lithiated ligand **8** is added in a drop-wise fashion (**Method B**) a dark purple to black solution forms immediately. After keeping a concentrated n-pentane solution at -30° C, crystals suitable for single-crystal XRD measurements could be obtained in a 73% yield referred to the amount of ligand utilized.

Complex **21** adopts a distorted square planar geometry around the chromium center. When comparing the distances between the two obtained chromium(II) complexes one can see, that in **21** the Cr-N distances are noticeably shorter with 2.261 (Cr1-N1) and 2.257 (Cr1-N2). In contrast to that, **20** adopts distances of 2.381 (Cr1-N1) and 2.371 (Cr1-N3) respectively. Interestingly, the distances from the *ipso* carbon to the chromium center do not differ so strongly with 2.011 in **21**, and 2.074 and 2.090 in **20**. Unfortunately, just like the already described chromium (III) complex(**16**), **21** has a disorder of the chlorine atoms. About 30% of the chlorine atoms are disordered with bromine atoms. When investigating the magnetic moment of **21**, a μ_{eff} of 4.8(5)μ_B was measured, which is in

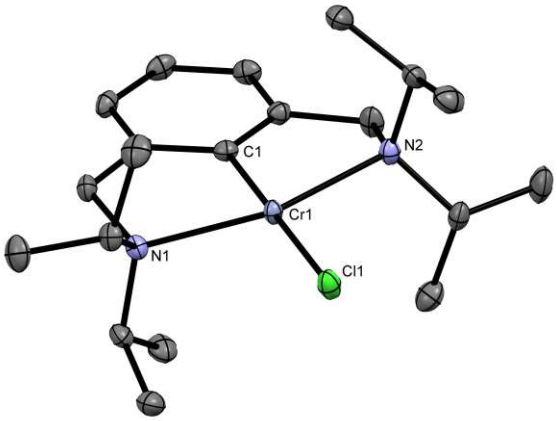

Figure 2.21: Crystal Structure of [Cr(NCN^{CH2}-*i*Pr)Cl] (**21**) with 50 % thermal ellipsoids. H-atoms omitted for clarity. Selected bond lengths (A) and bond angles (°): Cr1-C1 2.011, Cr1-N1 2.261, Cr1-N2 2.257, Cr-Cl1 2.455, C1-Cr1-Cl1 178.58, N1-Cr1-N2 158.53

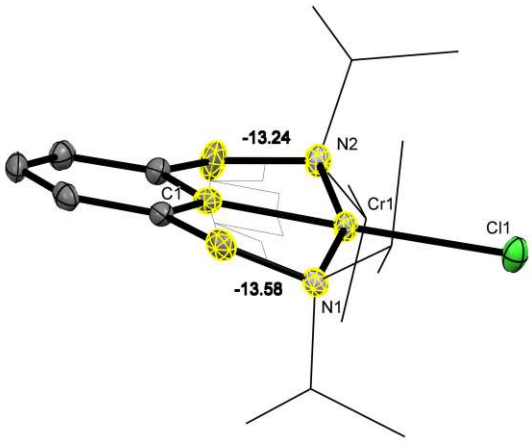

Figure 2.22: Crystal Structure of [Cr(NCN^{CH2}-*i*Pr)Cl] (**21**) with 50 % thermal ellipsoids. H-atoms omitted and *i*Pr-groups are depicted as wireframes for clarity. Torsion angles between the highlighted atoms (°): N2-C14-C1-Cr1 13.24, N1-C7-C1-Cr1 13.65

coherence with a d^4 high spin system. When comparing the coordination properties of **21** to literature-known PCP^O-systems[34] and PNP-systems,[104] the same trend, which was already observed with complex **16** prolongs. The observed Cr1-C1 bond length of 2.011 *Å* is considerably shorter than the reported lengths in the PCP^O(C-Cr)[34] - and monoanionic PNP-systems (N-Cr),[104] which exhibit bond lengths of 2.083 for both complexes. The difference in donating properties between the ligand frameworks becomes more apparent when the bond lengths of the neutral donor atoms to the metal centers are compared. Here complex **21** features bond lengths of 2.257 and 2.261 *Å*, whereas the chromium-phosphorus-bonds measure in at 2.452 and 2.457 *Å* respectively.[34] When comparing this result to the PNP counterparts, the difference becomes more apparent, with bond-lenghts of 2.484 and 2.489 *Å*.[104] Moreover, it is worth mentioning, that the measured lengths also differ to structurally related NCN complexes, featuring Bis(imino)aryl NCN ligands.[78] *Liu et al.* reported even shorter lengths for the carbon-chromium and the nitrogen-chromium bonds, measuring 1.985*Å*, 2.200 *Å* and 2.186 *Å* respectively.
It is important to note, that the torsion angles of **21** are significantly lower than in **16** described before. **21** features torsion angles of 13.24 and 13.56° out of the benzene plane of the ligand-framework, underlining the slightly distorted square planar geometry.

After characterizing complex **21** its reactivity towards other ligands was investigated. First, gaseous NO was chosen to react with a toluene solution of **21**, forming a dark red to brown solution instantly.
Conducted IR measurements of the obtained dark red solid exhibited a strong adsorption at 1702 cm^{-1}, which differs substantially from the results *Himmelbauer*[34] and *Pecak*[105] ob-

tained, when they investigated the reactivity of corresponding chromium PCP complexes and cobalt NCN complexes respectively.

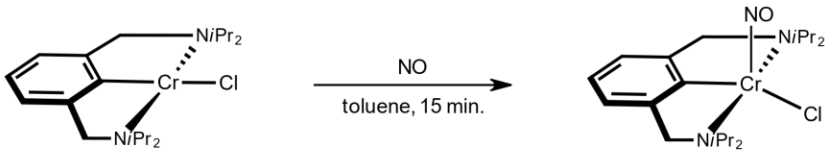

21 **22**

Figure 2.23: Reaction of **21** with NO in toluene

They reported adsorptions at 1654 cm^{-1} and 1609 cm^{-1} respectively. The literature examples feature a linear and bent NO-coordination mode respectively. Measurements of the magnetic moment in d_2-DCM revealed a effective magnetic moment μ_{eff} of $1.8(1)\mu_B$, which is in good correlation with literature data.[34,105] Due to the fact, that all attempts to obtain crystals of **22** for XRD analysis were unsuccessful, the structure of **22** was further investigated by performing DFT-calculations on the proposed structure. Because of this, it was made clear that the significant difference observed during IR-measurements, is most likely the result of a changed coordination mode of the NO-ligand to the metal center. In contrast to the literature examples, the NO-moiety in **22** likely coordinates in a linear coordination mode.

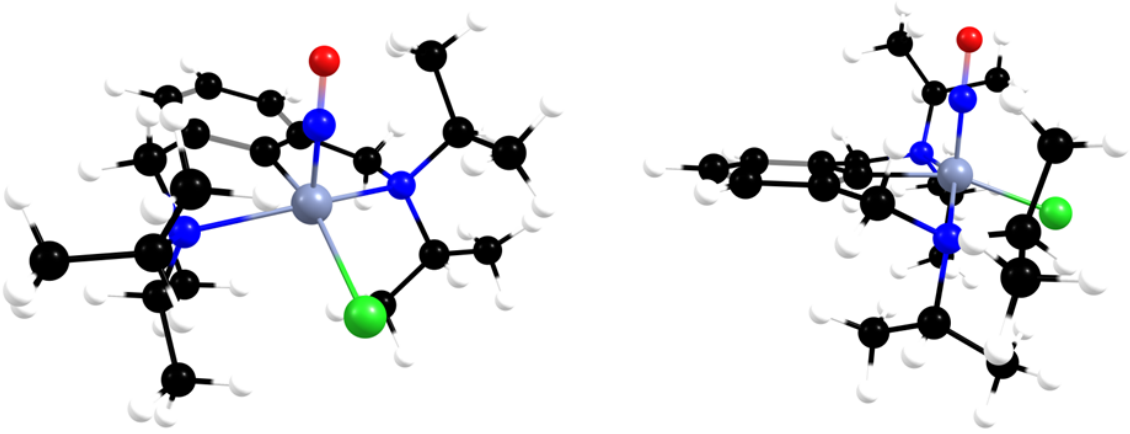

Figure 2.24: Optimized geometry of **22** at a BP86/def2-TZVP level of theory.

When cooling down a solution of ligand **8** in THF to -90° C and then adding *n*-BuLi to the solution and further adding neat or dispersed anhydrous $FeBr_2$ a dark yellow to brown solution is obtained. After prolonged reaction times (in comparison to complexes **20** and **21**), complex **23** could be extracted into large amounts of *n*-pentane to form bright yellow solutions.

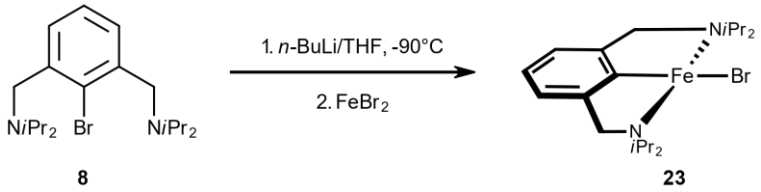

Figure 2.25: Reaction towards **23**

Due to the solubility in *n*-pentane, purification of the obtained compound was restricted to filtration techniques. Following the extraction, it was attempted to directly crystallize **23** by cooling the concentrated *n*-pentane solution down to -30° C, which in all conducted attempts led to the precipitation of micro-crystalline to amorphous solids. Measurements of the magnetic moment in d_6-benzene revealed a μ_{eff} of $2.8(1)\mu_B$, which is a higher value than expected for a d^6 high spin system in a square planar coordination geometry. Interestingly, *Nishibayashi et al.* observed a similar phenomenon when investigating structurally similar PCP-iron complexes.[106] Further attempts to crystallize both compounds from different solvents, solvent mixtures and different crystallisation techniques has not been successful yet. The addition of small amounts of benzene (in a ratio of 1:20) rapidly increases the solubility of both complexes and thus makes extraction far more efficient.

To gain further insights of the coordination properties of complex **23** it was reacted with gaseous nitric oxide, with the intention of saturating the complex coordinately and thus reducing its sensitivity.

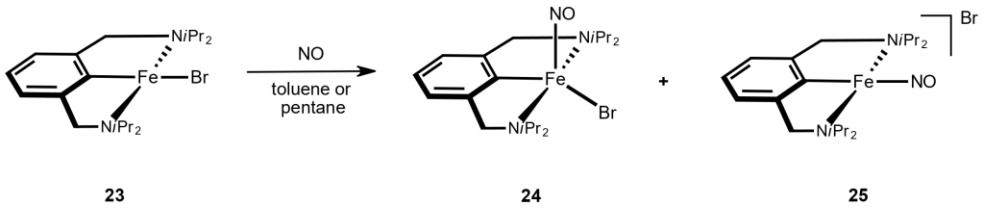

Figure 2.26: Proposed reaction towards **24** and **25**

When injecting nitric oxide in the head-space of a solution of **23** the colour changes from a bright yellow (*n*-pentane solution) or dark yellow (toluene-solution) to a dark red immediately. conducting IR-measurements on the obtained dark red to brown solid revealed an interesting result. The recorded spectrum gives rise to two distinct signals in the NO-range: one at 1775 cm $^{-1}$ and one at 1704 cm $^{-1}$.

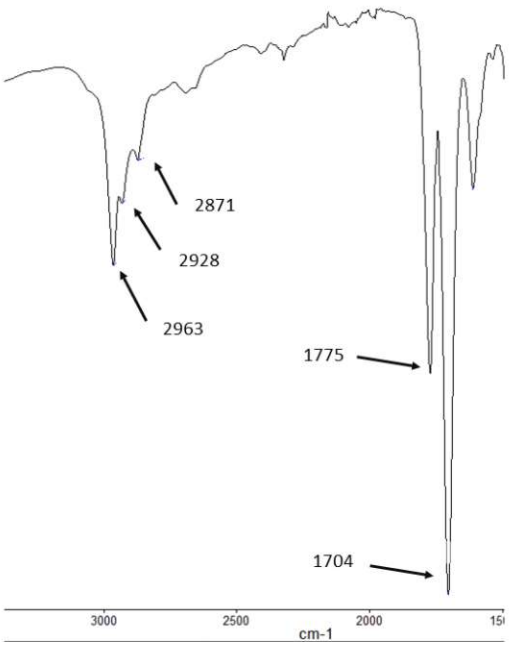

Figure 2.27: ATR IR spectrum of the mixture of **24** and **25**

Attempts in separating the two obtained species was not possible via solubility. Both species are near insoluble in *n*-pentane and feature similar solubility properties in solvents with higher polarities such as diethyl-ether. Furthermore, one of the two components could not be selectively crystallised from the mixture. Because of this, DFT- calculations were performed to get further insights of the possible geometries that could lead to the measured frequencies obtained via IR-spectroscopy. Through these calculations (BP86/def2-TZVP), it was found that the observed band at 1775 cm $^{-1}$ is in good agreement with the theoretically proposed square pyramidal structure of **24** with a calculated value of 1773 cm^{-1}.

For the second signal two possibilities come into mind: either a cationic species is formed, with a bromine atom as counter atom or a different isomer of **24**. When calculating the frequencies for one different isomer, with the nitric oxide moiety in *trans*-position to the *ipso*-carbon, one obtains a calculated frequency for the NO-vibration of 1808 cm $^{-1}$. With this result in mind, the hypothesis of a second isomer was abandoned.
For the second option, an easy experimental method was implemented. By reacting the mixture of **24** and **25** with a halogen scavenger, subtracting the bromine moiety and interchanging the counter-ion with a non-coordinating anion only one product should likely form.

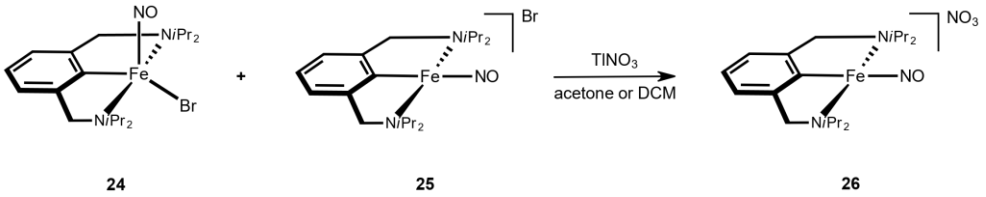

Figure 2.28: Reaction towards **26**

When adding anhydrous $TlNO_3$ to the mixture of **24** and **25** in DCM no immediate change in physical appearance was visible. After 18 hours, the start of a grey precipitation could be observed. After 48 hours no further precipitation was visible. Most likely TlBr precipitated due to its poor solubility in organic solvents. It was also discovered, that the reaction is noticeably faster, when degassed acetone is utilized as solvent.

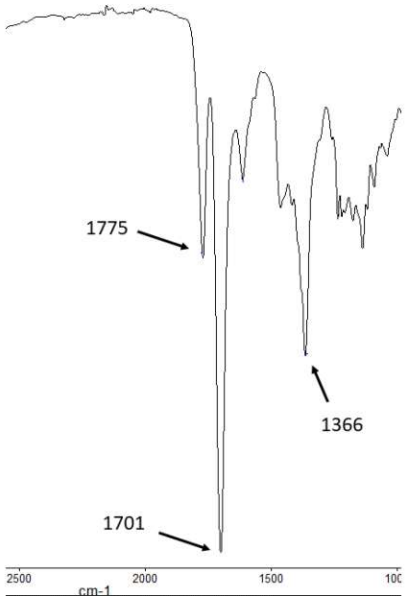

Figure 2.29: selected part of the ATR IR spectrum of the residue obtained from the reaction towards **26**.

Conducting IR-measurements on the residue, after the formed TlBr has been filtered of, still revealed two distinct frequencies. The frequency at 1775 cm^{-1} is still present, although at a reduced intensity. Further, the spectrum gives rise of a frequency at 1701 cm^{-1} and a additional intense adsorption at 1366 cm^{-1}, which can be attributed to the NO_3 counter-ion.

It is literature known, that iron(II)carbonyl-pincer-complexes feature a d^6 low-spin conformation.[30,32] This facilitates NMR spectroscopy with standard methodologies with these compounds. In order to obtain the analogues of already puplished PCP iron carbonyl

complexes,[30,32] gaseous carbon monoxide was injected into the headspace of solution of **23** in toluene or *n*-pentane.

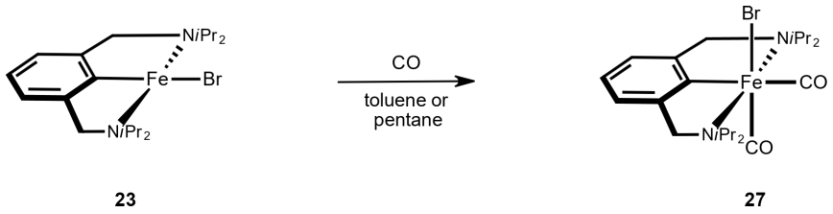

23 **27**

Figure 2.30: Reaction towards **27**

The difference in solubility also plays a major role in this reaction. When the reaction is performed in toluene, a dark green/brown solution forms instantly. Interchanging toluene for *n*-pentane results in a slower formation of a intense, clear green solution. After workup, conducted IR - measurements revealed two distinct absorption frequencies at 2022 cm $^{-1}$ and 1920 cm $^{-1}$, indicating the formation of a *cis*-dicarbonyl complex. Interestingly, the measured frequencies are in the range of literature known values for structural-analogoues for PCP- pincer complexes: the frequencies for PCP^{CH_2} complexes are 1993 cm $^{-1}$ and 1938 cm $^{-1}$,[30] and those for PCP^{NEt} are 2002 cm $^{-1}$ and 1934 cm $^{-1}$.[32] Iron Bis(oxazolinyl)phenyl NCN complexes feature CO absoptions at 2020cm $^{-1}$, 1969cm $^{-1}$ and 2026cm $^{-1}$, 1965cm $^{-1}$ respectively, depending on their chiral properties introduced by the utilized ligands.[39] The NMR - measurements carried out confirmed the low spin character of **27**, but the resolution was limited, so that satisfactory results can only be obtained from measuring single crystals of **27**. Unfortunately, all attempts to obtain single crystals of **27** suitable for X-ray diffraction analysis were unsuccessful.

When applying the transmetallation protocol (Method B) with cobalt, a double bridged complex is obtained. Here, every cobalt atom in the complex exhibits a tetrahedral coordination geometry. The formal oxidation state is of further interest, because the distance between the two cobalt atoms formally allows the existence of a Co-Co metal-bond.[107]

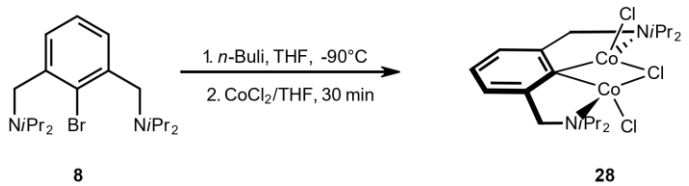

8 **28**

Figure 2.31: Reaction towards **28**

To gain further insight into the coordination properties of complex **28**, the magnetic moment was further evaluated via the Evans-method (d_8-toluene) one obtains a value of μ_{eff} =5.8(4)μ_B. This value is lower than the expected value, when no cobalt-cobalt

bond is assumed, with two cobalt(II) centers in the tetrahedral coordination. This is most likely due to the fact, that the chlorine atoms are miss-ordered with bromine atoms, and therefore no accurate mass can be used to calculate the exact value of μ_{eff}. This leads to the assumption, that every cobalt atom features a d^7 high spin configuration. Further the single crystal structure of **28** exhibits interestingly symmetric properties. For reasons of scientific accuracy, it must also be mentioned that the illustrations, figure 2.31 and figure 2.32, show the structure of **28** only with chlorine atoms. Here, the data show a disorder with bromine atoms.

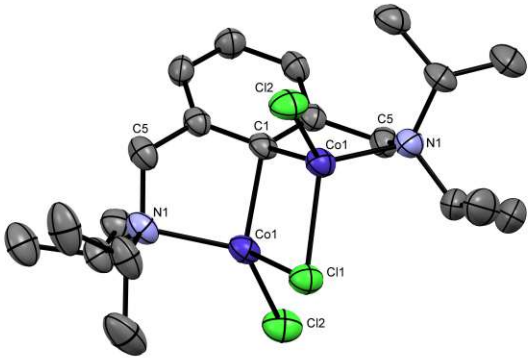

Figure 2.32: Crystal Structure of $[Co_2(NCN^{CH_2}\text{-}i\text{Pr})Cl_3]$ (**28**) with 50 % thermal ellipsoids. H-atoms omitted for clarity. Selected bond lengths ($\AA$) and bond angles (°): C1-Co1 2.114, Co1-Co1 2.694, Co1-Cl1 2.404, Co1-Cl2 2.338, Co1-N1 2.100, C1-Co1-Cl2 117.50, C1-Co1-Cl1 106.33, Co1-C1-Co1 79.16, N1-Co1-Cl2 124.10, N1-Co1-Cl1 133.55

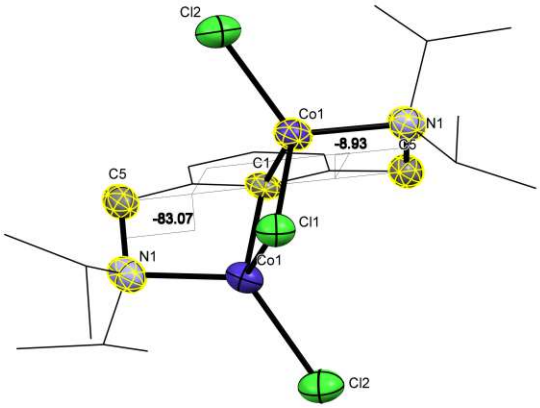

Figure 2.33: Crystal Structure of (**28**) with 50 % thermal ellipsoids. H-atoms omitted and most atoms are depicted as wireframes for clarity. Torsion angles of selected atoms (°): N1-C5-C1-Co1 (above plane): 8.93, N1-C5-C1-Co1 (below plane): 83.07

Interestingly, the single crystal structure of **28** reveals a level of symmetry, which is higher than expected . The distances of the nitrogen atoms towards the cobalt atoms are of the exact same length of 2.100 $\AA$ which is noticeably shorter than those reported in comparable PCP^{NH} complexes,[97] where the cobalt-phosphorous bonds measure 2.221-2.234 $\AA$. This result is in line with measured bond-lengths of structurally related NCN-cobalt complexes,[105] where these distances measure in the range from 2.033 to 2.044 $\AA$. Unsurprisingly, with a measured carbon-cobalt bond length of 2.114 $\AA$ in **28**, this result differs significantly from the before described literature-known compounds. The already published *ipso*-carbon-cobalt bonds measure in at 1.850 $\AA$ for the $[Co(NCN^{CH2}\text{-Et})Br]$-

complex[105] and 1.935$\AA$ for the [Co(PCP^{NH}-tBu)Cl]-complex[97]respectively. This drastic difference can be attributed to the uncommon coordination of ligand **8** to the two cobalt centers. When calculating the geometric indices for tetravalent systems τ_4 and $\tau_4^{'}$ supports the impression of a distorted terahedral structure one receives when examining the crystal structure of **28** ($\tau_4 = 0.86$ and $\tau_4^{'} = 0.83$, $\tau_4 = \tau_4^{'} = 1$ corresponding to a perfect tetrahedral geometry).[101–103,108]

2.3 Synthesis of the SCS pincer complexes

Due to the fact that SCS Pincer complexes with first row transition metals are exceedingly rare, the reactivity of the ligands **10, 11** and **13** towards nickel was exploited first. Van Koten's initial work with SCS Pincer ligands with mainly palladium and platinum was taken as inspiration for the synthesis of the nickel complexes of the ligands **10, 11** and **13**. Therefore, a solution of the ligands **10** and **11** was added to a solution of $Ni(COD)_2$. To further control the reaction, the precursor solution was cooled to -80°C. After a successful addition of the ligand solution, the mixture was allowed to react at that temperature for 30 minutes, before it was allowed to warm up to room temperature. Upon warming up, the colours of the solutions changed from an intensive yellow to orange (**11**) and orange-red (**10**).

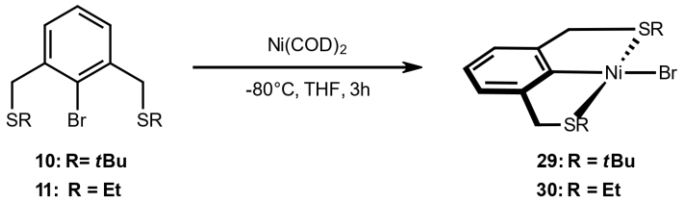

Figure 2.34: Reaction of **10** and **11** with $Ni(COD)_2$ towards the complexes **29** and **30**

Both complexes are air-stable and stable to moisture to a certain degree. Slow diffusion of *n*-pentane into concentrated DCM solution of **29** resulted in the formation of crystals suitable for single-crystal XRD measurements.

Interestingly, the solid state structure of **29** is highly symmetric. So the bond distances between the two sulfur donor atoms to the nickel center are of the exact same length with 2.222 A. Further worth noting is, that, besides its slightly bend structure, which is expected for complexes with carbon atoms as their linking groups, the bond angle between the *ipso*-carbon, nickel and the bromine atom measures exactly 180 degrees, which is the ideal angle for square planar geometries. Another special feature of this structure is that the torsion angles that the donor arms make with the plane of the benzene framework are also exactly equal at 19.80 degrees against the benzene plane. In the recorded ^{1}H-NMR spectrum the protons on the CH_2S*t*Bu (linkers) give rise to a broad singlet at 4.05 ppm (*cf.* ligand **10**, in d_2-*DCM*: 3.95 ppm) which is surprising when compared to literature.[88] In the SCS triad *van Koten* published with his SCS^{CH2}-Me ligand in 2008, he observed shifts which were shifted towards lower ppm-values when compared to the signal of the free ligand. The difference is most noticeable with the [Ni(SCS^{CH2}-Me)Br] complex, were he recorded a signal of 3.26 ppm, followed by 3.47 ppm for the [Pd(SCS^{CH2}-Me)Br] complex and 3.73-3.69 ppm for the [Pt(SCS^{CH2}-Me)Br]-complex respectively (*cf.* van Koten's ligand gives rise to a singlet at 3.85 ppm).[88]
Surprisingly, if compared to literature, complex **30** displays a similar result to those observed with **29**. Here, the protons of the CH_2S-Et (linkers) show a singlet signal in the recorded ^{1}H-NMR spectrum at 4.02 ppm (cf. ligand **11** in d_2-*DCM*: 3.88 ppm).

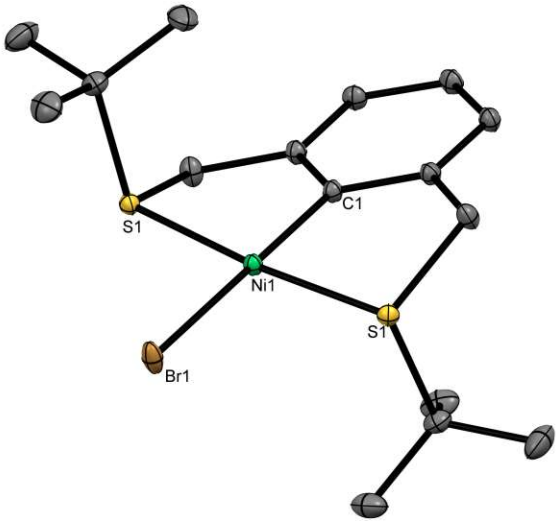

Figure 2.35: Crystal Structure of [Ni(SCS^{CH2}-*t*Bu)Br] (**29**) with 50 % thermal ellipsoids. H-atoms omitted for clarity. Selected bond lengths ($\AA$) and bond angles (°): Ni1-C1 1,902(), Ni1-S1 2.222(), Ni1-S1 2.222(), Ni1-Br1 2.400(), C1-Ni1-Br1 180.00, S1-Ni1-S1 173.03

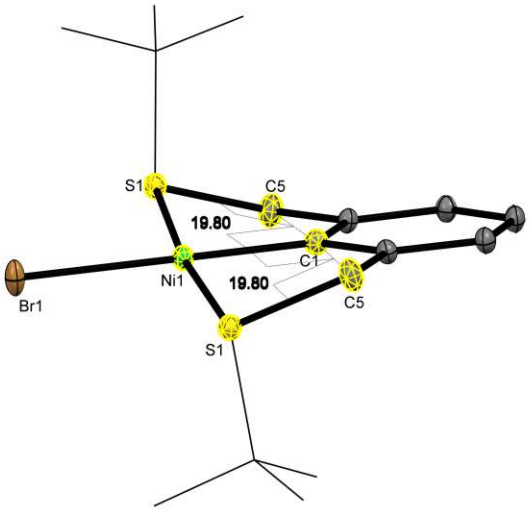

Figure 2.36: Crystal Structure of [Ni(SCS^{CH2}-*t*Bu)Br] (**29**) with 50 % thermal ellipsoids. H-atoms omitted and *t*Bu-groups are depicted as wireframes for clarity. Torsion angles: S1-C5-C1-Ni1: 19.80

Further modifications to compound **29** and **30** were unsuccessful. Inspired by literature[109] the attempt was made to obtain an borohydride species, which have been shown to be promising intermediates towards nickel-hydrides.[97] Unfortunately, a change of solvents and intermixing solvents, eg. MeOH/toluene, toluene, *i*-PrOH/toluene in combination with sodium borohydride had no change on the outcome of the reaction. Furthermore, the substitution of sodium-borohydride with lithium-borohydride in THF as solvent had no change in outcome. For all reactions, only ligand **10** or **11** and nickel(0) nanoparticles, visible as black suspension, could be recovered.

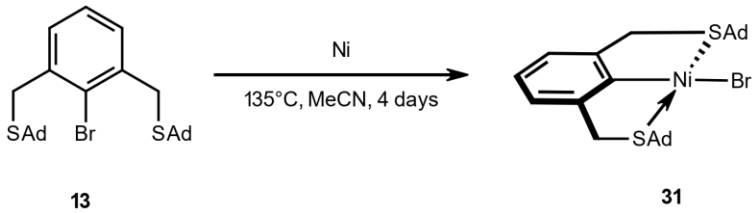

13 **31**

Figure 2.37: Reaction towards **31**

Attempts of obtaining the complex **31** via the same reaction protocol utilizing Ni(COD)$_2$ as metal precursor where unsuccessful and only ligand and nickel(0) nanoparticles could

most likely be recovered. Therefore, nickel powder and the ligand **13** were heated up to 135°C in MeCN in a closed vial for 4 days. ^{1}H-NMR measurements revealed a conversion of 63 % , but after that reaction time, a leak tightness of the reaction vessel could not be guarantied. Unfortunately, the similar solubilities of ligand **13** and complex **31** inhibited straightforward ways of purification. Fortunately, complex **31**, like complexes **29** and **30**, is relatively stable towards air an moisture. Thus, it could be successfully purified via silica chromatography in DCM/PE in a ratio of 1:2. Surprisingly, the recorded ^{1}H-NMR spectrum exhibits an interesting result for the protons on the CH_2S-Ad (linker). As expected and in line with the results observed with complexes **29** and **30**, the recorded signal is shifted to higher ppm. Interestingly, after purification now two peaks are visible, at 3.93 and 3.90 ppm respectively. For clarification, no signals of the free ligand (*cf.* a sharp singlet at 3.82 ppm, recorded in d_2-*DCM*) were visible in the recorded spectra. This signal can now be resolved in two ways: either a doublet at 3.91 ppm, or as two distinct signals at the shifts reported above. This may now indicate a loosely coordinating arm of the ligand, in the case of a doublet. Another possibility is the existence of two isomers of **31**. Since no evidence for the existence of two isomers was found in ^{13}C-NMR, the assumption of a non-/weakly coordinating arm applies here. The answer to this question may only be found by investigating the single-crystal structure of **31**. Unfortunately no crystals of sufficient quality for such measurements could be obtained from a multitude of different approaches towards synthesising such samples.

When the methodology of complexation, which was developed before for NCN chromium complexes, gets applied to the SCS-framework with cobalt, a dark solution forms instantly. Here, a mixture could be obtained and successfully separated from each other. Extracting the resulting residue with *n*-pentane, a dark yellow suspension was obtained.

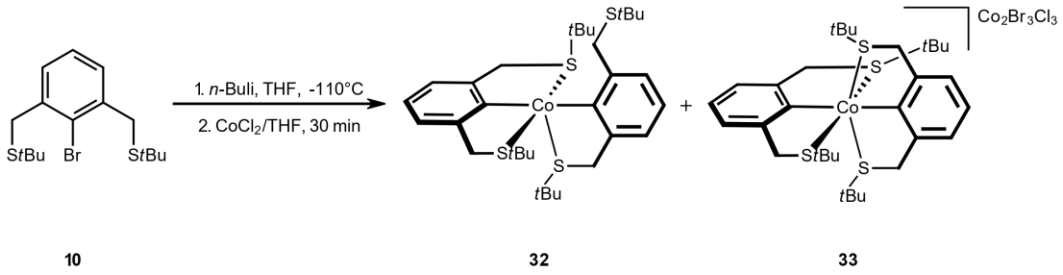

Figure 2.38: Reaction of **10** with $CoCl_2$

After further work-up, and storing the concentrated *n*-pentane solution of **32** at -30°C resulted in the deposition of dark red crystals of **32**, which where suitable for single-crystal XRD analysis. The distances in **32** from the *ipso*-carbon atoms to the cobalt center measure in at 1.922 $\AA$ and 1.985 $\AA$ respectivly. Further, the distances of the three sulfur donors are in the range of 2.226 to 2.319 $\AA$. The angle along the C11-Co1-C1 axis features a near linear angle of 177.66 °.

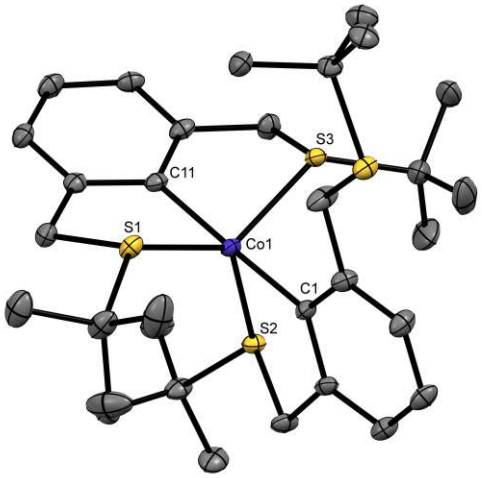

Figure 2.39: Crystal Structure of [Co-(κ^2-(SCS^{CH_2}-tBu))(κ^3-(SCS^{CH_2}-tBu))] (**32**) with 50 % thermal ellipsoids. H-atoms omitted for clarity. Selected bond lengths (A) and bond angles (°): C11-Co1 1.985, Co1-C1 1,922, Co1-S1 2.226, Co1-S2 2.319, Co1-S3 2.255, C11-Co1-C1 177.66, S1-Co1-S3 135.10, S3-Co1-S2 98.67, S2-Co1-S3 124.72

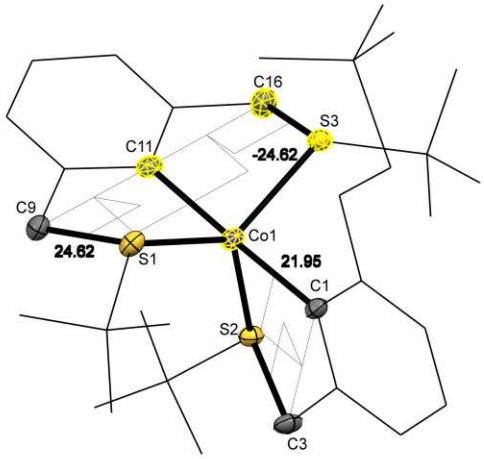

Figure 2.40: Crystal Structure of [Co-(κ^2-(SCS^{CH_2}-tBu))(κ^3-(SCS^{CH_2}-tBu))] (**32**) with 50 % thermal ellipsoids. H-atoms omitted and most of the ligand framework depicted as wireframes for clarity. Torsion angles (°): S3-C16-C11-Co1: 24.62, S1-C9-C11-Co1: 24.62, S2-C03-C1-Co1: 21.95

Complex **32** displays a geometry that is best described as trigonal bipyramidal, which was confirmed by the calculation of the geometry index τ_5 ($\tau_5 = 0.71$; $\tau_5 = 1$ corresponding to a perfect trigonal-bipyramidal geometry)[101–103,108] . Here, two ligand moieties coordinated in a κ^2-κ^3 fashion, where one sulfur moiety stays uncoordinated to the cobalt center. Measurement of the effective magnetic moment revealed a μ_{eff} =1.8(4)μ_B, which is in good agreement with a d^7 low-spin system with one unpaired electron. To obtain more insights about the coordination properties of **32**, EPR-spectroscopy was conducted.

Throughout this methodology the g-values were determined to g_x= 2.047, g_y=2.063 and g_z= 2.276 respectively. Further, hyperfine couplings to ^{59}Co are recorded at A_x= 21.2 G, A_y= 38.8 G and A_z= 115.52. To gain further knowledge about the frontier orbitals, DFT calculations were performed at a BP86/def2-TZVP level of theory. As expected, the z^2 orbital acts as LUMO for this system. The x^2-y^2 acts as SOMO for this system. Concluding, the other three d- orbitals (xy, xz, yz) are filled orbitals: HOMO-1, HOMO-2 and HOMO-3 respectively. A graphical representation of the frontier orbitals of **32** is given in Figure 2.42.

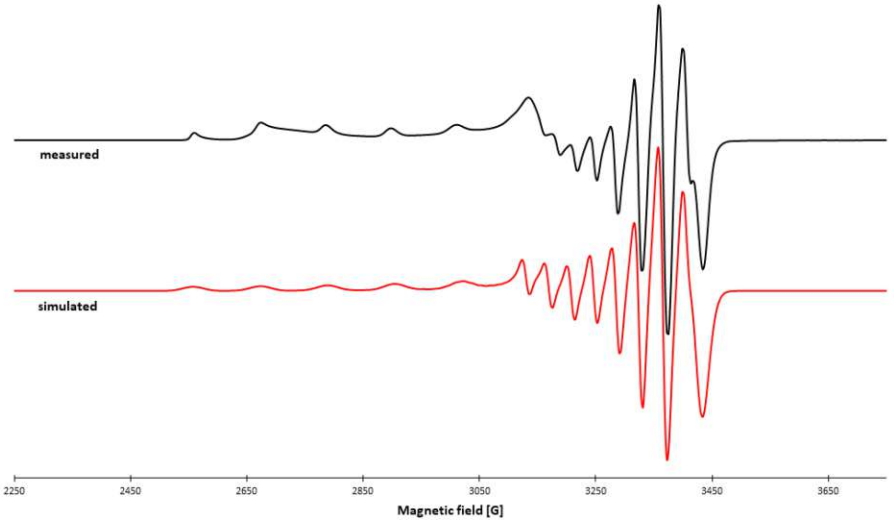

Figure 2.41: X-Band EPR spectrum of [Co-κ^2-(SCS^{CH_2}-tBu)-κ^3-(SCS^{CH_2}-tBu)] **32** in frozen toluene glass at 100 K at a microwave frequency of 9.86 GHz. The red line represents the simulation with g_x= 2.047, g_y=2.063, g_z= 2.276.

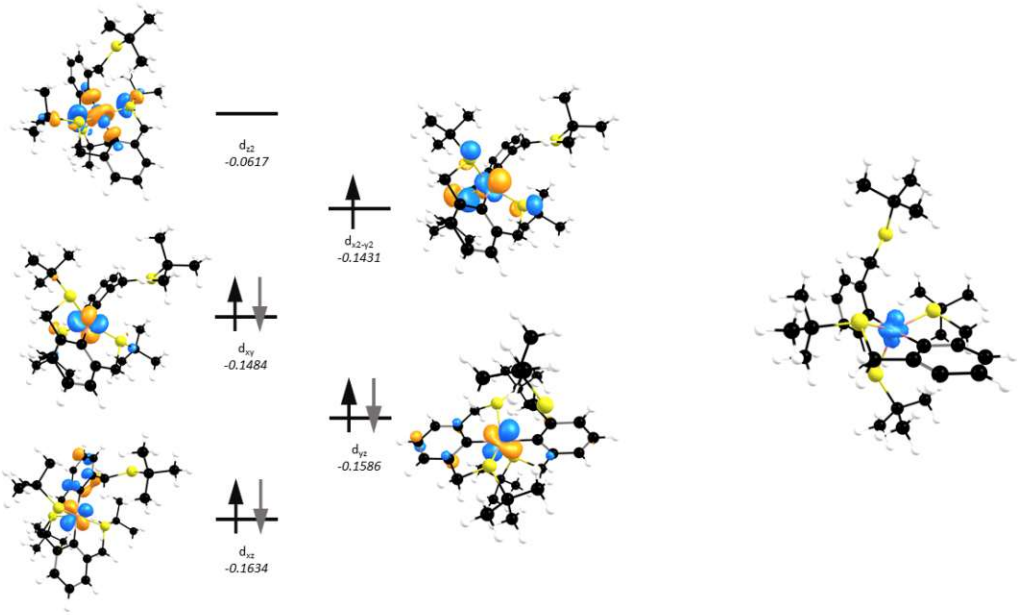

Figure 2.42: left: BP86/def2-TZVP computed frontier orbitals (d-splitting for **32**); right: spin density plot of **32**. Energy values are given in hartrees.Orbitals are computed at an iso-value of 0.05.

When further extracting the residue of the reaction, where **32** has already been extracted, with toluene, a brownish solution is obtained. After workup, dark green crystals which where suitable for single crystal XRD measurements could be obtained by slow diffusion of *n*-pentane into a concentrated DCM solution of **33**.

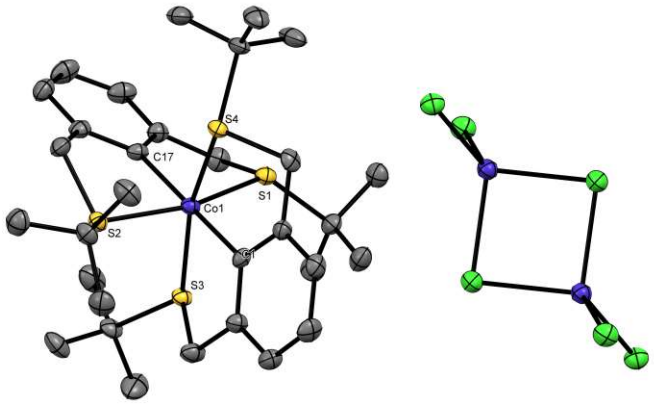

Figure 2.43: Crystal Structure of [Co-(κ^3-SCS^{CH_2}-*t*Bu)$_2$][$Co_2Br_3Cl_3$] (**33**) with 50 % thermal ellipsoids. DCM solvate-molecules are omitted for clarity purposes. Selected bond lengths ($\AA$) and bond angles (°): C1-Co1 1.979, Co1-C17 1.976, S1-Co1 2.252, S2-Co1 2.281, S3-Co1 2.253, S4-Co1 2.272, C1-Co1-C17 176.75, S1-Co1-S2 164.66, S3-Co1-S4 164.90

The structure revealed two ligand-moieties bound to one cobalt center in a κ^3-κ^3 fashion, as a DCM solvate. Interestingly another cobalt-halogen species crystallized in the same structure as well. The question arose, whether unreacted precursor material co-crystallized, or if the complex itself is a cationic species and the cobalt halogen moiety acts as counter-anion. Furthermore, close evaluation of the crystallographic data revealed a statistical miss-order along the halogen atoms of the possible anionic species.
When investigating the crystal packing depicted in figure 2.44, it is obvious, that the cobalt halogen moitey is not unreacted precursor material that co-crystallized. There are reports in literature that proof, that such Co_2Br_6 or Co_2Cl_6 units can act as mono- and dianionic molecules.[110,111] It must be mentioned that the majority of reports are about dianionic behaviour.

Closer observation of the coordination geometry of the pincer-unit visible in the single crystal structure of **33**, gives insight about a slightly distorted octahedral geometry with near linear angles along the three hypothetical axes. Further, quite symmetric bond-lengths are visible, with the *ipso*-carbon cobalt bonds measuring at 1.979 and 1.976 $\AA$ respectively. Additionally, the distances from all sulfur-donor atoms towards the cobalt center are in the range of 2.252 to 2.281 $\AA$.

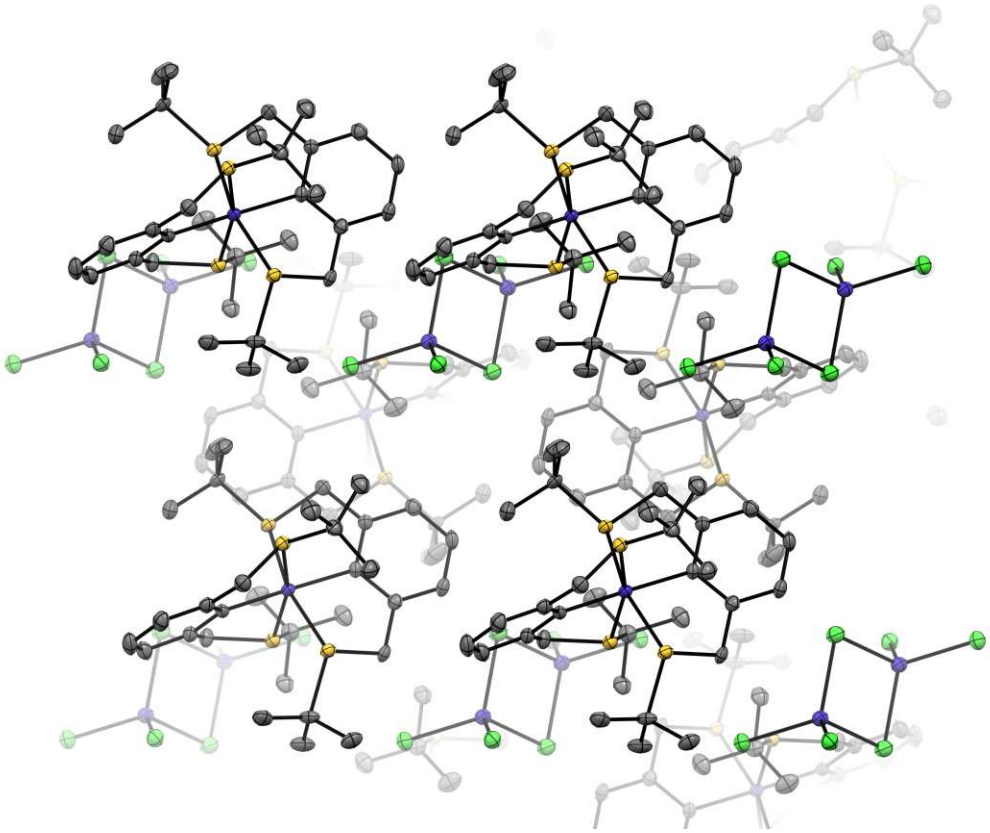

Figure 2.44: Crystal Structure of [Co-(κ^3-SCS^{CH_2}-tBu)$_2$][$Co_2Br_3Cl_3$] (**33**) with 50 % thermal ellipsoids. Crystal-packing of 2x2 unit cells. DCM solvate molecules omitted for clarity.

As literature suggests that these type of anions are di-anionic, it was now of further interest to determine the formal oxidation state of the cobalt-center, as this di-anionic behaviour would impose a cobalt center, in the unusual cobalt(IV) configuration. To now clarify the formal oxidation state of κ^3-κ^3 complex, the crystals obtained were reacted with NaBAr$^F_4$, in d_6-benzene.

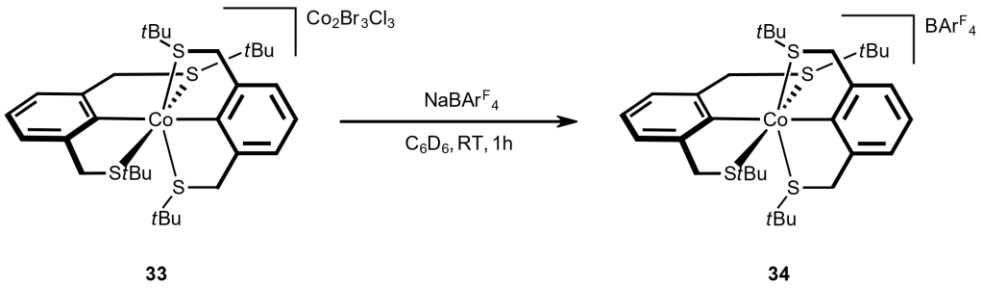

33 **34**

Figure 2.45: Reaction of **33** with NaBAr$^F{}_4$

^{1}H-NMR measurements revealed, that the obtained structure of **33**, contained a cobalt d^6 coordination center in a low-spin configuration, with a formal oxidation state of +3. Interestingly, here the CH_2S-tBu (linker) protons give rise to a sharp singlet at 3.58 ppm in d_6 benzene.
This results yields to the conclusion that, the counter anion must be a mixture of Co(II) and Co(III) centers, featuring one unpaired electron. As can be deduced from the crystal structure, the anionic species is a compound in which the stoichiometry of the chlorine and bromine atoms is statistically distributed. To gain further insights of the properties of the $(Co_2Cl_3Br_3)^{1-}$ moiety, X-band EPR spectroscopy measurements in frozen toluene glass where conducted.

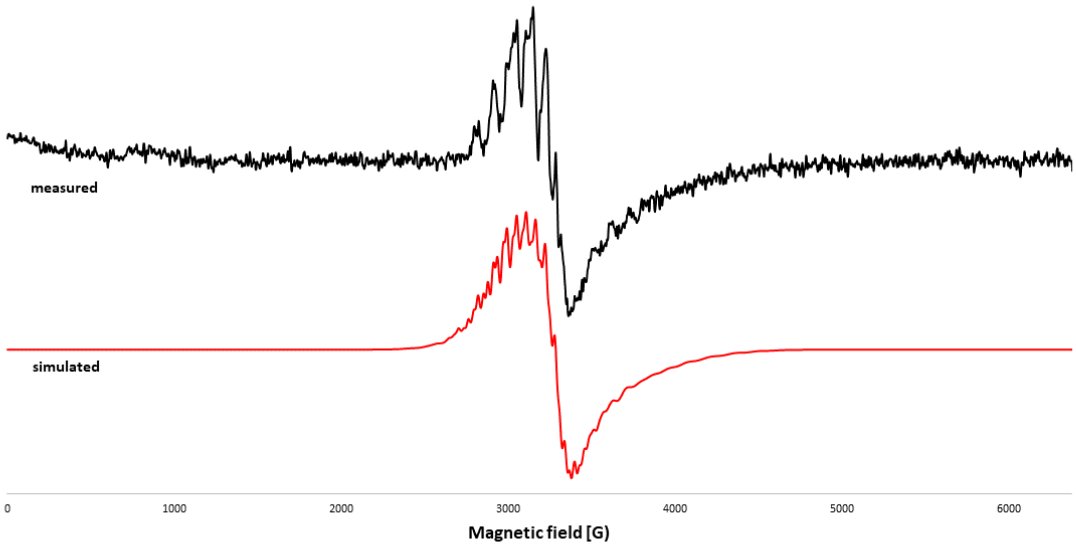

Figure 2.46: X-Band EPR spectrum of the anion of [Co(κ_3-SCS^{CH_2}-tBu)$_2$][$Co_2Cl_3Br_3$] **33** in frozen toluene glass at 100K at a microwave frequency of 9.86 GHz. The red line represents the simulation with $g_x = 2.173$ $g_y = 1.896$ $g_z = 2.048$.

Throughout this methodology the g-values were computed to g_x= 2.173, g_y= 1.896 and g_z= 2.047 respectively , which vary noticeably from the g value of a free electron (g = 2.002). Further, hyperfine couplings to ^{59}Co are recorded at A_x= 29.57 G, A_y= 110.73 G and A_z= 0.019 G for one cobalt center. The hyperfine coupling of the second cobalt atom are given as A_x= 54.3 G, A_y= 148.16 G and A_z= 0.008 G. The theoretical calculation of the spectrum fits the measured result quite well, if the complexity of the calculation is taken into account, which results from the statistical distribution of bromine and chlorine atoms in the anion.

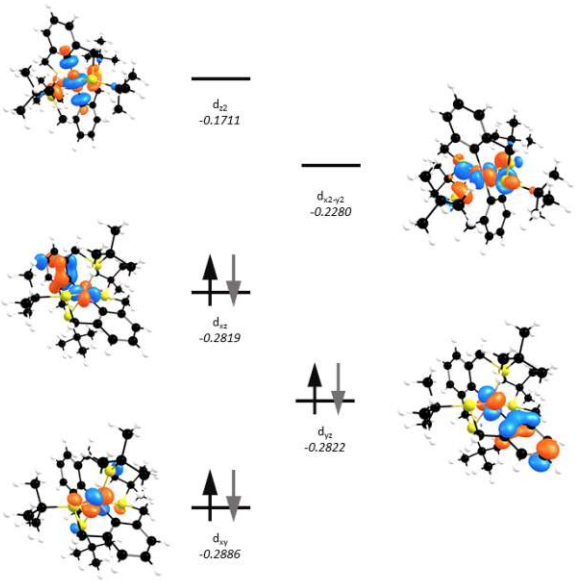

Figure 2.47: BP86/def2-TZVP computed frontier orbitals (d-splitting for **33**). Energy values are given in hartrees.

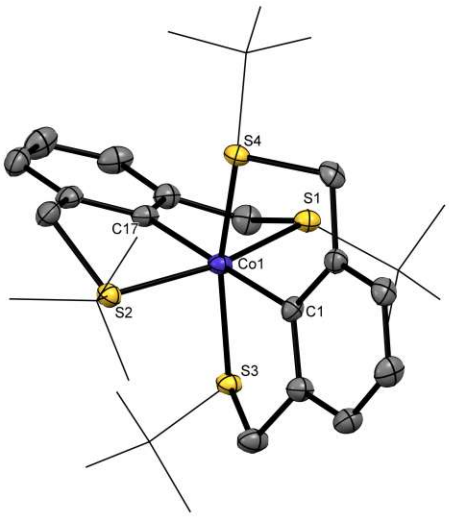

Figure 2.48: Crystal structure of the cationic part of **33**.

To obtain further insights into the electronic properties of the cationic contribution **33**, the complex was investigated by the means of DFT calculations. In line with the expectations for a closed shell d^6 system in a slightly distorted octahedral coordination geometry, the z^2 and the x^2-y^2 orbitals function as LUMO+1 and LUMO. Not surprisingly, the xz orbital is depicted as the HOMO, and the yz and xy orbitals as HOMO-1 and HOMO-2 respectively. The cationic character of **33** is further confirmed by a comparison of the bond-lengths in **33** with those observed in **32**. The observed lengths in **33** are remarkably shorter than those observed in **32**. The difference is not so large when comparing the cobalt-carbon bonds, ie. 1.196-1.979 $\mathring{A}$ in **33** compared to 1.922-1.985 $\mathring{A}$. However, the difference becomes more clear when comparing the distances between the cobalt atoms and the sulfur-donors. There, the distances in **33** measure in the range from 2.252 to 2.281 $\mathring{A}$, whereas in **32** the obtain values between 2.255 and 2.319 $\mathring{A}$.

3 Conclusion and Outlook

The results pointed out in this work have shown that NCN and SCS ligand frameworks differ substantially from known PCP systems. Throughout this work it could be demonstrated that NCN ligands are, for the investigated cases, not capable of undergoing complexation reactions following an oxidative addition pathway. Furthermore it could be outlined, that the outcome of transmetalation reactions in this case are method dependent (e.g. **20**, **21**, **34**). Additionally, these transmetalation protocols did not require expensive auxiliary reagents, like those published in literature. Moreover it could be demonstrated, that in the case of SCS ligands, cobalt when compared to nickel, forms different and unforeseen coordination geometries. Evaluations of the formal oxidation states and electronic properties of these complexes could be successfully determined via a variety of approaches. All compounds were characterized using a multitude of methods such as NMR (and Evans method), IR, EPR and single-crystal XRD-analysis. Furthermore, basic computational investigations of relevant compounds by the means of DFT calculations have been conducted.

The successful isolation of further modified complexes, for example alkylated complexes is of great interest and is subject of current investigations. Moreover, the investigation of possible pathways towards hydridic species of the presented chromium and iron complexes is of high interest, due to the versatile application possibilities of hydride-complexes in catalysis. The evaluation of possible catalytic potentials of all isolated compounds will be subject to further investigations.

"This is Spatel!"

Dr. Wolfi Edel, the other day in the lab

4 Experimental

All manipulations were performed under an inert atmosphere of Argon by using Schlenk techniques or in an MBraun inert-gas glovebox. The solvents were purified according to standard procedures. The deuterated solvents were purchased from Aldrich and dried over molecular sieves. Nitric oxide (NO 2.5) was purchased from MESSER GmbH (Gumpoldskirchen, Austria). ^{1}H, ^{13}C(^{1}H), and COSY NMR spectra were recorded on AVANCE-250, AVANCE-400 and AVANCE-600 spectrometers respectivly. ^{1}H and ^{13}C(^{1}H) NMR spectra were referenced internally to residual protio-solvent and solvent resonances, respectively, and are reported relative to tetramethylsilane . Infrared spectra were recorded in attenuated total reflection (ATR) mode on a PerkinElmer Spectrum Two FT-IR spectrometer. Elemental analysis was performed on an elementar vario MACRO (Elementar Analysensysteme GmbH, Germany) CHNS analyzer. High-resolution mass spectra were recorded on an Agilent 6545 QTOF equipped with an Agilent Dual AJS ESI ion source (Agilent Technologies, Santa Clara, USA). Measured accurate mass data for confirming elemental compositions were typically within 3 parts per million accuracy. In all experiments a direct infusion technique was used, and samples prepared in a glovebox.

Electron Paramagnetic Resonance (EPR) spectra were recorded on an X-band Bruker Elexsys-II E500 CW-EPR spectrometer (Bruker Biospin GmbH, Rheinstetten, Germany) equipped with a high sensitivity cavity (SHQE1119) at 100±1K. The instrument parameters were set as follows: microwave frequency, 9.43 GHz; modulation frequency, 100 kHz, and microwave power, 15.9 mW. The spectra were analyzed using Xepr software and the Anisotropic SpinFit simulation program (both Bruker Biospin GmbH).

4.1 Synthesis of the Ligands

2-Bromo-1,3-bis(bromomethyl)benzene (1)

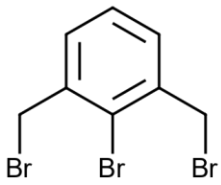

2-bromo-1,3-dimethylbenzene (20 g, 108 mmol) and N-bromosuccinimide (38.41 g, 216 mmol) where suspended in 160 mL CCl_4. The apparatus was flushed with N_2 twice. Then, azobisisobutylnitrile (AIBN) (20 mg, 0.121 mmol) was added to the mixture. Following the addition, the suspension was heated up to reflux for 3h before another 20 mg of AIBN were added in the same fashion. Then the mixture was refluxed overnight. After cooling down to room temperature, the suspension was filtered through a pad of silica, affording a clear solution. After evaporation of the solvent in vacuo the crude product was obtained as off-white solid. Finally, the crude product was recrystallized from *n*-hexane, affording the clean product as off-white needles. (24g, 58% yield)

^{1}**H-NMR** (400 MHz, Chloroform-*d*, 20°C, ppm): δ 7.42 (d, J = 7.6 Hz, 2H, CH), 7.29 (t, J = 8.2, 1H, CH), 4.65 (s, 4H, CH_2)

1,3-bis(bromomethyl)benzene (2)

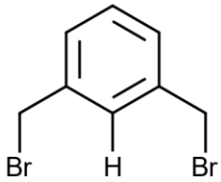

m-Xylene (15 g, 141.2 mmol) and N-bromosuccinimide (50.5 g, 283.7 mmol) and AIBN (20 mg, 0.121 mmol) were suspended in CCl_4 (120 mL). Then the apparatus got flushed with argon prior to heating up to reflux. After 2h at reflux, another tranche of AIBN (20 mg, 0.121 mmol) was added to the mixture. After refluxing over night, the mixture was allowed to cool to room-temperature, before it got filtered through a pad of silica, affording a clear solution. After evaporation of the solvent, the off-white crude product was recrystallized from *n*-hexane three times, to afford the clean product as white needles.(16.5 g, 44% yield)

^{1}**H-NMR** (400 MHz, Methylene Chloride-d_2, 20° C, ppm): δ 7.44 (q, J = 1.3 Hz, 1H, CH), 7.35 (d, J = 1.4 Hz 3H, CH), 4.51 (s, 4H, CH_2).
^{13}**C-NMR** (101 MHz, $CDCl_3$): δ 139.1 (s, *C*-CH_2Br), 130.12 (s, C-H), 129.83 (s, C-H), 129.60 (s, C-H), 33.58(s, C_2Br)

2-Bromo-1,3-bis(dibromomethyl)benzene (3)

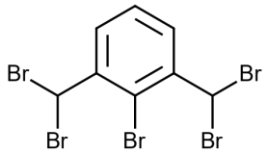

m-Xylene (5 g, 47.1 mmol) and N-bromosuccinimide (33.5 g, 188.4 mmol) and AIBN (20 mg, 0.121 mmol) where suspended in CCl_4 (100 mL). Then the apparatus got flushed with argon prior to heating up to reflux. After 3h at reflux, another tranche of AIBN (20 mg, 0.121 mmol) was added to the mixture. After refluxing over night, the mixture was allowed to cool to room-temperature, before it got filtered through a pad of silica, affording a clear solution. After evaporation of the solvent, the off-white crude product got recrystallized from *n*-hexane to afford the clean product as white needles. (4.1 g, 38% yield)

^{1}**H-NMR** (250 MHz, Chloroform-*d*,20° C, ppm): δ 8.09 (m, 2H, CH), 7.60 (t, J = 7.55 Hz 1H, CH), 7.15 (s, 2H, C*H*Br_2).

2-Bromo-1,3-bis(oxomehtyl)benzene(4)

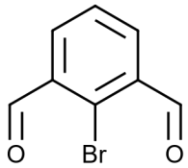

2-Bromo-1,3-bis(dibromomethyl)benzene (**3**) (4 g, 7.9 mmol) was suspended in formic acid (80%, 60 mL) and water (10 mL) and heated up to reflux over night. After cooling down to room temperature, all volatiles were evaporated under reduced pressure. After re-suspending the crude product in water, the product was extracted into DCM. Then, the product was dried over Na_2SO_4 and filtrated. After evaporation of the solvent, the product was obtained as brownish solid.(1.6g, 94 % yield)

^{1}**H-NMR** (250 MHz, Chloroform-*d*, 20° C, ppm): δ 10.55 (s, 2H, C*H*=O), 8.17 (d, J = 8.3 Hz, 2H, C*H*), 7.59 (t, J = 8.2 Hz, 1H, C*H*=O).

4.1.1 NCN-Pincer Ligands

1,1' (2-bromo-1,3-phenylene)-bis-(N,N-dimethylamine)(5)

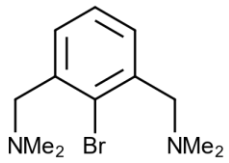

2-Bromo-1,3-bis(bromomethyl)benzene **(1)** (3.3 g, 9.62 mmol) and dimethylamine- hydrochloride (3.8 g, 46.59 mmol) got suspended in $CHCl_3$ (30 mL). Then, triethylamine (70 mL) was added, followed by the admixture of additional $CHCl_3$ (20 mL). The mixture was stirred at room temperature overnight. The reaction mixture was washed with water (300 mL total) and brine (300 mL total). Then the solution was dried with Na_2SO_4 and filtered. After evaporation of the solvent, the crude product was obtained as yellow oil. Purification was achieved via distillation (0.5 mbar, 137° C). The clean product was obtained as colourless oil. (1.3 g, 49% yield)

^{1}**H-NMR** (400 MHz, Chloroform-*d*, 20°C, ppm): δ 7.25 (d, 2H, CH), 7.17 (m, 1H, CH), 3.47 (s, 4H,CH_2), 2.23 (s, 12H, N-CH_3)
^{13}**C-NMR** (101 MHz, $CDCl_3$): δ 138.73 (s, *C*-CH_2), 129.44 (s, CH), 127.01 (s, CH), 126.62 (s, *ipso*C-Br), 64.12 (s, CH_2), 45.64 (s, N-*C*H_3)

1,1' (1,3-phenylene)-bis-(N,N-dimethylamine)(6)

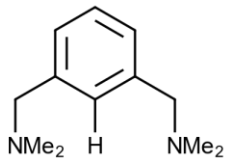

1,3-bis(bromomethyl)benzene **(2)** (3.95 g, 14.96 mmol) and dimethylamine-hydrochloride (2.7 g, 33.10 mmol) got suspended in $CHCl_3$ (30 mL). Then, triethylamine (70 mL) was added, followed by the admixture of additional $CHCl_3$ (20 mL). The mixture was stirred at room temperature overnight. The reaction mixture was washed with water (300 mL total) and brine (300 mL total). Then the solution was dried over Na_2SO_4 and filtrated. After evaporation of the solvent, the crude product was obtained as yellow oil. Purification was achieved via distillation (0.7 mbar, 117° C). The clean product was obtained as light orange oil. (1.1 g, 38 % yield)

^{1}**H-NMR** (400 MHz, methylene-chloride-d_2, 20°C, ppm): δ 7.27 (m, 1H, CH), 7.24(s, 1H, CH), 7.19 (m, 2H ,CH), 3.40 (s, CH_2), 2.21 (d, J = 1.0 Hz, 12 H, N-CH_3)
^{13}**C-NMR** (101 MHz, methylene-chloride-d_2): δ 139.88 (s, *C*-CH_2), 130.17 (s, CH), 128.45 (s, C-H), 126.57 (s,*ipso*-C-H), 64.79 (s, *C*H_2), 45.74 (s, N-*C*H_3)

1,1' (2-bromo-1,3-phenylene)-bis-(N,N-diethylamine)(7)

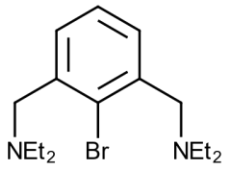

2-bromo-1,3-bis(bromomethyl)benzene **(1)** (3 g, 8.75 mmol) was suspended in toluene (30 mL). Then a solution of diethylamine (2.68 g, 36.75 mmol) in toluene (25 mL) was added in a dropwise fashion. After about 30 minutes, the formation of a white precipitate could be observed. The mixture was stirred at room temperature overnight. The reaction mixture was filtered, followed by the evaporation of all volatiles under reduced pressure. Purification was achieved via distillation (0.7 mbar, 151° C). The clean product was obtained as light yellow oil. (2.4 g, 84 % yield)

^{1}**H-NMR** (400 MHz, methylene-chloride-d_2, 20°C, ppm): δ 7.43 (d, J = 7.5 Hz, 2H, CH), 7.25(t, J = 7.5 Hz, 1H, CH), 3.64 (s, 4H,CH_2), 2.56 (q, J = 7.1 Hz, 8H, N-CH_2), 1.03 (t, J = 7.1 Hz, 12 H, N-CH_3)
^{13}**C-NMR** (101 MHz, methylene-chloride-d_2): δ 140.49(s, C-CH_2), 129.19 (s, CH), 126.97(s, C-H), 126.34(s, C-Br), 58.56 (s,CH_2), 64.02(s, CH_2CH_3), 45.64(s, CH_2CH_3)

1,1' (2-bromo-1,3-phenylene)-bis-(N,N-diisopropylamine)(8)

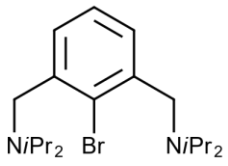

2-bromo-1,3-bis(bromomethyl)benzene **(1)** (3 g, 8.75 mmol) was suspended in toluene (30 mL). Then a solution of diisopropylamine (3.72 g, 36.75 mmol) in toluene (25 mL) was added in a dropwise fashion. After about 30 minutes, the formation of a white precipitate could be observed. The mixture was stirred at room temperature overnight. The reaction mixture was filtered, followed by the evaporation of all volatiles under reduced pressure. Purification was achieved via recrystallisation from n-hexane. The clean product was obtained as slighty orange, resinous solid. (3.1 g, 92% yield)

^{1}**H-NMR** (400 MHz, benzene-d_6, 20°C, ppm): δ 7.77 (dt, J = 7.6, 0.8 Hz, 2H, CH), 7.28 (t, J = 7.6 Hz, 1H, CH), 3.88 (s, 4H, CH_2), 2.94 (dt, J = 13.6, 6.6 Hz, 4H, N-CH_2), 0.94 (d, J = 6.6 Hz, 24 H, N-$CHCH_3$)
^{13}**C-NMR** (101 MHz, benzene-d_6): δ 141.77(s, C-CH_2), 128.23 (s, CH), 126.57(s, C-H), 124.44(s, C-Br), 49.80 (s,CH_2), 48.65 (s, N-$CH(CH_3)_2$, 20.53(s, N-$CHCH_3$))$_2$

(N,N' E,N,N'E)-N,N'((2-bromo- 1,3-phenylene)bis(methanylylidene))bis(2,4,6-trimethylaniline) (9)

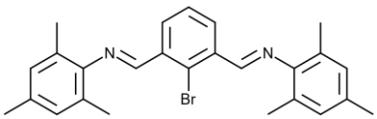

2-Bromo-1,3-bis(oxomehtyl)benzene **(4)** (1.5 g, 7.04 mmol) was dissolved in warm MeOH (35 mL, at 50° C) followed by the addition of 2,4,5-trimethylaniline (2.1 g, 15.5 mmol) via a syringe in a dropwise fashion. After stirring the mixture for 10 minutes, the product crystallized spontaneously from the reaction mixture. The crystals were collected via a glas frit, and washed with cold MeOH. Drying under reduced pressure afforded the clean product as bright yellow solid. (2.86 g, 91% yield)

^{1}**H-NMR** (400 MHz, methylene-chloride-d_2, 20°C, ppm): δ 8.77 (d, J = 0.6 Hz, 2H, CH=N), 8.41 (d, J = 7.7 Hz, 2H, CH), 7.61 (tt, J = 7.6, 0.7 Hz, 1H, CH), 6.95 (d, J = 0.7 Hz, 4H, *mesitylene*-CH), 2.32 (s, 6H, mesitylene -p - CH_3), 2.19 (s, 12H, mesitylene -o - CH_3).
^{13}**C-NMR** (101 MHz, methylene-chloride-d_2, 20°C): δ 161.79 (s, C=N), 148.36 (s,C-N), 135.78 (s,p-C-CH$_3$), 133.39 (s, *mesitylene*-CH), 131.18 (s, C-C=N), 128.73 (s, o-CCH$_3$), 128.18 (s, C-Br), 127.75 (s, CH), 126.88 (s, CH), 20.44 (s, p-CH$_3$), 18.05 (s, oCH$_3$)

4.1.2 SCS-Pincer Ligands

((2-bromo-1,3-phenylene)bis(methylene))bis(tert-butylsulfane) (10)

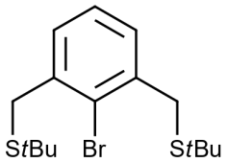

Tert-butylmercaptane (1.65 g, 18.37 mmol) was added to a NaOH (1.13 g, 26.26 mmol)-solution in dry methanol (35 mL) which resulted in a slight yellow colouration of the solution. 2-bromo-1,3-bis(bromomethyl)benzene **(1)** (3.00 g, 8.75 mmol) was added to the solution. The reaction mixture was stirred for 3 h at room temperature. After addition of water (15 mL) and diethylether (50 mL), a white precipitation was observed and the phases got separated. The aqueous phase got extracted with additional diethylether (15 mL). The combined organic phases were washed with a 10 % NaOH solution, dried over magnesium sulfate and the solvent removed. The product was obtained as a colourless solid (3 g, 93 % yield).

^{1}**H-NMR**(400 MHz, chloroform-d, 20° C, ppm): δ 7.34 (d, J = 7.5 Hz, 2H, ph), 7.21 (t, J = 7.0 Hz, 1H, ph), 3.95 (s, 4H, CH2), 1.41 (s, 18H).
^{13}**C-NMR** (101 MHz, chloroform-d): δ 138,98 (s, C-CH$_2$), 129.58 (s, CH), 128.98 (s, C-Br), 127.14 (s, C-H), 43.03 (s,C(CH$_3$)$_3$), 34.37 (s, CH$_2$), 30.61 (s, S-C(CH$_3$)$_3$)

((2-bromo-1,3-phenylene)bis(methylene))bis(ethylsulfane)(11)

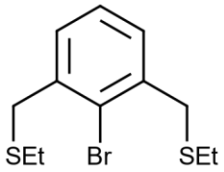

Ethanethiol (1.14 g, 18.37 mmol) was added to a NaOH (1.13 g, 26.26 mmol)-solution in dry methanol (35 mL) which resulted in a slight yellow colouration of the solution. 2-bromo-1,3-bis(bromomethyl)benzene **(1)**(3 g, 8.75 mmol) was added to the solution. The reaction mixture was stirred for 3 h at room temperature. After addition of water (15 mL), brine (10 mL) and diethylether (50 mL), a white precipitation was observed and the phases got separated. The aqueous phase was extracted with additional diethylether (15 mL). The combined organic phases were washed with a 10 % NaOH solution, dried over magnesium sulfate and the solvent removed. The product was obtained as a colourless solid (2.43g, 91 % yield).

^{1}**H-NMR**(400 MHz, methylene-chloride-d_2, 20° C, ppm): δ 7.26 (m, 1H, ph), 7.24 (t, 2H, ph), 3.88 (s, 4H, CH2), 2.52 (q, J = 7.4 Hz, 4H, S-CH_2), 1.25 (t, J = 7.4 Hz, 6H, S-CH_3). ^{13}**C-NMR** (101 MHz, methylene-chloride-d_2): δ 139.26 (s, C-CH_2), 129.23 (s, CH), 126.8 (s, C-H), 126.42 (s, C-Br), 37.04 (s,CH_2), 25.82 (s, S-CH_2CH_3), 14.39 (s, S-CH_2CH_3)

1-Adamantanethiol (12)

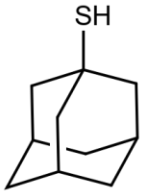

1-Bromoadamantane (4.2 g, 19.52 mmol) was suspended in glacial acetic acid (20 mL). Then, thiourea (3 g, 39.41 mmol) and 45% hydrobromic acid (9.8 mL) were added subsequently. The mixture was refluxed at 115° C under an argon atmosphere for 5h. Then the mixture was allowed to cool down to room-temperature and was stirred at that temperature overnight. The synthesized iso-thiouroniuimsalt was then filtered and subsequently hydrolyzed with aqueous NaOH (3.95 g, 98.75 mmol, in 80 mL) and ethanol (30 mL), allowing the mixture to stir for 24h. After acidification of the obtained solution with 2M HCl (50 mL), the product was extracted with chloroform, DCM and petrolether subsequently (60 mL each). The combined organic layers got were dried over Na_2SO_4, filtered and all volatiles evaporated under reduced pressure. The product was obtained as resinous, colourless solid. (2.50 g, 76.10% yield)

^{1}**H-NMR**(400 MHz, methylene-chloride-d_2, 20° C, ppm): δ 1.92 (m, 3H), 1.84 (d, J = 2.9 Hz, 6H), 1.59 (m, 6H, CH_2)

^{13}**C-NMR** (101 MHz, methylene-chloride-d_2): δ 47.54 (s, S-C), 35.76 (s, CH$_2$), 30.28(s, CH)

((2-bromo-1,3-phenylene)bis(methylene))bis(adamantylsulfane) (13)

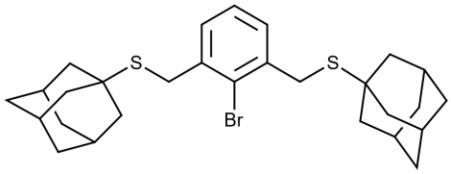

1-Adamantanethiol (**12**) (1 g, 5.94 mmol) was added to a NaOH (0.71 g, 17.82 mmol)-solution in dry methanol (50 mL) which resulted in a slight yellow colouration of the solution. 2-bromo-1,3-bis(bromomethyl)benzene **(1)**(0.97 g, 2.83 mmol) was added to the solution. The reaction mixture was stirred for 5 h at room temperature. After addition of water (20 mL), brine (10 mL) and diethylether (30 mL), a white precipitation was observed and the phases got separated. The aqueous phase got extracted with additional 20 mL diethylether. The combined organic phases were washed with a 10 % NaOH solution, dried over Na_2SO_4 and the solvent removed. The product was obtained as a colourless solid (1.1 g, 97 % yield).

^{1}**H-NMR**(400 MHz, methylene-chloride-d_2, 20° C, ppm): δ 7.23 (d, J = 7.5 Hz, 2H, CH), 7.11 (dd, J = 8.2, 7.0 Hz, 1H, CH), 3.82 (s, 4H, CH_2), 1.99 – 1.94 (m, 6H), 1.84 (d, J = 3.0 Hz, 12H), 1.65 – 1.61 (m, 12H).
^{13}**C-NMR** (101 MHz, methylene-chloride-d_2): δ 139.26 (s, C-CH$_2$), 129.23 (s, CH), 126.8 (s, C-H), 126.42 (s, C-Br), 37.04 (s,CH$_2$), 25.82 (s, S-CH$_2$CH$_3$), 14.39 (s, S-CH$_2$$CH_3$)

4.2 Synthesis of the Complexes

$[Co(MeCN)_2(THF)_4][Co(CO)_4]_2$ (14)

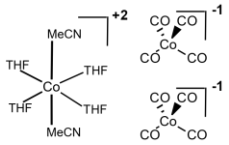

The ligand **(9)** (100 mg, 0.22 mmol) and Co_2CO_8 (76 mg, 0.22mmol) where heated up to 80 °C in MeCN (3.5 mL) in a closed microwave reaction vial. After 4h the dark turbid solution was allowed to cool down to room-temperature. After evaporation of the solvent, the residue was extracted into toluene (5 mL total) and filtered through a short pad of celite. After evaporation of the solvent, the residue was washed with *n*-pentane twice (2 mL each), yielding a dark brown residue. The product was crystallized by the slow diffusion of *n*-pentane into a saturated THF solution and obtained as dark green crystals, suitable for single crystal XRD analysis. (108 mg, 63% yield)
IR(ATR, cm^{-1}): 1835 (ν_{CO})

4.2.1 NCN Pincer Complexes

$[Ti(NCN^{CH_2}\text{-Et})Cl_3]$ (15)

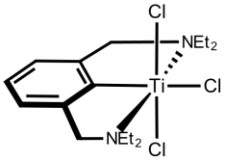

The ligand **(7)** (75 mg, 0.23 mmol) was dissolved in THF (5 mL) and subsequently cooled to -90° C. After stirring at that temperature for 5 minutes, *n*-BuLi (0.15 mL, 1.6 M, 0.24 mmol) was added in a dropwise fashion, yielding a clear yellow solution. This solution was kept at low temperatures for additional 10 minutes before it was allowed to warm up to 0° C. Then, it was added in a dropwise fashion to a solution of $TiCl_4(THF)_2$ (80 mg, 0.24 mmol) in THF (5 mL), forming a red/brown solution immediately. The mixture was left stirring for additional 15 minutes before the solvent was evaporated under reduced pressure. The residue was extracted into toluene (5 mL) and filtrated through a syringe filter (PTFE, 0.2 μm). The clear, dark red solution was reduced to about 1 mL, before the product was precipitated via the addition of *n*-pentane (10 mL). The mother liquor was decanted of, and the residue was washed with additional *n*-pentane (2 mL). After drying the residue under reduced pressure, a brown solid was obtained. (54 mg, 58% yield)

^{1}**H-NMR**(250 MHz, methylene-chloride-d_2, 20° C, ppm): δ 7.52 (s, CH), 7.25 (d, J = 11.9 Hz, 2H, CH), 3.58 (d,J = 2.5 Hz, 4H, CH_2), 2.56 – 2.52 (m, 8H), 1.08 - 1.04 (m, 12H)

[Cr(NCN^{CH_2}-Et)(THF)Cl$_2$](16)

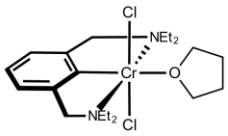

The ligand **(7)** (400 mg, 1.23 mmol) was dissolved in 13 ml THF and subsequently cooled to -90 °C. After stirring at that temperature for 10 minutes, *n*-BuLi (1.52 mL, 1.6M, 2.46 mmol) was added dropwise via a syringe. The light yellow solution was stirred at -90 °C for 2.5h. After warming up to -30°C, neat $CrCl_3(THF)_3$ (460 mg, 1.23 mmol) was added portion-wise under stirring, resulting in the formation of a dark green solution. The solution was allowed to warm up to room temperature and left stirring overnight. After evaporation of the solvent, the green residue was taken up in dry toluene (7 mL) and filtered trough a pad of celite. After removal of the toluene, the purple residue was washed 3 times with *n*-pentane (10 mL each). Careful drying under reduced pressure yielded a light-purple solid (340mg, 63 % yield). Crystals suitable for X-ray crystallography could be obtained via slow diffusion of *n*-pentane into a saturated THF solution of **(16)** as dark green crystals. μ_{eff} =3.7(2)μ_B (Evans Method, d_8-THF)

[Cr(NCN^{CH_2}-Me)(THF)Cl$_2$](17)

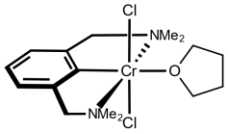

The ligand **(5)** (100 mg, 0.36 mmol) was dissolved in 7 ml THF and subsequently cooled to -90° C. After stirring at that temperature for 10 minutes, *n*-BuLi (0.46 mL, 1.6M, 0.73 mmol) was added dropwise via a syringe. The light yellow solution was stirred at -90° C for 2.5h. After warming up to -30° C, neat $CrCl_3(THF)_3$ (133.8 mg, 0.36 mmol) was added portionwise during stirring, resulting in the formation of a dark green solution. The solution was allowed to warm up to room temperature and left stirring overnight. After evaporation of the solvent, the light green residue was taken up in dry toluene (5 mL) and filtered trough a pad of celite. After removal of the toluene, the light green residue was washed 3 times with *n*-pentane (3mL each). Careful drying under reduced pressure yielded a light-green solid. (95 mg, 68 % yield) μ_{eff} =3.7(4)μ_B (Evans Method, d_8-THF)

[Cr(NCN^{CH_2}-*i*Pr)Cl$_2$](18)

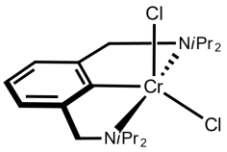

The ligand **(8)** (100mg, 0.24 mmol) was dissolved in 7 ml THF and subsequently cooled to -90 °C. After stirring at that temperature for 10 minutes, *n*-BuLi (0.21 mL, 1.6 M, 0.35 mmol) was added dropwise via a syringe. The light yellow solution was stirred at -90° C for 2.5h. After warming up to -30° C, neat $CrCl_3(THF)_3$ (112 mg, 0.30 mmol) was added portionwise during stirring, resulting in the formation of a dark, mud-green solution. The solution was allowed to warm up to room temperature and left stirring overnight. After evaporation of the solvent, the light green residue was taken up in dry toluene (5 mL) and filtered trough a pad of celite. After removal of the toluene, the light green residue was washed 3 times with *n*-pentane (3 mL each). Careful drying under reduced pressure yielded a olive-green solid. (70 mg, 63 % yield) μ_{eff} =3.7(2)μ_B (Evans Method, d_8-THF);

[Cr(NCN^{CH_2}-Et)Cl](19)

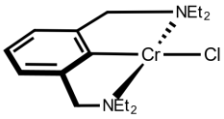

The ligand **(7)** (150 mg, 0.45 mmol) was dissolved in 9 mL THF and subsequently cooled to -90 °C. After stirring at that temperature for 10 minutes, *n*-BuLi (0.37 mL, 1.6M, 0.59 mmol) was added dropwise via a syringe. The light yellow solution was stirred at -90 °C for 2.5h. After warming up to 0° C, neat $CrCl_2$ (53 mg, 0.43 mmol) suspended in THF (5mL) was added drop-wise under stirring, resulting in the formation of a dark purple solution. The solution was allowed to warm up to room temperature and left stirring for additional 15 minutes. After evaporation of the solvent, the dark residue was taken up in *n*-pentane (7 mL) and filtered trough a syringe filter (PTFE, 0.2 μm). Careful drying under reduced pressure yielded a dark-purple solid (88 mg, 58 % yield). Crystals suitable for X-ray crystallography could be obtained by cooling a saturated solution of **(19)** in *n*-pentane to -30° C. μ_{eff} =4.7(8)μ_B (Evans Method, d_6-benzene)

[Cr-(κ^2-NCN^{CH_2}-*i*Pr)$_2$](20)

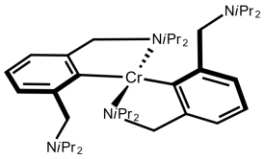

The ligand **(8)** (100 mg, 0.26 mmol) was dissolved in 7 ml THF and subsequently cooled to -90° C. After stirring at that temperature for 10 minutes, n-BuLi (0.18 mL, 1.6 M, 0.30 mmol) was added dropwise via a syringe. $CrCl_2$ (38 mg, 0.30 mmol) got suspended in 4 ml THF and further suspended, partly dissolved by placing vial containing the suspension in an ultrasonic-bath for 30 minutes. The now light blue suspension was added in a dropwise fashion to a still cold, light yellow solution of the afore prepared lithium-species. This resulted in the immediate formation of a dark blue solution. After the addition was completed, all volatiles got immediately removed under reduced pressure. The residue was extracted with *n*-pentane (6 mL total) and filtered through a syringe filter (PTFE, 0.2 μm).The solvent was removed under reduced pressure, yielding a blue/black solid. Crystals suitable for X-ray crystallography where obtained by cooling a saturated *n*-pentane solution to -30° C as sapphire blue cuboids. (45mg, 37% yield, calculated to the toal amount of ligand utilized)μ_{eff} =4.7(3)μ_B) (Evans Method, d_6-benzene)

[Cr(NCN^{CH_2}-*i*Pr)Cl](21)

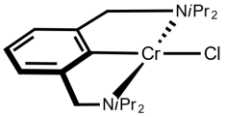

$CrCl_2$ (38 mg, 0.30 mmol) was suspended in THF (15 ml) and then placed in an ultrasonic bath for 1h to form a light blue solution. The ligand **(6)** (100mg, 0.26 mmol) was dissolved in THF (5 ml) and subsequently cooled to -90° C. After stirring at that temperature for 10 minutes, *n*-BuLi (0.18 mL, 1.6M, 0.30 mmol) was added dropwise via a syringe. The orange solution was further stirred at that temperature for 30 minutes, before it was allowed to warm up to 0° C over the course of an hour. Then it was further left stirring at that temperature for another hour. Then the lithiated species was added in a dropwise fashion to the produced THF-solution of $CrCl_2$. Upon addition, a dark, purple to black coloured solution formed immediately. The solution was allowed to stir for 15 minutes at room temperature before all volatiles where evaporated in vacuo. The dark residue was extracted into *n*-pentane (7 mL in total) and filtered through a syringe filter (PTFE, 0.2 μm). The filtrate was reduced (1.5 mL of total volume) and left at -30° C to afford the complex as dark purple crystalline plates, which were suitable for X-ray diffraction analysis. The mother liquor was decanted off and the crystals where dried under reduced pressure to obtain a near black crystalline solid. (75 mg, 73% yield) μ_{eff} =4.8(5)μ_B (Evans Method, d_6-benzene)

[Cr(NCN^{CH_2}-*i*Pr)(NO)Cl](22)

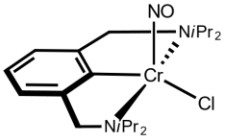

Nitric oxide was injected into the headspace of a prepared solution of [Cr(NCN^{CH_2}-*i*Pr)Cl] **(21)** (50 mg, 0.12 mmol) in toluene (6 mL) at room temperature. Upon exposure, the colour of the solution immediately changed from a mud green colour to an intensive red. The solution was left stirring for additional 30 minutes, before all volatiles got evaporated in vacuo. The product could be obtained as a dark red solid. (51 mg, 95 % yield)

IR(ATR, cm^{-1}): 1702 (ν_{NO})

[Fe(NCN^{CH_2}-*i*Pr)Br](23)

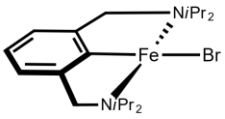

$FeBr_2$ (59 mg, 0.27 mmol) was dissolved in THF (7 mL) to give an orange solution. A solution of the ligand **(8)** (100 mg, 0.26 mmol) in THF (5mL) was cooled to -80° C. After stirring at that temperature for 10 minutes, *n*-BuLi (0.18 mL, 1.6 M, 0.30 mmol) was added dropwise via a syringe. The orange solution was further stirred at that temperature for 30 minutes, before it was allowed to warm up to 0° C over the course of an hour. Then it was further left stirring at that temperature for another hour. Then the lithiated species was added in a dropwise fashion to the produced THF-solution of $FeBr_2$. The resulting dark yellow to brown mixture was further stirred at room temperature for 1 hour, before all volatiles got evaporated in vacuo. The remaining brown residue was extracted with *n*-pentane (20 mL) and filtered through a syringe filter (PTFE, 0.2 μm). The resulting clear yellow solution was reduced to a volume of 5 mL, before it was filtered through a syringe filter (PTFE, 0.2 μm) again. The filtrate was then kept at -30° C for a week,during which a yellow amorphous solid precipitated. (57 mg, 51 % yield) $\mu_{eff} = 2.8(5)\mu_B$ (Evans Method, d_6-benzene)

[Fe(NCN^{CH_2}-*i*Pr)(NO)Br](24)

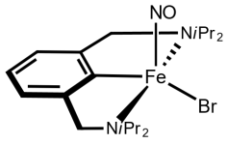

Nitric oxid was injected into the headspace of in situ generated **(23)** (following the same protocol as described in **(23)**) in toluene (5 mL) at room temperature, whereupon the colour changed from a dark yellow to intensive red immediately. After 20 minutes, all volatiles were evaporated in vacuo, yielding a dark red solid. **(24)** was not obtained in pure form, because it was not separable from putative **(25)**.

IR(ATR, cm^{-1}): 1773 (ν_{NO})

[Fe(NCN^{CH_2}-*i*Pr)(NO)]Br(25)

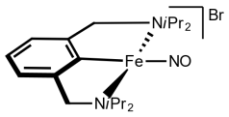

Nitric oxid was injected into the headspace of in situ generated **(23)** (following the same protocol as described in **(23)**) in toluene (5 mL) at room temperature, whereupon the colour changed from a dark yellow to an intensive red immediately. After 20 minutes, all volatiles were evaporated in vacuo, yielding a dark red solid. **(25)** was not obtained in pure form, because it was not separable from **(24)**.

IR(ATR, cm^{-1}): 1702 (ν_{NO})

Reaction towards [Fe(NCN^{CH_2}-*i*Pr)(NO)](NO$_3$(26)

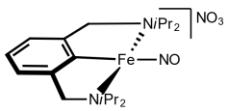

The residue from **(24/25)** (50 mg) was treated with $TlNO_3$ (52 mg, 0.19 mmol) in degassed acetone (5 mL) and was left stirring at room temperature for 24 hours. After 2 hours, a white/grey solid started precipitating. The mixture was filtered through a pad of celite, followed by the removal of the solvent. The dark red residue was re-extracted into DCM, and filtered through a pad of celite again. After removal of the solvent, a dark red solid was obtained. **24** could not be separated completely. μ_{eff} =1.9(3)μ_B (Evans Method, d_2-DCM), measured from the mixture of **24** and **26**.
IR(ATR, cm^{-1}): 1701 (ν_{NO}), 1366 (ν_{NO_3})

[Fe(NCN^{CH_2}-*i*Pr)(CO)$_2$Br](27)

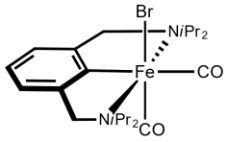

(23) was generated in situ: $FeBr_2$ (59 mg, 0.27 mmol) was dissolved in THF (7mL) to give an orange solution. A solution of **(8)** (100 mg, 0.26 mmol) in THF (5mL) was prepared and *n*-Buli was added dropwise at room temperature. The orange solution was stirred for 15 additional minutes before it was added in a dropwise fashion to the $FeBr_2$ solution. The resulting dark yellow to brown solution was stirred for additional 10 minutes before all volatiles where evaporated in vacuo. The following workup was conducted in analogy to as previously described for **(23)**, with the variation that the remaining solution was reduced to a volume of 10 mL. In the headspace of this yellow *n*-pentane solution of [Fe(NCN^{CH_2}-*i*Pr)Br] **(23)** carbon monoxide gas was injected at room temperature. This resulted in a intense green colouration of the forming suspension. The suspension was further stirred at a CO pressure of 1 bar for additional 10 minutes before all volatiles got evaporated in vacuo. The residue was extracted with of *n*-pentane (15 mL) and the extract was filtered through a a syringe filter (PTFE, 0.2 μm). After evaporation of the solvent, the product could be obtained as green solid. (54 mg, 50% yield)

IR(ATR, cm^{-1}): 2022, 1920 (ν_{CO})

[Co$_2$(NCN^{CH_2}-*i*Pr)Br$_3$](28)

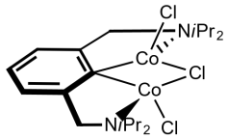

$CoCl_2$ (28 mg, 0.21 mmol) got suspended in THF (10 mL) and placed in an ultrasonic bath for 30 minutes to form an intense blue solution. The ligand **(6)** (75 mg, 0.19 mmol) was dissolved in 5 mL THF and subsequently cooled to -90° C. After stirring at that temperature for 10 minutes, *n*-BuLi (0.14 mL, 1.6M, 0.22 mmol) was added dropwise via a syringe. The orange solution was further stirred at that temperature for 30 minutes, before it was allowed to warm up to 0° C over the course of 30 minutes. Then, the lithiated ligand was added in a dropwhise fashion to the intense blue solution of $CoCl_2$, forming a dark solution. The mixture was allowed to stir for additional 20 minutes before all volatiles got evaporated under reduced pressure. The black residue was extracted into toluene/ *n*-pentane (50:50 mixture, 10 mL total) and filtered through a syringe filter (PTFE, 0.2 μm). The dark solution was reduced to 5 mL and stored at -30° C, whereupon dark green crystals suitable for XRD measurements precipitated from the solution. (45 mg, 39% yield (calculated to the ligand)) μ_{eff} =5.3(3)μ_B (Evans Method, d_8-toluene)

4.2.2 SCS Pincer Complexes

[Ni(SCS^{CH_2}-*t*Bu)Br](29)

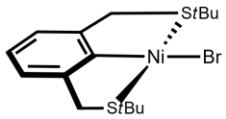

$Ni(COD)_2$ (80 mg, 0.28 mmol) was dissolved in THF (13 mL) and cooled to -90° C. Then, a prepared solution of **(10)**(100 mg, 0.28 mmol) in THF (4 mL) was added dropwise to the solution. The mixture was stirred for 30 minutes at -90° C, then allowed to warm up to room-temperature, and stirred for additional 2.5 h, whereupon a change in color towards red took place. After evaporation of the solvent, the residue got extracted into toluene (6 mL) and filtrated through a pad of celite. The volume of the filtrate was reduced to about 1 mL. Then, the product was precipitated upon addition of *n*-pentane (12 mL). After evaporation of all volatiles under reduced pressure, the residue was washed thrice with *n*-pentane (4 mL each) and dried in vacuo. Crystals suitable for X-ray crystallography could be obtained via two ways: *n*-pentane diffusion into a saturate DCM solution or via slow evaporation of DCM at RT. The product was obtained as orange powder. (91 mg, 78% yield)
^{1}**H-NMR** (400 MHz, Methylene Chloride-d_2, 20° C, ppm): δ 6.89 (dd, J = 8.0, 7.0 Hz, 1H), 6.77 (d, J = 7.9 Hz, 2H), 4.05 (s, 4H), 1.59 (s, 18H).
^{13}**C-NMR** (101 MHz, Methylene Chloride-d_2, 20° C, ppm): δ 154.51 (s, CH), 151.58 (s, *ipso*-C), 124.88 (s, *C*-CH_2), 120.61 (s, CH), 51.27 (s, CCH_3) , 43.33 (s, CH_2), 30.77 (s, CH_3)

[Ni(SCS^{CH_2}-Et)Br](30)

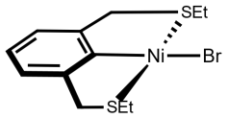

$Ni(COD)_2$ (75 mg, 0.27 mmol) was dissolved in THF (13 mL) and cooled to -90° C. Then, a prepared solution of **(11)** (91 mg, 0.29 mmol) in THF (4 mL) was added dropwise to the solution. The mixture was stirred for for 30 minutes at -90° C, then allowed to warm up to room-temperature, and stirred for additional 2.5 h, whereupon a dark yellow colouration took place. After evaporation of the solvent, the residue got extracted into toluene (6 mL) and filtrated through a pad of celite. The volume of the filtrate was reduced to about 1 mL. Then the product was precipitated upon addition of *n*-pentane (12 mL). After evaporation of all volatiles under reduced pressure, the residue was washed thrice with *n*-pentane (3 mL each) and dried in vacuo. The product was obtained as yellow powder. (75 mg, 76% yield)

^{1}**H-NMR** (400 MHz, Methylene Chloride-d_2, 20° C, ppm): δ 6.87 (dd, J = 8.1, 6.9 Hz, 1H, CH), 6.75 (m, 2H, CH), 4.02 (s, 4H, CH_2), 3.00 (q, J = 7.3 Hz, 4H, SCH_2), 1.49 (t, J = 7.3 Hz, 6H, CH_3).

[Ni(SCS^{CH_2}-Ad)Br](31)

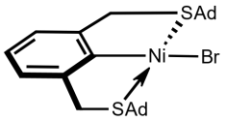

The ligand **(13)** (100mg, 0.19 mmol) and nickel powder (60 mg, 1.02 mmol) were heated up to 135°C in MeCN (3.5 mL) in a closed microwave vial. After 6 h a slight yellow coloration took place, which, after completed reaction time (4 days) changed to a orange/brown colour. After allowing the solution to cool down to room temperature, the mixture was diluted with additional MeCN (4 mL) and filtered through a syringe filter (PTFE, 0.2 μm). After evaporation of the solvent, the crude product was purified via silica gel chromatography (DCM:PE 2:1). Product was obtained as intense orange solid. (71 mg, 63 % yield)

^{1}**H-NMR**(400 MHz, methylene-chloride-d_2): δ 6.78 (dt, J = 8.0, 6.8 Hz, 1H, CH), 6.65 (dd, J = 14.5, 7.5 Hz, 2H, CH), 3.91 (d, 4H, CH_2), 2.14 (dd, J = 6.1, 3.1, 12H), 2.02 (t, J = 3.4 Hz, 6H), 1.64 (q, J = 2.9 Hz, 12H).
^{13}**C-NMR** (101 MHz, methylene-chloride-d_2): δ 152.23 (s, C-CH_2), 124.43 (s, CH), 120.24(s, C-H), (C-Ni not detected), 43.13 (s,CH_2), 35.87 (d, J = 4.6 Hz, S-CHCH$_2$-Ad), 30.31 (d, J = 3.8 Hz, S-CH$_2$$CH_2$-Ad)

[Co-(κ^2-(SCS^{CH_2}-*t*Bu))(κ^3-(SCS^{CH_2}-*t*Bu))](32)

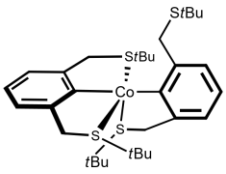

$CoCl_2$ (59 mg, 0.45 mmol) got suspended in THF (15 mL) and placed in an ultrasonic bath for 30 minutes to form an intense blue solution. The ligand **(10)** (150 mg, 0.41 mmol) were dissolved in THF (5 mL) and subsequently cooled to -105° C. After stirring at that temperature for 10 minutes, n-BuLi (0.29 mL, 1.6M, 0.47 mmol) was added dropwise via a syringe. The red solution was further stirred at that temperature for 30 minutes, before it was allowed to warm up to 0° C over the course of 30 minutes. Then, the lithiated ligand was added in a dropwise fashion to the intense blue solution of $CoCl_2$, forming a dark solution. The mixture was allowed to stir for additional 45 minutes before all volatiles got evaporated under reduced pressure. The dark residue was extracted with n-pentane (12 mL) and filtered through a syringe filter (PTFE, 0.2 μm). The dark yellow solution was reduced to a volume of 5 mL. Storing the solution at -30° C over night led to the deposition of red crystals, suitable for XRD analyis. (53 mg, 21 % yield. calculated to the max. possible amount, with ligand utilized) μ_{eff} =1.8(2))μ_B (Evans Method, d_6-benzene)

[Co-(κ^3-(SCS^{CH_2}-*t*Bu))$_2$][$Co_2Br_3Cl_3$](33)

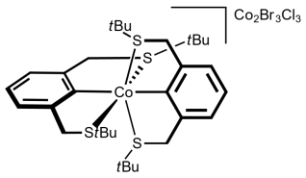

The formation **(33)** occours during the synthesis of **(32)**. After the successful separation of **(32)** by the extraction into *n*-pentane. The remaining residue was extracted with toluene (5 mL) and filtered through a syringe filter (PTFE, 0.2 μm). After evaporation of the solvent, a brown solid was obtained. (102 mg, 23 % yield). Crystals suitable for XRD measurements could be obtained by *n*-pentane diffusion into a saturated DCM solution of **(33)**.

Reaction towards [Co-(κ^3-(SCS^{CH_2}-*t*Bu))$_2$][BAr^F_4](34)

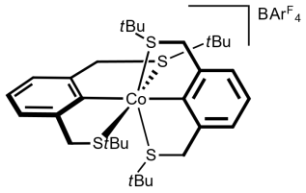

33 (15 mg, 0.014 mmol) was dissolved in benzene- d_6. Then $NaBAr^F_4$ (13 mg, 0.014 mmol) were added and the mixture was stirred for 1.5 h. After that time, the mixture was filtered through a syringe filter (PTFE, 0.2 μm) into a NMR-tube.

^{1}**H-NMR** (400 MHz, benzene-d_6, 20° C, ppm): δ 7.44 (s, CH, 4 H, BArF), 7.35 (s, CH, 8 H, BArF), 7.08-6.93 (m, 6 H, CH), 3.58 (s, 8 H, SCH_2), 1.20 (s, 36 H, CH_3).

5 Bibliography

[1] McNaught, A. D.; Wilkinson, A. *IUPAC Compendium of Chemical Terminology* **2014**, *2291*, 2293.

[2] Schlögl, R. *Angewandte Chemie - International Edition* **2015**, *54*, 3465–3520.

[3] Armor, J. N. *Catalysis Today* **2011**, *163*, 3–9.

[4] Fechete, I.; Wang, Y.; Védrine, J. C. *Catalysis Today* **2012**, *189*, 2–27.

[5] Berton, G.; Leeuwen, P. W. N. M. V. **2008**, 1989–2006.

[6] European Commission, **2014**, 41.

[7] Henckens, T. *Governance of the World's Mineral Resources* **2021**, 61–70.

[8] Bobba, S.; Carrara, S.; Huisman, J.; Mathieux, F.; Pavel, C. *European Commission*; 2020; p 100.

[9] Moulton, C. J.; Shaw, B. L. *J. Chem. Soc., Dalton Trans.* **1976**, 1020–1024.

[10] van Koten, G. *Pure Appl. Chem* **1989**, *61*, 1681–1694.

[11] Kadassery, K. J.; MacMillan, S. N.; Lacy, D. C. *Dalton Transactions* **2018**, *47*, 12652–12655.

[12] Li, Y.; Collett, J. D.; Guan, H. *Comprehensive Coordination Chemistry III*, 3rd ed.; Elsevier Inc., 2021; pp 505–606.

[13] Kameo, H.; Ishii, S.; Nakazawa, H. *Dalton Transactions* **2012**, *41*, 11386–11392.

[14] Zhang, J.; Foley, B. J.; Bhuvanesh, N.; Zhou, J.; Janzen, D. E.; Whited, M. T.; Ozerov, O. V. *Organometallics* **2018**, *37*, 3956–3962.

[15] Ke, I. S.; Gabbaï, F. P. *Inorganic Chemistry* **2013**, *52*, 7145–7151.

[16] Derrah, E. J.; Martin, C.; Mallet-Ladeira, S.; Miqueu, K.; Bouhadir, G.; Bourissou, D. *Organometallics* **2013**, *32*, 1121–1128.

[17] Mastalir, M.; Schweinzer, C.; Weil, M.; Pittenauer, E.; Allmaier, G.; Kirchner, K. *Monatshefte fur Chemie* **2016**, *147*, 1183–1187.

[18] Peris, E.; Crabtree, R. H. *Chemical Society Reviews* **2018**, *47*, 1959–1968.

[19] Choi, J.; MacArthur, A. H.; Brookhart, M.; Goldman, A. S. *Chemical Reviews* **2011**, *111*, 1761–1779.

[20] Ramírez-Contreras, R.; Cosio, M. N.; Park, S.; Bhuvanesh, N.; Ozerov, O. V. *Journal of Organometallic Chemistry* **2021**, *938*, 1–5.

[21] Crabtree, R. *Comprehensive Coordination Chemistry III*.

[22] Tolman, C. A. *Chemical Reviews* **1977**, *77*, 313–348.

[23] Abbenhuis, H. C.; van Belzen, R.; Grove, D. M.; Klomp, A. J.; van Mier, G. P.; Spek, A. L.; van Koten, G. *Organometallics* **1993**, *12*, 210–219.

[24] Seligson, A. L.; Trogler, W. C. *Journal of the American Chemical Society* **1991**, *113*, 2520–2527.

[25] Teratani, T.; Koizumi, T.-a.; Yamamoto, T.; Tanaka, K.; Kanbara, T. *Dalton Trans.* **2011**, *40*, 8879–8886.

[26] Begum, R. A.; Powell, D.; Bowman-James, K. *Inorganic Chemistry* **2006**, *45*, 964–966.

[27] Komiyama, Y.; Kuwabara, J.; Kanbara, T. *Organometallics* **2014**, *33*, 885–891.

[28] Wang, Q. Q.; Begum, R. A.; Day, V. W.; Bowman-James, K. *Journal of the American Chemical Society* **2013**, *135*, 17193–17199.

[29] Lawrence, M. A.; Green, K. A.; Nelson, P. N.; Lorraine, S. C. *Polyhedron* **2018**, *143*, 11–27.

[30] Eder, W.; Himmelbauer, D.; Stöger, B.; Veiros, L. F.; Pignitter, M.; Kirchner, K. *Dalton Transactions* **2021**, *50*, 13915–13924.

[31] Himmelbauer, D.; Mastalir, M.; Stöger, B.; Veiros, L. F.; Kirchner, K. *Organometallics* **2018**, *37*, 3631–3638.

[32] Himmelbauer, D.; Mastalir, M.; Stöger, B.; Veiros, L. F.; Pignitter, M.; Somoza, V.; Kirchner, K. *Inorganic Chemistry* **2018**, *57*, 7925–7931.

[33] *Organometallics* **2018**, *37*, 3475–3479.

[34] Himmelbauer, D.; Stöger, B.; Veiros, L. F.; Pignitter, M.; Kirchner, K. *Organometallics* **2019**, *38*, 4669–4678.

[35] Himmelbauer, D.; Stöger, B.; Veiros, L. F.; Pignitter, M.; Kirchner, K. *Organometallics* **2019**, *38*, 4669–4678.

[36] Albrecht, M.; Kocks, B. M.; Spek, A. L.; Van Koten, G. *Journal of Organometallic Chemistry* **2001**, *624*, 271–286.

[37] Albrecht, M.; Lindner, M. M.; van Koten, G. *Dalton Transactions* **2011**, *40*, 8733–8744.

[38] Chuchuryukin, A. V.; Huang, R.; Lutz, M.; Chadwick, J. C.; Spek, A. L.; Van Koten, G. *Organometallics* **2011**, *30*, 2819–2830.

[39] Hosokawa, S.; Ito, J. I.; Nishiyama, H. *Organometallics* **2010**, *29*, 5773–5775.

[40] Benito-Garagorri, D.; Bocokić, V.; Mereiter, K.; Kirchner, K. *Organometallics* **2006**, *25*, 3817–3823.

[41] Rimml, H.; Venanzi, L. M. *Journal of Organometallic Chemistry* **1983**, *259*, C6–C7.

[42] Steenwinkel, P.; Gossage, R. A.; Van Koten, G. *Chemistry - A European Journal* **1998**, *4*, 759–762.

[43] De Aguiar, S. R.; Stöger, B.; Pittenauer, E.; Allmaier, G.; Veiros, L. F.; Kirchner, K. *Organometallics* **2016**, *35*, 3032–3039.

[44] Li, Y.; Krause, J. A.; Guan, H. *Organometallics* **2018**, *37*, 2147–2158.

[45] Gorgas, N.; Stöger, B.; Veiros, L. F.; Kirchner, K. *ACS Catalysis* **2016**, *6*, 2664–2672.

[46] Gorgas, N.; Stöger, B.; Veiros, L. F.; Kirchner, K. *ACS Catalysis* **2018**, *8*, 7973–7982.

[47] Pecak, J.; Fleissner, S.; Veiros, L. F.; Pittenauer, E.; Stöger, B.; Kirchner, K. *Organometallics* **2021**, *40*, 278–285.

[48] Evans, D. F. *J. Chem. Soc.* **1959**, 2003–2005.

[49] Schubert, E. M.; Birdwhistell, R. K. **1959**, 1955.

[50] Ostfeld, D.; Cohen, I. A. *Journal of Chemical Education* **1972**, *49*, 829.

[51] Goswami, M.; Chirila, A.; Rebreyend, C.; de Bruin, B. *Topics in Catalysis*; Springer US, 2015; Vol. 58; pp 719–750.

[52] Villamena, F. A. In *Reactive Species Detection in Biology*; Villamena, F. A., Ed.; Elsevier: Boston, 2017; pp 163–202.

[53] Presley, T.; Kuppusamy, P.; Zweier, J. L.; Ilangovan, G. *Biophysical Journal* **2006**, *91*, 4623–4631.

[54] Himmelbauer, D. *Synthese und Charakterisierung von PCP Pincer Komplexen mit unedlen Metallen* **2020**,

[55] El-Agamey, A.; McGarvey, D. J. *Carotenoids* **2008**, 119–154.

[56] Desrosiers, M.; Schauer, D. A. *Nuclear Instruments and Methods in Physics Research, Section B: Beam Interactions with Materials and Atoms* **2001**, *184*, 219–228.

[57] Roessler, M. M.; Salvadori, E. *Chemical Society Reviews* **2018**, *47*, 2534–2553.

[58] Grove, D. M.; Koten, G. V.; Louwen, J. N.; Noltes, J. G.; Spek, A. L.; Ubbels, H. J. C. *Journal of the American Chemical Society* **1982**, *3*, 6609–6616.

[59] Grove, D. M.; van Koten, G.; Ubbels, H. J.; Zoet, R.; Spek, A. L. *Organometallics* **1984**, *3*, 1003–1009.

[60] van der Zeijden, A. A.; van Koten, G. *Inorganic Chemistry* **1986**, *25*, 4723–4725.

[61] *Coordination Chemistry Reviews* **2004**, *248*, 2275–2282.

[62] Slagt, M. Q.; Klein Gebbink, R. J.; Lutz, M.; Spek, A. L.; Van Koten, G. *Journal of the Chemical Society, Dalton Transactions* **2002**, 2591–2592.

[63] Mehendale, N. C.; Bezemer, C.; van Walree, C. A.; Klein Gebbink, R. J.; van Koten, G. *Journal of Molecular Catalysis A: Chemical* **2006**, *257*, 167–175.

[64] Dijkstra, H. P.; Meijer, M. D.; Patel, J.; Kreiter, R.; Van Klink, G. P.; Lutz, M.; Spek, A. L.; Canty, A. J.; Van Koten, G. *Organometallics* **2001**, *20*, 3159–3168.

[65] Valdés, H.; González-Sebastián, L.; Morales-Morales, D. *Journal of Organometallic Chemistry* **2017**, *845*, 229–257.

[66] Wu, L. Y.; Hao, X. Q.; Xu, Y. X.; Jia, M. Q.; Wang, Y. N.; Gong, J. F.; Song, M. P. *Organometallics* **2009**, *28*, 3369–3380.

[67] Grove, D. M.; van Koten, G.; Ubbels, H. J.; Zoet, R.; Spek, A. L. *Organometallics* **1984**, *3*, 1003–1009.

[68] Chnme, N. C. H.; Grove, D. M.; Murrall, N. W.; Welch, A. J. *Journal of the American Chemical Society*

[69] Cloutier, J. P.; Zargarian, D. *Organometallics* **2018**, *37*, 1446–1455.

[70] Cloutier, J. P.; Rechignat, L.; Canac, Y.; Ess, D. H.; Zargarian, D. *Inorganic Chemistry* **2019**, *58*, 3861–3874.

[71] Cloutier, J. P.; Vabre, B.; Moungang-Soumé, B.; Zargarian, D. *Organometallics* **2015**, *34*, 133–145.

[72] Beilin, S. I.; Dolgoplosk, B. A. *Journal of Organometallic Chemistry* **1976**, *10*, 237–239.

[73] Wehman-Ooyevaar, I. C.; Kapteijn, G. M.; Grove, D. M.; Smeets, W. J.; Spek, A. L.; Van Koten, G. *Journal of the Chemical Society, Dalton Transactions* **1994**, 703–711.

[74] Steenwinkel, P.; James, S. L.; Gossage, R. A.; Grove, D. M.; Kooijman, H.; Smeets, W. J.; Spek, A. L.; Van Koten, G. *Organometallics* **1998**, *17*, 4680–4693.

[75] Ito, J. I.; Hosokawa, S.; Khalid, H. B.; Nishiyama, H. *Organometallics* **2015**, *34*, 1377–1383.

[76] Hosokawa, S.; Ito, J. I.; Nishiyama, H. *Organometallics* **2012**, *31*, 8283–8290.

[77] Hosokawa, S.; Ito, J. I.; Nishiyama, H. *Organometallics* **2013**, *32*, 3980–3985.

[78] Liu, Z.; Gao, W.; Liu, X.; Luo, X.; Cui, D.; Mu, Y. *Organometallics* **2011**, *30*, 752–759.

[79] Caise, A.; Griffin, L. P.; McManus, C.; Heilmann, A.; Aldridge, S. *Angewandte Chemie International Edition* **2022**,

[80] Kanbara, T.; Okada, K.; Yamamoto, T.; Ogawa, H.; Inoue, T. *Journal of Organometallic Chemistry* **2004**, *689*, 1860–1864.

[81] Akaiwa, M.; Kanbara, T.; Fukumoto, H.; Yamamoto, T. *Journal of Organometallic Chemistry* **2005**, *690*, 4192–4196.

[82] Kruithof, C. A.; Berger, A.; Dijkstra, H. P.; Soulimani, F.; Visser, T.; Lutz, M.; Spek, A. L.; Gebbink, R. J.; Van Koten, G. *Dalton Transactions* **2009**, 3306–3314.

[83] Kuwabara, J.; Munezawa, G.; Okamoto, K.; Kanbara, T. *Dalton Transactions* **2010**, *39*, 6255–6261.

[84] Okamoto, K.; Kanbara, T.; Yamamoto, T.; Wada, A. *Organometallics* **2006**, *25*, 4026–4029.

[85] Pollino, J. M.; Weck, M. *Synthesis* **2002**, 1277–1285.

[86] Van Manen, H. J.; Fokkens, R. H.; Van Veggel, F. C.; Reinhoudt, D. N. *European Journal of Organic Chemistry* **2002**, 3189–3197.

[87] Patterson, J. P.; Cotanda, P.; Kelley, E. G.; Moughton, A. O.; Lu, A.; Epps, T. H.; O'Reilly, R. K. *Polymer Chemistry* **2013**, *4*, 2033–2039.

[88] Kruithof, C. A.; Dijkstra, H. P.; Lutz, M.; Spek, A. L.; Gebbink, R. J.; Van Koten, G. *Organometallics* **2008**, *27*, 4928–4937.

[89] Suijkerbuijk, B. M.; Martínez, S. D.; Van Koten, G.; Klein Gebbink, R. J. *Organometallics* **2008**, *27*, 534–542.

[90] Bonnet, S.; Lutz, M.; Spek, A. L.; Van Koten, G.; Klein Gebbink, R. J. *Organometallics* **2010**, *29*, 1157–1167.

[91] Hosseini-Kharat, M.; Zargarian, D.; Alizadeh, A. M.; Karami, K.; Saeidifar, M.; Khalighfard, S.; Dubrulle, L.; Zakariazadeh, M.; Cloutier, J. P.; Sohrabijam, Z. *Dalton Transactions* **2018**, *47*, 16944–16957.

[92] Himmelbauer, D.; Mastalir, M.; Stöger, B.; Veiros, L. F.; Kirchner, K. *Organometallics* **2018**, *37*, 3631–3638.

[93] Peterson, S. M.; Helm, M. L.; Appel, A. M. *Dalton Transactions* **2015**, *44*, 747–752.

[94] Matsumoto, T.; Takamine, H.; Tanaka, K.; Chujo, Y. *Organic Letters* **2015**, *17*, 1593–1596.

[95] Bibal, C.; Mazières, S.; Gornitzka, H.; Couret, C. *Polyhedron* **2002**, *21*, 2827–2834.

[96] Moya-López, J. F.; Elhalem, E.; Recio, R.; Álvarez, E.; Fernández, I.; Khiar, N. *Organic and Biomolecular Chemistry* **2015**, *13*, 1904–1914.

[97] Murugesan, S.; Stöger, B.; Weil, M.; Veiros, L. F.; Kirchner, K. *Organometallics* **2015**, *34*, 1364–1372.

[98] McGowan, K. P.; Abboud, K. A.; Veige, A. S. *Organometallics* **2011**, *30*, 4949–4957.

[99] Hirao, Y.; Katayama, Y.; Mitsunuma, H.; Kanai, M. *Organic Letters* **2020**, 0–4.

[100] Fu, A.; Zhao, L.; Li, C.; Luo, M.; Zeng, X. *Organometallics* **2021**, *40*, 2204–2208.

[101] Ferbinteanu, M.; Cimpoesu, A. F.; Mariusandruh, A.; Rochon, F. D. *Polyhedron* **1998**, *17*, 3671–3679.

[102] Okuniewski, A.; Rosiak, D.; Chojnacki, J.; Becker, B. *Polyhedron* **2015**, *90*, 47–57.

[103] Rosiak, D.; Okuniewski, A.; Chojnacki, J. *Polyhedron* **2018**, *146*, 35–41.

[104] Ott, J. C.; Isak, D.; Melder, J. J.; Wadepohl, H.; Gade, L. H. *Inorganic Chemistry* **2020**, *59*, 14526–14535.

[105] Pecak, J.; Eder, W.; Tomsu, G.; Stöger, B.; Pignitter, M.; Kirchner, K. *European Journal of Inorganic Chemistry* **2021**, *2021*, 4280–4285.

[106] Ashida, Y.; Egi, A.; Arashiba, K.; Tanaka, H.; Kuriyama, S.; Yoshi-Zawa, K.; Nishibayashi, Y. *chemrxiv*

[107] Xie, Y.; Miao, Q.; Deng, W.; Lu, Y.; Yang, Y.; Chen, X.; Liao, R. Z.; Ye, S.; Tung, C. H.; Wang, W. *Inorganic Chemistry* **2022**, *61*, 2204–2210.

[108] Addison, A. W.; Rao, T. N.; Reedijk, J.; van Rijn, J.; Verschoor, G. C. *J. Chem. Soc., Dalton Trans.* **1984**, 1349–1356.

[109] Himmelbauer, D.; Schratzberger, H.; Käfer, M. G.; Stöger, B.; Veiros, L. F.; Kirchner, K. *Organometallics* **2021**, *40*, 3331–3340.

[110] Smart, K. A.; Vanbergen, A.; Lednik, J.; Tang, C. Y.; Mansaray, H. B.; Siewert, I.; Aldridge, S. *Journal of Organometallic Chemistry* **2013**, *741-742*, 33–39.

[111] Sun, J. S.; Zhao, H.; Ouyang, X.; Clérac, R.; Smith, J. A.; Clemente-Juan, J. M.; Gómez-Garcia, C.; Coronado, E.; Dunbar, K. R. *Inorganic Chemistry* **1999**, *38*, 5841–5855.

6 Appendix

6.1 Crystallographic Data

complex	**[Cr(NCN ^{CH2}-*i*Pr)Cl]**	**[Cr-(κ^2-NCN ^{CH2}-*i*Pr)$_2$]**	**cluster**
empirical formula	$C_{20}H_{35}ClCrN_2$	$C_{40}H_{70}CrN_4$	$C_{48}H_{81}Cl_3Cr_3N_6O_2$
molecular weight (g mol^{-1})	407.35	659.00	1035.47
crystal size (mm)	0.15 x 0.14 x 0.11	0.20 x 0.18 x 0.23	0.18 x 0.23 x 0.21
color, shape	violet, block	blue, block	green, block
crystal system	orthorombic	monoclinic	triclinic
space group	P21	P21	P-1
a ($\AA$)	7.7465(7)	11.7557(13)	13.028(2)
b ($\AA$)	13.1236(12)	13.6484(15)	13.064(2)
c ($\AA$)	20.2570(19)	11.9682(13)	18.689(3)
α(°)	90	90	74.763(3)
β (°)	90	90.433(4)	81.190(3)
γ (°)	90	90	89.143(4)
V ($\AA^3$)	2059.4(3)	1920.2(4)	3031.8(9)
Z	4	2	8
ρ (g cm^{-3})	1.314	1.140	-
T (K)	100	100	100
μ (mm^{-1})	1.357	1.140	
F(0 0 0)	867	724	1230
θ_{min} (°)	2.815	2.26	1.143
θ_{max} (°)	27.660	30.32	30.011
No.refl. measured	38995	21912	17569
No. of unique reflns.	4416	9297	11900
no. of reflns. I> 2σ	3978	-	-
no. of params.	226	424	-
R_1 (all data)	0.0355	0.0735	-
wR_2 (all data)	0.0572	0.1076	-
GooF	1.039	0.989	-

complex	**[Cr(NCN ^{CH2}-Et)Cl_2(THF)]**	**[Ni(SCS ^{CH2} - *t*Bu)Br]**	**[Co_2(NCN ^{CH2}-*i*Pr)Cl_2Br]**
empirical formula	$C_{19}H_{31}Cl_2CrN_2O$	$C_{16}H_{25}S_2NiBr$	$C_{20}H_{35}ClCo_2N_2Br_2$
molecular weight (g mol^{-1})	426.36	420.10	621.56
crystal size (mm)	0.18 x 0.21 x 0.24	0.19x 0.20 x 0.17	0.23 x 0.24 x 0.17
color, shape	green, block	orange, block	green, block
crystal system	monoclinic	orthorhombic	tetragonal
space group	P n	P2n	P42/n
a ($\AA$)	8.1644(19)	9.809(4)	16.3566(6)
b ($\AA$)	8.940(2)	14.592(5)	16.3566(6)
c ($\AA$)	14.933(4)	12.700(5)	20.5658(11)
α(°)	90	90	90
β (°)	96.234(6)	90	90
γ (°)	90	90	90
V ($\AA^3$)	1083.5(4)	1817.6(12)	5502.1(5)
Z	2	4	8
ρ (g cm^{-3})	1.307	1.535	1.501
T (K)	100	100	100
μ (mm^{-1})	0.784	-	0.744
F(0 0 0)	450	2496	2496
θ_{min} (°)	2.278	2.52	2.49
θ_{max} (°)	29.475	36.62	19.13
No.refl. measured	19404	32845	162793
No. of unique reflns.	5805	4395	9922
no. of reflns. I> 2σ	-	3612	3336
no. of params.	239	102	130
R_1 (all data)	0.1477	0.0306	0.0995
wR_2 (all data)	0.1960	0.0454	0.1368
GooF	1.019	1.017	1.087

complex	**[Co(κ^2-SCS^{CH2}-*t*Bu)(κ^3-SCS^{CH2}-*t*Bu)]**	**[Co (κ^3-(SCS^{CH2}-*t*Bu)][$Co_2Br_3Cl_3$]**
empirical formula	$C_{32}H_{53}S_4Co$	$C_{33}H_{52}S_4Co_3Br_{1.59}Cl_{3.41}$
molecular weight (g mol^{-1})	624.91	942.88
crystal size (mm)	0.19 x 0.25 x 0.21	0.16x 0.29 x 0.23
color, shape	red, block	green, block
crystal system	monoclinic	triclinic
space group	P21/c	P-1
a ($\AA$)	9.9832(9)	9.8600(16)
b ($\AA$)	19.6159(16)	10.7422(18)
c ($\AA$)	16.6052(15)	19.023(3)
α(°)	90	80.148(5)
β (°)	90.064(3)	86.304(5)
γ (°)	90	88.002(5)
V ($\AA^3$)	3251.8(5)	1980.5(6))
Z	4	2
ρ (g cm^{-3})	1.276	1.581
T (K)	100	100
μ (mm^{-1})	0.804	2.908
F(0 0 0)	1344	963
θ_{min} (°)	1.038	2.65
θ_{max} (°)	29.050	26.19
No.refl. measured	35456	11599
No. of unique reflns.	8611	6912
no. of reflns. I> 2σ	7345	6848
no. of params.	344	416
R_1 (all data)	0.0545	0.1178
wR_2 (all data)	0.1181	0.1098
GooF	0.821	0.992

7 List of figures